MODELLING OF MECHANICAL BEHAVIOUR OF CONCRETE STRUCTURES

by

JIANPING JIANG, B.Sc., M.Eng.

A THESIS

Submitted to the School of Graduate Studies

in Partial Fulfilment of the Requirements

for the Degree

Doctor of Philosophy

McMaster University

April 1988

DOCTOR OF PHILOSOPHY (1988) McMASTER UNIVERSITY

(Civil Engineering and Engineering Mechanics) Hamilton, Ontario

Canada

TITLE: Modelling of Mechanical Behaviour of Concrete Structures

AUTHOR: Jianping Jiang

B.Sc. (Nanjing Instutite of Technology, China)

M.Eng. (McMaster University)

SUPERVISORS: Dr. F.A. Mirza and Dr. S. Pietruszczak

NUMBER OF PAGES: xiv, 224

ABSTRACT

This thesis deals with numerical modelling of mechanical behaviour of reinforced concrete structures. The main objective of this study is to establish a rational constitutive model for concrete subjected to monotonic or cyclic loadings and to analyze nonlinear behaviour of reinforced concrete structures by finite element method.

The constitutive model described here is built within the framework of rate-independent theory of plasticity. In the present study, the emphasis is placed on an adequate modelling of basic trends in the behaviour of concrete, e.g. compaction-dilatancy transition, sensitivity of material characteristics to confining pressure, gradual transition in failure mechanisms from a brittle to a ductile mode and phenomenon of cyclic degradation of material stiffness and strength, etc. The proposed model is suitable for describing strain hardening and softening response of concrete under any complex state of stress. In order to describe rigorously the strain softening response, an appropriate criterion for strain localization is derived from considerations of stability of the constitutive relations. The model is verified for a number of loading paths by comparing the numerical results with the experimental data available in the literature.

The finite element modelling of reinforced concrete slabs is also presented. In this finite element model, the post-cracking behaviour of concrete and tension stiffening effect are modelled using the proposed constitutive theory. Moreover, some common problems related to numerical instability are carefully studied. The numerical results are compared with the experimental data and the results obtained from other analytical models.

ACKNOWLEDGEMENTS

The author would like to express his sincerest gratitude to his supervisors, Dr. F.A. Mirza and Dr. S. Pietruszczak for their constant guidance, criticism, and encouragement during the course of the research and preparation of the thesis.

Thanks are also due to Dr. R.G. Drysdale, Dr. J.D. Embury and Dr. A. Ghobarah, the members of Supervisory Conmmittee, for their interests and suggestions.

The financial support of the Natural Science and Engineering Research Council of Canada and McMaster University are gratefully acknowledged.

Finally, this thesis is dedicated to the author's family for their understanding and support, and especially to his wife, Xiaolu, for her patience and understanding througth the duration of this study.

TABLE OF CONTENTS

TABLES OF CONTENTS (Cont'd)

TABLES OF CONTENTS (Cont'd)

LIST OF FIGURES

LIST OF TABLES

CHAPTER 1

INTRODUCTION

1.1 General Remarks

Concrete as a structural material has been very widely used in civil engineering projects since the late nineteenth century. During the past several decades, a large number of developments in the technology of concrete, structural design and the theory of modern structural analysis have taken place. In particular, the developments in design philosophy are reflected in the virtual elimination of working stress design and its replacement by the ultimate strength design method in codes of practice. The advances in analytical methodology manifest in the vast engineering applications of computer-oriented numerical techniques such as the finite element technique and the increasing usage of sophisticated material models, e.g. nonlinear elastoplastic constitutive model. Despite these advances, the rational modelling of mechanical behaviour of concrete structures still remains a difficult problem due to the following complexities involved:

(1) Concrete is a heterogenous, multiphase system which on a macroscopic scale is a mixture of cement paste, sand and coarse aggregate. At the microscopic level, it contains numerous microcracks and voids. As a result, the mechanical behaviour is extremely complicated.

(2) The response of a reinforced concrete structure is heavily influenced by cracking of concrete and yielding of reinforcement. Appropriate modelling of such slow crack propagation in concrete has been a difficult topic for many years.

(3) The modelling of interface behaviour between concrete and steel reinforcement is also very difficult, as the mechanical characteristics are still not clearly understood.

(4) The shear transfer mechanism at cracked concrete sections has a significant influence on the behaviour. Both experimental and analytical investigations of such effect are very complicated.

(5) The time-dependent behaviour such as creep and shrinkage of concrete and the dynamic behaviour as caused by fluctuating loads are even more complex than the behaviour under monotonically increasing loads.

Of all the complexities mentioned above, the path-dependent constitutive behaviour of concrete is a very essential one, which to a large extent effects the behaviour of reinforced concrete structures. Consequently, the constitutive modelling of concrete has become a very important topic for many researchers. Although various models have been proposed(ref.[1]), ranging from the very simple to the very sophisticated, many aspects of concrete behaviour are still not well understood or described appropriately. One particular problem is how to

model the post-cracking behaviour of concrete including the strain softening effect. Since some portions of a structural system may reach this stage prior to the overall failure, the post-cracking behaviour should not be ignored when analyzing reinforced concrete structures. In fact, any inadequate modelling of the post-cracking behaviour in a numerical analysis may cause instabilities. Therefore, the development of a simple, effective and consistent constitutive model for concrete, capable of describing both the pre- and post-cracking behaviour, remains very important.

1.2 Brief Review of the Literature

The state-of-the-art review on modelling of the mechanical behaviour of reinforced concrete structures by numerical techniques, such as finite element method, has been reported in detail in ref.[1]. Therefore, the literature review presented here is very comprehensive and focuses on the topics to be investigated in this study.

1.2.1 Constitutive Models for Concrete

The stress-strain behaviour of concrete under biaxial or triaxial state of stress has been investigated experimentally and

analytically by many researchers. Various models have been proposed, which have borrowed different theoretical frameworks primarily from continuum mechanics, e.g. non-linear elasticity (refs.[2-5]), rate-independent plasticity(refs.[6-11]), endochronic theory(refs.[12,13]), and plastic-fracturing theory(refs.[14,15]), etc.

The elasticity-based models were mostly developed using the theory of hyperelasticity or that of hypoelasticity. The hyperelastic models in ref.[2] assume a path-independent reversible response with no memory of deformational history, whereas the hypoelastic models in refs.[3-5] approximate a path-dependent irreversible process with limited memory and no pronounced reference state. Although the hyperelastic models can simulate many characteristics of concrete such as nonlinearity, dilatation and stress-induced anisotropy, they fail to account for load-history effects and is lack of continuity for a neutral loading path. The hypoelastic models with variable moduli of tangential material stiffness can describe the instantaneous behaviour in terms of stress rate and strain rate tensors. However, they usually encounter an inherent difficulty in the formulation of their constitutive relations, i.e. the instantaneous constitutive matrix becoming anisotropic in the nonlinear range even if the isotropic behaviour is assumed initially. Moreover, they do not model accurately the behaviour of concrete at high stress levels or near failure and different constitutive relations may be required when an unloading occurs at different stress levels.

All of the above defects associated with the elasticity-based models can be well overcome by the application of plasticity theory. In the early stages of developments of plasticity-based models, the perfect-plasticity formulation was suggested to approximate the actual stress-strain behaviour. This has been widely used to obtain upper and lower bounds on collapse loads for reinforced concrete structures. However, such formulation does not account for strain hardening and softening effects. In the strain hardening concepts as employed in refs.[6-11], the hardening effects have been attributed to a progressive propagation of microcracks in a concrete medium due to increasing external loads. Because of the inherent heterogeneity and the randomness of microcracks, most of the models proposed treat the material as an isotropic one until formation of a distinct macrocrack. It is obvious that the plasticity-based models have the advantage of offering more freedom in modelling cyclic behaviour of concrete. In fact, some of the models do have the capability of predicting the cyclic response of concrete. However, only a few of these models can adequately simulate the sensitivity of material characteristics to the applied confining pressure, and almost none is capable of describing a smooth transition from ductile to brittle behaviour. Therefore, it seems inevitable that further modifications are necessary.

An alternative approach to describe the complex behaviour of concrete is based on the endochronic theory of plasticity, developed originally by Valanis[16] for metals. The first application of this theory to concrete was proposed by Bazant et al[12]. The basic concept

involved in this theory is that of intrinsic time which is similar to the role of effective plastic strain in the classical theory of plasticity. This model can reflect many aspects of concrete behaviour such as nonlinearity, volume dilatancy, confining pressure sensitivity, etc. However, the final form of the constitutive relations is very complicated and involves unacceptably large number of material parameters.

In the plastic-fracturing theory, refs.[14,15], the inelastic behaviour is due to combination of pure plastic slip and microcracking. The pure plastic strain component is evaluated from the classical theory of plastic flow while the fracturing strain component is obtained by using the potential functions in strain space. It has been reported that this model predicts the nonlinear behaviour of concrete very well, refs.[14,15]. However, many complexities arise in the process of defining two loading functions in stress and strain spaces, respectively.

1.2.2 Finite Element Modelling of Concrete Structures

One of the earliest papers published on the application of finite element method to reinforced concrete structures was contributed by Ngo and Scordelis[17] in 1967. Since then, the finite element method has been successfully applied to studying behaviours of variety of reinforced concrete structural systems, including planar members,

plates and shells, axisymmetric structures and three-dimensional structural systems. Ngo and Scordelis[17] analyzed simple beams in which the concrete and steel reinforcement were represented by two-dimensional constant strain triangular elements. Linear constitutive relations were used in the analysis and the discrete crack concept with pre-defined crack patterns was first brought into the finite element modelling of cracked concrete. Instead of using pre-defined crack patterns, Nilson[18] modified this approach to trace the discrete cracks individually by progressive splitting of nodes and then defining a new topology for the subsequent analysis. In his study, nonlinear behaviour of concrete was modeled by hypoelastic type of constitutive relations and an incremental loading technique was implemented in the analysis. Soon thereafter a second and basically different crack model was developed by Rashid[19] and Franklin[20], simultaneously. In this model a discrete crack is numerically replaced by many finely spaced cracks perpendicular to the principal tensile stress direction. The latter model is called the smeared crack model. This formulation has been widely adopted by many researchers, refs.[21,22].

Subsequently, many more investigations were undertaken predominantly to study the overall behaviour of more complex structures such as reinforced concrete plates and shells, refs.[23-26], nuclear reactor vessels, refs.[27,28], etc. The objective of those investigations was primarily to determine the basic failure mechanisms which, for a number of these structures, were not well understood. Some of the fundamental aspects of reinforced concrete behaviour, such as

bond-slip, aggregate interlocking, tension stiffening effect, etc. were also explored. More detailed information can be found in ref.[1].

With increased applications of the finite element method to reinforced concrete structures, questions have been raised regarding the objectivity of solutions by the finite element method. The major issue is the sensitivity of the solution to the grid size used. It has been indicated in ref.[29] that when the uniaxial tensile strength of concrete is used as a criterion for crack propagation in a smeared crack model, infinitesimally small element sizes may produce a self-propagating crack requiring negligible energy. To avoid such problem several criteria based on fracture mechanics concepts have been suggested, refs.[29,30]. However, further investigation and improvements are still necessary in order to achieve finite element solutions which maintain proper grid objectivity.

1.3 Purpose and Scope

The purpose of this thesis is to develop a constitutive model for describing basic characteristics of concrete, including post-cracking response and to implement this model into finite element analysis of reinforced concrete structures such as reinforced concrete slabs and concrete beams.

In the development of rational constitutive relations for

concrete the emphasis is placed on modelling of the progressive transition from compaction to dilatancy, sensitivity of material characteristics to confining pressure and smooth transition in failure mechanisms from a ductile to a brittle mode. The proposed elastoplastic model is suitable for describing both monotonic and cyclic loading histories. To describe rigorously the strain softening response, an appropriate strain localization criterion is derived from considerations of stability of the constitutive relations. The proposed model is verified for a number of loading paths by comparing the numerical results with the experimental data available in the literature.

In the context of finite element analysis of reinforced concrete structures, the proposed constitutive model is used to investigate post-cracking behaviour and tension stiffening effect. Furthermore, some common problems of numerical instability such as mesh size and incremental load step size sensitivities are carefully studied. The numerical results are compared with the experimental test data and the results obtained from other analytical models.

In Chapter 2 the experimental observations of basic properties of concrete under various stress states are first discussed. Subsequently, the fundamental assumptions incorporated in the proposed constitutive relations are outlined. The mathematical details concerning the form of failure surface, yield and plastic potential loci are provided, followed by a discussion of strain hardening and

softening characteristics and introduction of 'size effect' into the constitutive framework. Subsequently, the identification procedure for material parameters involved in the formulation is described. Finally, the performance of the model is verified for various loading histories imposed on concrete with different strengths.

Chapter 3 deals with convexity of yield loci for pressure sensitive materials such as concrete. First, a general criterion for convexity in the octahedral plane is derived. This criterion is subsequently applied to examine the convexity of various functions proposed in the literature. The chapter is concluded by a discussion of some newly proposed convex generalizations.

Extension of the constitutive model, described in Chapter 2, to cover the cyclic behaviour of concrete is the major task of Chapter 4. An initial active loading process is modelled by the concept discussed in Chapter 2, whereas for loading histories experiencing stress-reversals, the formulation invokes a set of neutral loading loci defining the conditions of neutral state, ref.[31]. The field of hardening moduli is specified through an appropriate interpolation rule which enables one to simulate adequately the effect of cyclic degradation of the material stiffness and strength. The effectiveness of the model is verified for some typical cyclic loading histories and the results are compared with the experimental data available in the literature.

In Chapter 5, the brittle-ductile transition in concrete is treated as a bifurcation problem. This is based on the postulate that strain softening phenomenon is the result of localization of deformation into a shear band. From this postulate a necessary condition for strain localization is derived. To determine whether the bifurcation is physically feasible, an additional condition for strain localization is postulated using the concept of maximum second rate of energy dissipation. Subsequently, both conditions are employed to predict the brittle-ductile transition.

Chapter 6 describes finite element modelling of reinforced concrete structures. First, a general description of nonlinear finite element analysis of structures involving strain softening effect is provided, including formulation of finite element method, solution procedure for nonlinear analysis and numerical implementation of elastoplastic constitutive models. Subsequently, the finite element analyses of reinforced concrete slabs are carried out. The post-cracking behaviour and tension stiffening effect are modelled using the proposed constitutive theory. The numerical results are compared with the experimental data from literature and the results obtained by other investigators. Some numerical instability problems are carefully examined for both reinforced concrete slabs and plain concrete beams. In the later case the emphasis is focussed on studying the numerical solution aspects related to unstable material response. Both conventional and unconventional (i.e. incorporating the so-called 'size parameter' in the constitutive relations) analysis are performed and

their results are compared with each other.

Finally, some conclusions from this study and a few recommendations for future investigation are presented in Chapter 7.

CHAPTER 2

CONSTITUTIVE MODELLING OF CONCRETE RESPONSE UNDER MONOTONIC LOADING

2.1 Introduction

In the analysis and design of reinforced concrete structures, it is essential to investigate and understand the basic characteristics of reinforced concrete materials under various loading conditions, especially, the nonlinear response of plain concrete to applied loadings. Moreover, a realistic solution to a structural problem involving plain or reinforced concrete elements depends, to a large extent, on the choice of a set of appropriate constitutive relations which adequately describe the mechanical behaviour of concrete. Consequently, over the past decades a considerable amount of research has been focused on both experimental investigation and numerical prediction of progressive failure of plain concrete subjected to complex loading histories.

It is well known that the mechanical behaviour of concrete is very complicated and path-dependent because of the inherent heterogeneity and the randomness of microcracks. It seems unlikely that any phenomenological approach will ever be able to embrace all possible variations in material characteristics for different loading histories and environmental conditions. In this Chapter, a rate-independent

constitutive theory applicable to concrete and rock-like materials is presented. The proposed theory adequately reflects certain typical trends in concrete behaviour. These trends are: a progressive transition from compaction to dilatancy; sensitivity of material characteristics to confining pressure exhibiting a continuous transition in failure mechanisms from a ductile to a brittle mode. The proposed concept is built within the framework of theory of plasticity. The deformation process is governed by a non-associated flow rule and involves a progressive evolution of the yield surface which is described in terms of an appropriate hardening/softening parameter. The emphasis here is placed on adequate modelling of mechanical response of concrete under monotonic loading conditions. The extension of the model to fluctuating loading histories will be considered in Chapter 4.

This Chapter is divided into four main parts. In the first part, a brief discussion on some of the key facets of concrete behaviour as observed from many experiments is provided in order to set up a physical background for the subsequent mathematical description of the behaviour. In the second part, basic assumptions incorporated in the formulation of constitutive relations are outlined. The mathematical details concerning the form of failure surface, yield and plastic potential loci are provided, concluded by a general derivation of constitutive equations. The third part is concerned with identification of material parameters involved in the proposed model. Finally, in the fourth part, an extensive discussion on numerical effectiveness of the model is presented. The performance of the model

is verified for various stress histories.

2.2 Experimental Observations

In order to develop a realistic constitutive model for concrete, a knowledge of the physical processes involved in the stress-strain behaviour of the material is necessary. This requires a clear understanding of the basic characteristics of the mechanical behaviour of concrete under various loading conditions. This section summarizes some typical mechanical properties of concrete observed from tests under uniaxial, biaxial and triaxial states of stress reported in the literature. No attempt will be made here to fully review the literature on properties of concrete since such information can be found in several textbooks[32-35]. A brief review of some basic properties of concrete can also be found in refs.[36-40]. Therefore, the following discussions are mainly confined to the mechanical properties of normal-weight concrete subjected to short-term and quasi-static loadings. The cyclic behaviour of concrete will be discussed in Chapter 4.

2.2.1 Uniaxial Behaviour

From the standpoint of modelling stress-strain relationship of concrete, the uniaxial behaviour of the material under compression or tension is the simplest case which has been studied by many

investigators[41-45]. It has been found that a virgin concrete specimen contains a large number of defects in the transition zone between coarse aggregates and mortar, as schematically depicted in Fig. 2.1. These defects in the transition zone may be classified as two kinds, i.e. bond cracks at the interface between aggregate and cement paste and mortar cracks in the matrix. Most of the cracks are caused by segregation, shrinkage, or thermal deformation in the matrix. Upon application of external load, these defects may start to propagate and at the same time some additional cracks may be developed. All those cracks or defects tend to further propagate and coalesce as the load increases. This characteristic of progressive cracking plays a major role in determining the nonlinear behaviour of concrete.

Figure 2.2, after ref.[46], presents the stress-strain behaviour of concrete subjected to uniaxial compression. Here, f_c' denotes maximum compressive strength of concrete. As indicated in the figure, four stages of progressive failure can be identified on the ascending branch:

Stage 1, when a stress applied is below about 30 percent of f_c', the cracks existing in the transition zone remain almost unchanged. Thus, a nearly linear-elastic response is observed on the stress-strain diagram.

Stage 2, for a stress between 30 to 50 percent of f_c', the bond cracks begin to increase in lengths, widths, and numbers due to stress concentrations at the crack tips, while the mortar cracks remains unchanged. At this stage, the stress-strain curve starts to

deviate appreciably from a nearly straight line as the stress increases.

Stage 3, at 50 to 60 percent of f_c', the mortar cracks begin to propagate in the matrix and may tend to bridge the existing cracks. With further increase in stress up to 75 percent of f_c', the cracks in the transition zone become unstable. At the same time the proliferation and propagation of mortar cracks in the matrix become pronounced. Due to such mechanisms of progressive cracking the stress-strain curve now tends to bend considerably toward the horizontal response.

Stage 4, for a stress above 75 percent of f_c', the largest cracks reach their critical lengths and coalescence becomes active. As the stress applied approaches the maximum strength, the failure state is reached, and thereafter the stress-strain curve begins to descend. Thus, concrete enters an unstable stage, which is commonly referred to as strain softening behaviour.

It may be noted from Fig. 2.2(b) that the propagation of cracks during an active loading not only contributes to the stress-strain nonlinearity as discussed above, but also causes volume expansion near the maximum strength. Such a smooth transition from compaction to dilatancy prior to failure is also observed in certain geological materials, e.g. rocks and dense sand.

As far as the uniaxial behaviour of concrete under tension is concerned, Fig. 2.3 (ref.[1]) shows that the stress-strain curve has a similar shape to that obtained in uniaxial compression test, ref.[47].

However, there are still some differences in behaviour. For example, under uniaxial tension, concrete has a markedly lower strength (e.g. $f_t' \approx 5$ to 10% of f_c'), ref.[46] and appears to be more brittle than its behaviour under compression. Since concrete under uniaxial tension tends to arrest cracks much less frequently than under uniaxial compression, the interval of stable crack propagation is expected to be relatively short. Although the failure in tension is mainly caused by a few bridging cracks rather than by numerous cracks as usually observed in compression tests, the descending branch of stress-strain curve still exists due to reduction in the effective area, ref.[48].

It should be pointed out that the stress-strain behaviour of concrete are influenced by the rate of loading; a higher rate of loading results in an apparently stiffer response and higher strength, ref.[49]. A detailed discussion of such rate-dependent type of behaviour is beyond the scope of the present study, and will not be dealt with here.

2.2.2 Biaxial Behaviour

The investigation of mechanical properties of concrete under biaxial state of stress is being pursued very actively by many researchers at the present time. Considerable experimental data are now available in the literature(refs.[3,50-54]) regarding strength, deformational characteristics, and microcracking behaviour of concrete.

Figures 2.4 to 2.6 show the typical stress-strain curves obtained by Kupfer et al.[50] for concrete under biaxial compression(Fig. 2.4), biaxial tension-compression(Fig. 2.5), and biaxial tension(Fig. 2.6). The biaxial stress interaction curves are presented in Fig. 2.7.

These experimental results, Kupfer et al.[50], clearly indicate that under biaxial compression concrete exhibits an increased strength up to 27 percent higher than the strength under uniaxial compression and an increased degree of ductility near the peak stress(Fig. 2.4). Under biaxial tension-compression(Fig. 2.5), concrete exhibits a noticeably reduced strength and ductility as compared to the case of biaxial compression. For biaxial tension(Fig. 2.6), the strength of concrete is approximately equal to the strength under uniaxial tension. From the biaxial strength envelope of concrete (Fig. 2.7), it is clear that the magnitude of uniaxial compressive strength virtually does not influence the shape of the biaxial stress interaction diagram. Nelissen[54] also observed that the strength envelope is independent of loading path although there is some indication that nonproportional loading may produce a lower strength than the proportional loading for light-weight concrete, ref.[55].

It can also be observed from the tests mentioned above that under biaxial compressive state of stress, concrete shows a volumetric strain behaviour similar to that observed under uniaxial compression as illustrated in Fig. 2.8. The transition from compaction to dilatancy is largely attributed to progressive growth of major cracks in concrete.

It is also noteworthy that concrete strength and ductility is strongly influenced by the magnitude of confining pressure. This pressure-dependent behaviour will become more obvious after the discussion on behaviour of concrete under triaxial state of stress in the next subsection.

2.2.3 Triaxial Behaviour

The available experimental data on triaxial behaviour of concrete is very fragmentary. In the earlier studies on triaxial compressive behaviour of concrete(refs.[56,57]), it was found that the axial strength of concrete increases with increasing confining pressure as shown in Figs. 2.9 and 3.0. This phenomenon was not fully understood until the work by Palaniswamy et al.[4]. From their experimental results, two distinct modes of behaviour were observed for all paste, mortar and concrete specimens depending upon whether the applied pressure is below or above a certain value, $(\sigma_3)_t$, which is referred to as brittle-ductile transition pressure. For an applied pressure below $(\sigma_3)_t$, concrete behaves as a quasi-brittle(plastic-softening) material and the failure mode is cleavage or brittle type, similar to that observed in uniaxial compression. If the applied confining pressure exceeds $(\sigma_3)_t$, concrete behaves as a quasi-ductile(plastic-hardening) material and the failure mode is crushing or ductile type. In the case of increasing confining pressure, a gradual transition from brittle to ductile behaviour is expected. In fact, this gradual

transition behaviour from cleavage to crushing under increasing confining pressure was observed by Cowan[58] and Berg[59].

It is interesting to point out here that concrete exhibits nonlinear stress-strain behaviour even under purely hydrostatic compressive loading(refs.[60,61]) as shown in Fig. 2.11. It should also be noted that under triaxial loading concrete still exhibits the transition from compaction to dilatancy, ref.[62].

In regard to the failure surface(or maximum strength surface) under general triaxial loading conditions, it is reported in ref.[46] that concrete has a fairly consistent (i.e. path independent) failure surface which is a function of the three principal stresses(σ_1 ,σ_2 ,σ_3) as shown schematically in Fig. 2.12(a). For lower confining pressure, the deviatoric sections(or π-planes) of the failure surface are noncircular but convex; for high confining pressure, these deviatoric sections are nearly circular. This is very different from metals in the sense that the failure surface is significantly influenced by the confining pressure as well as by the third stress invariant. From the limited test results reported in the literature, it seems that this surface is independent of loading path, refs.[63,64]. More detailed discussion on the failure surface will be given in the next section.

2.3 Elastoplastic Constitutive Model for Concrete

In the present study, the following stress invariants are used in formulating the constitutive relations for concrete, i.e.

$$I = -\sigma_{ii} \; ; \qquad \bar{\sigma} = \left(\frac{1}{2} s_{ij} s_{ij} \right)^{1/2}$$

$$\theta = \frac{1}{3} \sin^{-1}\left(-\frac{3\sqrt{3}}{2} \frac{J_3}{\bar{\sigma}^3} \right) ; \quad -\frac{\pi}{6} \leq \theta \leq \frac{\pi}{6} \tag{2.1}$$

In the equations above $s_{ij} = \sigma_{ij} - 1/3\delta_{ij}\sigma_{kk}$ denotes the stress deviator and δ_{ij} is the Kronecker delta; and θ represents the angle measure of the third stress invariant $J_3 = 1/3 s_{ij} s_{jk} s_{ki}$. Here, a positive sign is assigned to tensile stress and strain and the usual implied summation convention is adopted.

In what follows, an elastoplastic constitutive model for concrete under monotonic loadings is proposed. This model invokes the concept of a path-independent failure surface, $F(\sigma_{ij})=0$, which is introduced a priori. The progressive failure of the material due to microcracking is described in terms of evolution of a family of yield surfaces, $f(\sigma_{ij},\xi)=0$, where ξ is a suitably defined damage parameter. The instantaneous direction of plastic flow is determined by a non-associated flow rule, which involves existence of a family of plastic potential surfaces defined in a parametric form $\Psi(\sigma_{ij})=const$. The material characteristics are largely affected by

the value of the confining pressure. The formulation allows for a smooth transition from a ductile(stable) to brittle(unstable) response by employing an appropriate form of strain hardening/softening function. In what follows, the major assumptions embodied in the proposed model are outlined together with relevant mathematical details, also see ref.[65].

2.3.1 Failure Surface and Yield Loci

In order to formulate a general failure criterion for concrete under a multiaxial state of stress, a proper definition of failure must be introduced first. The definition of failure in the literature differs between researchers and practical engineers. In some cases failure is defined in terms of a maximum attainable stress. In others failure is defined by the onset of dilatancy or sometimes by a sudden increase in strain rate(in a stress-controlled test). In the present study the failure criterion defines maximum strength of concrete under any possible combination of stresses. It is known that failure modes of concrete, in general, fall into two categories: brittle and ductile, depending on the value of applied confining pressure. In this definition of failure, brittle mode is associated with formation of major cracks at failure(peak stress) and material displays a strain softening response in the post-failure regime, while ductile model is defined by development of many small cracks prior to failure and material undergoes a strain hardening response only.

A number of different failure criteria for concrete have been reported in the literature. These criteria include: one-parameter description such as the Rankine or Griffith criterion of maximum tensile stress failure and the Tresca criterion of shearing stress failure; two-parameter description including the Mohr-Coulomb and Drucker-Prager criteria; three-parameter description referring to the Mohr-Coulomb criterion with a small tension cut-off and others given in refs.[7,66,67]; and four- and five-parameter descriptions with nonlinear relation between the octahedral normal and shear stresses, see refs.[11,68-73]. Some of these criteria have been successfully applied to constitutive description of concrete behaviour, but some seem to be unrealistic. Here, no attempt is made to review or criticize these criteria because detailed information can be found elsewhere[47,74]. Instead, more concern is given to a new formulation of failure criterion as proposed recently in ref.[65].

In the geometric sense, the characteristics of a failure surface in a three-dimensional stress space can be best described by its cross-sectional shape in the deviatoric plane (π-plane) and its meridians in the meridional planes. In the deviatoric plane the shape of the surface varies from a curvilinear triangle for a low confining pressure to a nearly circular shape at a high confining pressure. In the meridional planes a parabolic shape is observed as shown in Fig. 2.12(b) for two extreme meridians corresponding to $\theta=-\pi/6$ and $\theta=\pi/6$. In both the deviatoric and the meridional planes the surface is always smooth and convex.

Based on the experimental evidence as discussed above, the following form of the failure surface is proposed

$$F = a_1\left(\frac{\bar{\sigma}}{g(\theta)f_c'}\right) + a_2\left(\frac{\bar{\sigma}}{g(\theta)f_c'}\right)^2 - \left(a_3 + \frac{I}{f_c'}\right) = 0 \qquad (2.2)$$

where a_1, a_2, and a_3 are dimensionless material constants; f_c' represents the uniaxial compressive strength of concrete.

In the principal stress space, Eq.(2.2) represents an irregular cone with smooth curved meridians and a noncircular convex cross-section in the deviatoric plane(π-plane). The shape of the π-plane sections, defined through the function $g(\theta)$, is strongly influenced by the magnitude of the confining pressure. Thus, $g(\theta)$ should be defined in such a way that for low confining pressures it generates a curvilinear triangle, and a nearly circular shape for high confining pressures. There is a number of formulations of $g(\theta)$ available in the literature. Unfortunately, some of them do not assure convexity whereas those which do, usually involve very complicated functions. This problem will be fully examined in the next chapter. Here, the following simple form is adopted, also see ref.[75].

$$g(\theta) = \frac{(\sqrt{1+a} - \sqrt{1-a})K}{K\sqrt{1+a} - \sqrt{1-a} + (1-K)\sqrt{1-a\sin 3\theta}}, \qquad a \to 1 \qquad (2.3)$$

which satisfies $g(\pi/6)=1$ and $g(-\pi/6)=K$ and guarantees convexity for $K \geq 0.5587$ for $a=0.9999$, and this will be proved in the next chapter. In Eq.(2.3), the parameter K is defined as $K = \bar{\sigma}_t/\bar{\sigma}_c$, where $\bar{\sigma}_t$ and $\bar{\sigma}_c$ represent the maximum deviatoric stress intensity in extension($\theta=-\pi/6$) and compression ($\theta=\pi/6$) domains, respectively(see Fig. 2.12(c)). In the present study K is assumed to be function of I, i.e. $K=K(I)$, and the following simple function describing the variation of K is selected

$$K = 1 - K_0 \exp\left(-K_1 \left(a_3 + \frac{I}{f_c'} \right) \right) \tag{2.4}$$

where K_0 and K_1 are material constants. It should be noted that according to Eqs.(2.3) and (2.4) the shape of the π-plane section does change from a curvilinear triangle for low confining pressures to a nearly circular at high pressures, e.g. in Eq.(2.4) as $I \to \infty$ then $K \to 1$.

For a further discussion, Eq.(2.2) can be written, for convenience, in the following parametric form (via back-substitution of the positive root of Eq.(2.2))

$$F = \bar{\sigma} - g(\theta)\bar{\sigma}_c = 0 \tag{2.5}$$

where

$$\bar{\sigma}_c = \frac{-a_1 + \sqrt{a_1^2 + 4a_2(a_3 + \dfrac{I}{f_c'})}}{2a_2} f_c' \quad . \tag{2.6}$$

For the sake of simplicity, a similar functional form can now be employed to define the family of yield loci, namely

$$f = \bar{\sigma} - \beta(\xi) g(\theta) \bar{\sigma}_c = 0 \tag{2.7}$$

where $\beta(\xi)$ represents an appropriate hardening/softening function and the parameter ξ is defined by

$$\xi = \int d\xi \quad \text{and} \quad d\xi = \frac{d\bar{\varepsilon}^p}{\bar{\Phi}} \quad . \tag{2.8}$$

In Eq.(2.8), $d\varepsilon^p$ is a measure of plastic distortions, i.e.

$$d\varepsilon^p = (de^p{}_{ij} de^p{}_{ij})^{1/2}; \qquad de^p{}_{ij} = d\varepsilon^p{}_{ij} - \frac{1}{3}\delta_{ij} d\varepsilon^p{}_{kk} \tag{2.9}$$

whereas $\bar{\Phi}$=const. is a factor defined through a parametric equation

$$\Phi(I,\theta) = [g(\theta)(a_3 + I/f_c')]^2 = \bar{\Phi} \quad .$$

Employment of parameter $\bar{\Phi}$ in Eq.(2.9) is motivated by the experimental evidence. The proposed functional form, viz. Eq.(2.10), allows one to simulate typical trends in the variation of material characteristics with both I and θ, to be discussed later in this chapter.

It should be noted that according to Eq.(2.7) the size of the yield locus undergoes gradual expansion in the course of deformation. When $\beta \to 1$, the yield locus asymptotically approaches the failure surface. On the other hand, for an initial active loading process $\beta=0$ is assumed which means that the size of the initial yield locus is reduced to zero. This assumption is justified from the experimental observations since many test data indicate that a virgin concrete element exhibits irreversible deformation almost immediately after application of an external load. Therefore, in the proposed approach, the elastic domain is in fact reduced to an infinitesimal size. It should be noted that the concept of diminishing elastic domain has already been adopted by other investigators[11,76].

2.3.2 Plastic Potential Surfaces

According to theory of plasticity, refs.[77-79], when the state of stress reaches the yield locus, $f=0$, the material undergoes plastic deformations. In this theory the direction of plastic strain vector is

defined through a flow rule by assuming the existence of a plastic potential function(or surface), to which the incremental strain vector are orthogonal. Then the increments of the plastic strain can be expressed as

$$d\varepsilon^{p}_{ij} = d\lambda \frac{\partial \Psi}{\partial \sigma_{ij}} \tag{2.11}$$

which is referred to as the flow rule. In Eq.(2.11), $\Psi(\sigma_{ij})$=constant is the plastic potential surface, and $d\lambda$ is a positive factor of proportionality, which is nonzero only when plastic deformations take place.

As discussed previously, in the compression domain the concrete always exhibits a smooth transition from compaction to dilatancy prior to failure. This dilatancy is also observed in certain geological materials(e.g. dense sand) and can be adequately modelled by assuming a non-associated flow rule and defining an appropriate form of plastic potential surface, ref.[80]. After recognizing this analogy, the plastic potential function adopted in this study is similar in form to that suggested in ref.[80],i.e.

$$\Psi = \bar{\sigma} + \eta_c g(\theta) \bar{I} \ln(\bar{I}/\bar{I}_0) = 0 \tag{2.12}$$

where $\bar{I} = a_0 f_c' + I$ and a_0 is a constant which defines the location of

the apex of the plastic potential surface in the tensile domain. Moreover, parameter η_c represents the value of $\eta=\bar{\sigma}/(g(\theta)\bar{I})$ at which the transition from compaction to dilatancy occurs, i.e. at $\eta=\eta_c$, $d\varepsilon^p_{ij}=0$. It is assumed that such transition takes place along the locus defined by

$$\bar{f} = \bar{\sigma} - \alpha g(\theta)\bar{\sigma}_c = 0 \qquad (2.13)$$

in which α is a material constant.

Figure 2.13 shows the meridional section of the family of plastic potential surfaces. In order to satisfy the condition of irreversibility following from the second law of thermodynamics, i.e. $\sigma_{ij}d\varepsilon^p_{ij}\geq 0$, all the plastic potential surfaces are assumed to convex with respect to the origin of the stress space. To comply with the convexity requirement an appropriate evolution law for the family of surfaces $\Psi=0$ defined by Eq.(2.12) must be provided. Denote by η_0 the value of η_c at $I=0$ and $a_0=a_3$

$$\eta_0 = \frac{\alpha(-a_1 + \sqrt{a_1^2 + 4a_2a_3})}{2a_2a_3} \qquad (2.14)$$

and let the corresponding plastic potential surface, Eq.(2.12), be $\Psi_0=0$, see Fig. 2.13. It is assumed that for $\eta_c<\eta_0$ all the subsequent plastic potential surfaces are obtained by an isotropic

expansion of $\Psi_0=0$ under $a_0=a_3=const$. If the stress point falls inside the domain enclosed by $\Psi_0=0$, the family of surfaces $\Psi=0$ satisfies the constrains $\eta_c=\eta_0$ and $a_0<a_3$. These constraints imply that inside $\Psi_0=0$ all the subsequent surfaces are reduced in size and the apex gradually migrates towards the origin, $0<a_0<a_3$. Mathematical details concerned with identification of the current plastic potential surface are provided in Appendix A.

It should be noted that in the strain softening range, the deformation process is again described in terms of a non-associated flow rule with the plastic potential specified by Eq.(2.12). The zero dilatancy locus, as defined in the stable regime by Eq.(2.13), is assumed to undergo gradual contraction with decreasing value of β

$$\bar{f} = \bar{\sigma} - \beta\alpha g(\theta)\bar{\sigma}_c = 0 \ . \tag{2.15}$$

The above functional form enables one to model the progressive dilation of concrete during the unstable phase as reported by van Mier[81].

2.3.3 Generalized Hardening/Softening Function

Mechanical response of concrete is strongly influenced by the magnitude of confining pressure. At relatively high pressures, a pattern of numerous microcracks develops and material characteristics display a stable nature with a ductile failure mechanism. As the

confining pressure decreases, a gradual transition from ductile to brittle behaviour takes place. In the brittle regime, distinct macrocracks form leading to an unstable material response.

In the present discussion the transition from a stable (ductile) to unstable(brittle) response is modelled by an appropriate strain hardening/softening function. The form of this function is selected to reflect a gradual change in material characteristics from strain hardening (for high confining pressures) to strain softening with the rate progressively increasing with the decreasing pressure. The following general form of the function $\beta(\xi)$ is assumed

$$\beta = \frac{\xi}{A + B\xi}[1 - \bar{\phi}_r(1 - \exp(-C\langle \xi - \xi_f \rangle^Y))] \tag{2.16}$$

where

$$C = \bar{\phi}_s H[\langle((\frac{I}{f_c'})_T - (\frac{I}{f_c'})_f)/(a_3 + (\frac{I}{f_c'})_f)\rangle]^{\mu} \tag{2.17}$$

and the symbol $\langle\ \rangle$ is defined according to

$$\langle x \rangle = \begin{cases} 0 & \text{if } x \leq 0 \\ x & \text{if } x > 0 \ . \end{cases} \tag{2.18}$$

In Eq.(2.16) A and B are material constants, ξ_f represents the value of ξ corresponding to the value of $\beta=\beta_f$, and C is a variable.

defined by Eq.(2.17), which controls the rate of strain softening in the post-failure range. In Eq.(2.17) $(I/f_c')_f$ is evaluated at $\beta=\beta_f$ and $(I/f_c')_T$ denotes a normalized value of confining pressure at which a transition from ductile to brittle behaviour takes place. Moreover, γ, μ and H represent material constants and the parameter $\bar{\phi}_r$ defines the residual strength of the material. Finally, parameter $\bar{\phi}_s$ is referred to as a 'size parameter' and its significance is discussed in detail in the forthcoming subsection.

According to Eq.(2.16), the onset of strain softening takes place in the brittle regime for $(I/f_c')_f<(I/f_c')_T$ at $\beta=\beta_f$, corresponding to $\xi=\xi_f$. The value of β_f can be chosen a priori. In such a case, the onset of unstable response is described in terms of a path-independent criterion which implies the existence of a strain-softening surface, $F_b=f(\sigma_{ij},\beta_f)=0$, in the brittle regime. In general, however, the value of β_f should be determined more rigorously using an appropriate strain localization criterion derived from considerations of stability of the constitutive relations (bifurcation problem). This approach will be explored in Chapter 5.

It can be shown that, according to Eqs.(2.16) and (2.17), for $\gamma>1.0$, the following conditions are satisfied

$$(d\beta/d\xi)_{\xi=\xi_f^-} = (d\beta/d\xi)_{\xi=\xi_f^+}; \qquad \lim_{\xi\to\infty} \beta \equiv 1 - \bar{\phi}_r = \beta_r \,. \tag{2.19}$$

The first condition in Eq.(2.19) is to maintain continuity at the transition point (from stable to unstable). It is also evident that in the ductile regime where C=0, Eq.(2.16) reduces to a hyperbolic form

$$\beta = \frac{\xi}{A + B\xi} \tag{2.20}$$

implying a stable response. On the other hand, in the brittle regime, $I \to -a_3 f_c'$ leads to $C \to \infty$ and then a perfect brittle response is obtained. Hence, the generalized strain hardening/softening function defined by Eqs.(2.16) and (2.17) satisfies all mathematical requirements of a continuous function which represents variation of material characteristics from ductile to brittle behaviour.

It should be noted that in the brittle regime, non-uniform deformation mode consists of either sliding along asperities or, in certain circumstances, an abrupt fracture, i.e. opening of tensile microcracks. The former mechanism is completely described by Eqs.(2.16) and (2.17), whereas the latter one involves an instantaneous reduction of all stress components to zero. The fracture domain(OAB) is shown schematically in Fig. 2.12(b). If the stress path, after reaching the failure surface, penetrates into this domain, an abrupt fracture takes place. If, on the other hand, the residual strength envelope (as implicitly defined by parameter $\bar{\phi}_r$) is reached first, an unlimited plastic flow commences. At this time, the extent of the fracture domain can not be defined precisely due to lack of adequate experimental data.

One can only speculate that this domain is confined to a vicinity of the tensile branch of hydrostatic axis.

2.3.4 Introduction of 'Size Effect' into Constitutive Framework

It has been recognized by many researchers, refs.[82,83], that strain softening phenomenon is associated with a transition from a uniform into a certain non-uniform deformation mode (e.g. strain localization). Thus, the actual rate of strain softening can not be regarded, in a strict sense, as a material property. Experimental observations in refs.[41,84,85] seem to suggest that strain softening in plain concrete is essentially due to non-homogeneous deformation resulting from macroscopic cracking and material sliding. As a result, the observed rate of strain softening is affected by various factors, e.g. the shape and size of specimen, testing machine set-up and its stiffness, and specimen end conditions(lubricated or nonlubricated). Different combinations of these factors may result in different mechanisms associated with the strain softening phenomenon. A review and discussion on this subject can be found in refs.[82,83].

The approach presented here is based on the concept of 'equivalent continuum' similar to that introduced in ref.[86]. The strain softening is considered as a local phenomenon occurring in a 'smeared' sense at a material point. As mentioned above, the unstable

strain softening characteristics display sensitivity to the size of the specimen. Such 'size effect' can be introduced into the constitutive framework in a purely phenomenological manner without referring to the actual post bifurcation mechanism. Here, the 'size effect' has been incorporated through parameter $\bar{\phi}_s$ in Eq.(2.17). This parameter $\bar{\phi}_s$ is supposed to relate the rate of strain softening to the geometrical aspects. Instead of considering the details of the sample geometry, it is assumed, for simplicity, that its total volume constitutes a characteristic parameter which affects the softening response, i.e.

$$\bar{\phi}_s = \phi_s(I,V) = const. \tag{2.21}$$

where V represents the volume of the sample. More specifically, parameter $\bar{\phi}_s$ can be assumed in the following parametric form

$$\bar{\phi}_s = 1 + \alpha_1(I)\alpha_2(V/V_s)=const. \tag{2.22}$$

where V_s denotes a representative(or standard) volume for which the strain softening characteristics are assumed to be known. Function α_2 should be selected in such a manner as to reflect a progressive increase in the rate of strain softening with increasing volume ratio V/V_s. Moreover, for $V=V_s$ there must be $\alpha_2=0$ which implies $\bar{\phi}_s=1$. Assume, for instance, the following simple representation

$$\alpha_2(V/V_s) = (V/V_s)^{\lambda} - 1 \tag{2.23}$$

which satisfies the above constraints. In Eq.(2.23) λ represents a constant.

Degree of sensitivity of strain softening rate to geometrical aspects can vary with the confining pressure as well. This is accounted for by introducing function $\alpha_1(I)$ in Eq.(2.22). The range of variation of this function should be in the interval $0 \leq \alpha_1 \leq 1$. $\alpha_1=0$ implies that the strain softening characteristics remain unaffected by the volume of the sample, whereas $\alpha_1=1$ expresses the maximum sensitivity. As a result, the following trigonometric function is introduced to represent $\alpha_1(I)$, i.e.

$$\alpha_1(I) = \sin[(a_3 + (I/f_c')_f)/(a_3 + (I/f_c')_T)]\Pi \ . \qquad (2.24)$$

Here, if $(I/f_c')_f \to -a_3$ or $(I/f_c')_f \to (I/f_c')_T$ then $\alpha_1 \to 0$, and $\max(\alpha_1)=1$. Fig. 2.14 shows the strain softening characteristics for different V/V_s ratios as predicted by the above specified functions.

Incorporation of parameter $\bar{\phi}_s$ in Eq.(2.17), requires further investigation concerning the static admissibility of the $\bar{\sigma}$ vs. $\bar{\varepsilon}$ characteristics. An additional constraint on the value of the softening parameter H has been derived and can be found in Appendix B.

It should be noted that the introduction of the 'size effect' into the proposed constitutive framework is not only motivated by the

experimental evidence, but more importantly by the objective to reduce numerical instabilities caused by improper modelling of the strain softening response. The latter aspect will be addressed in Chapter 6 in conjunction with the finite element analysis of concrete structures using the proposed constitutive theory.

2.3.5 Formulation of Constitutive Equations

After introduction of the constitutive framework and definitions of parameters, the corresponding incremental constitutive equations can now be derived. Assuming additivity of the elastic and plastic strain rates, the generalized Hooke's law takes the form

$$d\sigma_{ij} = D^{e}_{ijkl}(d\varepsilon_{kl} - d\varepsilon^{p}_{k}) \qquad (2.25)$$

where D^{e}_{ijkl} represents the elasticity matrix. During an active loading process, the consistency condition, $df=0$, has to be satisfied, i.e.

$$\frac{\partial f}{\partial \sigma_{ij}} d\sigma_{ij} + \frac{\partial f}{\partial \beta}\frac{d\beta}{\partial \xi} d\xi = 0 \qquad (2.26)$$

in which $f(\sigma_{ij},\xi)=0$ is defined according to Eq.(2.7). Introducing the non-associated flow rule, Eq.(2.11), into Eq.(2.8) yields

$$d\xi = d\lambda \left(dev \frac{\partial \Psi}{\partial \sigma_{ij}} \; dev \frac{\partial \Psi}{\partial \sigma_{ij}} \right)^{1/2} / \bar{\Phi} \qquad (2.27)$$

in which $dev(\partial\Psi/\partial\sigma_{ij})$ represents the deviatoric part of $\partial\Psi/\partial\sigma_{ij}$, with $\Psi(\sigma_{ij})$=constant given by Eq.(2.12). Then substituting Eq.(2.25) into Eq.(2.26) and utilizing Eq.(2.27) the following is obtained,

$$d\lambda = \left(\frac{\partial f}{\partial \sigma_{ij}} D^{e}_{ijkl} d\varepsilon_{kl} \right) / (H_e + H_p) \qquad (2.28)$$

where

$$H_p = - \frac{\partial f}{\partial \beta} \frac{d\beta}{d\xi} \frac{\left(dev \frac{\partial \Psi}{\partial \sigma_{ij}} \; dev \frac{\partial \Psi}{\partial \sigma_{ij}} \right)^{1/2}}{\bar{\Phi}} \; ; \quad H_e = \frac{\partial f}{\partial \sigma_{pq}} D^{e}_{pqrs} \frac{\partial \Psi}{\partial \sigma_{rs}} . \qquad (2.29)$$

and H_p represents the plastic hardening/softening modulus.

The parameter $d\lambda$ in Eq.(2.27) can also be defined in terms of stress increments $d\sigma_{ij}$. Introducing Eq.(2.27) directly into Eq.(2.26) yields

$$d\lambda = \left(\frac{\partial f}{\partial \sigma_{ij}} d\sigma_{ij} \right) / H_p . \qquad (2.30)$$

Finally, substitution of Eq.(2.28) in Eq.(2.26) leads to the constitutive equations in a conventional form

$$d\sigma_{ij} = (D^e_{ijkl} - \frac{D^e_{ijpq} \frac{\partial \Psi}{\partial \sigma_{pq}} \frac{\partial f}{\partial \sigma_{mn}} D^e_{mnkl}}{H_e + H_p}) \, d\varepsilon_{kl} \, . \tag{2.31}$$

Equation (2.31) describes an active loading process in the incremental form, during which the irreversible deformations are generated. In the hardening regime, where $H_p>0$, such loading histories are constrained to the stress path satisfying the following conditions, i.e.

$$f = 0 \quad \text{and} \quad \frac{\partial f}{\partial \sigma_{ij}} d\sigma_{ij} > 0 \, . \tag{2.32}$$

It should be noted that the inequality in Eq.(2.32) implies $d\lambda>0$ in Eq.(2.30). This ensures, in view of convexity of the plastic potential given by Eq.(2.12), that the energy dissipated during plastic flow is always positive.

In the softening regime, where $H_p<0$, the postulate of irreversibility again requires the positiveness of $d\lambda$. In order to distinguish between elastoplastic loading and elastic unloading, the definition of $d\lambda$ in Eq.(2.28) can be employed and gives

$$f = 0 \quad \text{and} \quad \frac{\partial f}{\partial \sigma_{ij}} D^e_{ijkl} d\varepsilon_{kl} > 0 \tag{2.33}$$

as the criterion for an active loading process. According to this criterion, plastic deformations will occur whenever the stress increment obtained from the elastic solution, $d\sigma'_{ij}=D^{e}_{ijkl}d\varepsilon_{kl}$, is directed outside of the yield surface. It should be noted that the criterion in Eq.(2.33) is only valid for cases when $H_e+H_p>0$, i.e. there exists a locally unique response in stress rate for any specified strain rate. For the cases when $H_e+H_p<0$, the deformation process ceases to be locally controlled. In order to overcome such situations, the specified value of the softening parameters must satisfy the constraint obtained from the consideration of static admissibility (see Appendix B).

All the mathematical details concerning with the determination of constitutive Equation (2.31) are provided in Appendix C.

2.4 Identification of Constitutive Parameters

After establishing the constitutive relationship, next step is to properly identify all material parameters involved according to the experimental information available. In this section, the procedure for calibrating the material parameters which are required by the proposed model is discussed together with the relevant results as obtained by using the available test data.

In general, the proposed model involves the following material parameters:

- parameters a_1, a_2, a_3, K_0 and K_1, defining the failure envelope, Eq.(2.2);
- parameters A and B, involved in strain hardening function, Eq.(2.20);
- parameters H, γ, μ, associated with strain softening response; as well as transition pressure $(I/f_c')_T$, and parameters $\bar{\phi}_r, \bar{\phi}_s$, Eqs.(2.16) and (2.17);
- dilatancy parameter α, Eq.(2.13).

In addition, the elastic properties should also be specified, i.e. Young's modulus E and Poisson's ratio υ.

Most of the above listed parameters can be determined a priori based on extensive experimental data available in the literature. Thus, the effective number of parameters required to identify the model can be substantially reduced. The details concerning the identification procedure are summarized below.

(i) Parameters Defining the Failure Envelope

The parameters a_1, a_2, a_3, K_0 and K_1 are related to the form of the failure surface. In order to identify these parameters two steps were followed. First, along the compressive meridian ($\theta=\pi/6$), Eq.(2.2) was fitted to the data provided in refs.[4,87-90] by the least square approach. It was assumed that $a_3 = 0.3$, which corresponds to f_t'

$= 0.1f_c'$, with f_t' representing the uniaxial tensile strength of concrete. Subsequently, the form of the extension branch ($\theta=-\pi/6$) was determined. In this case, two failure states were chosen to be satisfied exactly. Namely, uniaxial tension state $f_t' = 0.1f_c'$ and a biaxial compression state $f_{bc} = -1.16f_c'$, see ref.[50]. Thus, throughout the identification process, f_c' (i.e. uniaxial compressive strength) was assumed as the only independent parameter.

The procedure described above resulted in the following values for the parameters

$$a_1=1.9253,\ a_2=0.5653,\ a_3=0.3,\ K_0=0.43416,\ K_1=0.07439\ . \tag{2.34}$$

Figure 2.15 presents meridional sections of the failure surface in both compression and extension domains. The vertical and horizontal axes are both normalized with respect to f_c', and the proposed analytical form is compared with the experimental data provided in refs.[4,87-90].

When selecting the material constants according to Eq.(2.34), the only information required to identify the form of the failure surface is the value of f_c'. In case when the results of an uniaxial tension test are also available, an exact value of f_t' can be used instead of an average approximation $f_t'=0.1f_c'$. Substituting the conditions of uniaxial tension ($\sigma_1=f_t'$, $\sigma_2=\sigma_3=0$) and biaxial compression ($\sigma_3=0$, $\sigma_1=\sigma_2=f_{bc}$) into Eqs.(2.4) and (2.5) leads to the following modifications of parameters a_3, K_0 and K_1

$$a_3 = 3\, f_t'/f_c'$$

$$K_1 = \ln\left(\frac{1 - K_t}{1 - K_{bc}}\right) / \left((f_t'/f_c') - 2(f_{bc}/f_c')\right)$$

$$K_0 = (1 - K_t)\exp(2K_1(f_t'/f_c')) \qquad (2.35)$$

where K_t and K_{bc} represent the value of K corresponding to uniaxial tension and biaxial compression, respectively,

$$K_t = \frac{2\sqrt{3}}{3} \frac{a_2 f_t'/f_c'}{-a_1 + \sqrt{a_1^2 + 8a_2 f_t'/f_c'}}$$

$$K_{bc} = -\frac{2\sqrt{3}}{3} \frac{a_2 f_{bc}/f_c'}{-a_1 + \sqrt{a_1^2 + 4a_2(3f_t'/f_c' - 2f_t'/f_c')}} \qquad (2.36)$$

and $f_{bc} = -1.16 f_c'$ may be assumed according to ref.[50].

(ii) Hardening Function Parameters

The expression defining the hardening function, Eq.(2.20), contains two material constants A and B. Both parameters can be identified by fitting Eq.(2.20) to the test data plotted in ($\bar{\sigma}/\bar{\sigma}_f$, $\bar{\varepsilon}^p$) plane, where $\bar{\sigma}_f = g(\theta)\bar{\sigma}_c$. Using the data from a series of I=constant tests provided in ref.[91], the following values were arrived through trial and error procedure.

$$A = 0.000085 \quad \text{and} \quad B = 0.95 \; . \qquad (2.37)$$

The results of the numerical simulations showing the variations of β vs. $\bar{\varepsilon}^p$ characteristics in both compression and extension are presented in Figs. 2.16(a) and 2.16(b), respectively.

In the subsequent section, predictions of numerous experimental test for different types of concrete (f_c' ranging from 15.3 to 62.1 N/mm^2) are provided. It can be seen from the results that the values of parameters A and B as defined by Eq.(2.37) are not affected by the actual uniaxial strength of concrete. Thus, they can be adopted a priori.

(iii) Dilatancy Parameter

This parameter defines the locus along which the transition from compaction to dilatancy takes place, Eq.(2.13). Experimental evidence reported in refs.[50,91] indicates that in various types of concrete the maximum volumetric strain is reached at approximately 95 percent of the failure stress. Consequently, α=0.95 may be assumed in Eq.(2.13).

(iv) Strain Softening Parameters

At the present time, the parameters H, μ, γ, $(I/f_c')_T$ and $\bar{\phi}_r$, $\bar{\phi}_s$ in Eqs.(2.16) and (2.17) can not be determined precisely due to lack of adequate experimental data. The existing experimental evidence in refs.[4,92], however, supports the proposed conceptual

framework, i.e. there is a brittle-ductile transition value of confining pressure $(I/f_c')_T$ which corresponds to initiation of the strain softening response.

In this study, value of $\gamma=2$ has been assumed which satisfies requirements imposed by Eq.(2.19). Then, the rate of strain softening is controlled by parameters H and μ. Both constants can be determined from, for example, uniaxial compression test by matching(trial and error process) the actual strain softening characteristics. The parameter $\bar{\phi}_r$, Eqs.(2.16) and (2.19), defines implicitly the form of the residual strength envelope. It is recognized that $\bar{\phi}_r$ may depend on the confining pressure viz. a parametric equation $\bar{\phi}_r=\phi_r(I)=$const. It seems, however, that a sufficient accuracy in numerical predictions may be attained by assuming $\bar{\phi}_r=$constant, which implies that the residual strength locus has a similar analytical form to that of the yield surface. Experimental investigations reported in refs.[93,94] indicate that

$$\beta_r = \lim_{\xi\to\infty} \beta = 0.2 \text{ to } 0.3 \qquad (2.38)$$

for both uniaxial tension and compression tests. Consequently, according to Eq.(2.19), $\bar{\phi}_r=0.7$ to 0.8 can be assumed in Eq.(2.16).

Figure 2.17 shows the variation of material characteristics with the confining pressure as predicted by the proposed model. For the

strain softening branch, some arbitrary values of H=1000 and u=6 (together with $\beta_{f=0.95}$) were selected with the objective to demonstrate the basic trends in material response. The simulations were completed assuming $\bar{\phi}_s=1$ in Eq.(2.17). The characteristic obtained is, in qualitative sense, quite satisfactory and reflects a smooth brittle-ductile transition as the confining pressure increases. The influence of parameter $\bar{\phi}_s$ has been discussed in section 2.3.4, which will not be repeated here.

2.5 Numerical Verification

In this section the performance of the proposed model is verified via comparison with the experimental results for a number of loading paths imposed on different types of concrete (f_c' ranging from 15.3 to 62.1 N/mm^2). The loading histories considered are indicated in Fig. 2.18 and include:

Path 1: initially applied hydrostatic compression followed by loading along the compressive meridian($\theta=\pi/6$) under $d\bar{\sigma}>0$ with I=const.

Path 2: initially applied hydrostatic compression followed by loading along the extension meridian($\theta=-\pi/6$) under $d\bar{\sigma}>0$ with I=const.

Path 3: initially applied hydrostatic compression followed by uniaxial compression(under $\sigma_1=\sigma_3$=const.).

Path 4: proportional loading histories including uniaxial

tension, uniaxial compression, biaxial tension and biaxial compression.

The results of numerical simulations are presented in Figs. 2.19 to 2.24. The predictions in Figs. 2.19 to 2.23 are restricted to the strain-hardening regime due to lack of sufficient experimental data in the strain-softening range. Figures 2.19 and 2.20 present the simulations for stress paths 1 and 2, respectively. Some of these results have already been referred to in section 2.4 for the purpose of identification of material parameters. Figs. 2.19(a) and 2.20(a) show the normalized deviatoric characteristics (normalized deviatoric stress vs. deviatoric strain), whereas Figs. 2.19(b) and 2.20(b) present the corresponding volume change (normalized deviatoric stress vs. volumetric strain). In these figures, numerical predictions are compared with the experimental data provided in ref.[91]. The predictions plotted in Fig. 2.21 are corresponding to path 3 and the behaviour of two different types of concrete is simulated (f_c' =15.3 N/mm^2 and f_c' =62.1 N/mm^2) under different initial confining pressures. A complete stress-strain history is provided and the results are compared with the test data quoted from ref.[91]. Figures 2.22 and 2.23 are concerned with uniaxial and biaxial loading programs starting at zero confining pressures(path 4). Figure 2.22 shows the material characteristics as predicted in compression tests, whereas Fig. 2.23 refers to tension tests. Experimental data from ref.[50] is used for comparison. Finally, Fig. 2.24 presents the simulation of another uniaxial compression test(at I=0 initially) for which the experimental

data is available as reported in ref.[95]. In this case, a complete deformation history is traced including the unstable branch. Prior to failure, concrete undergoes compaction with progressively decreasing rate. During the strain softening phase, a significant dilation is predicted which is in accordance with the existing experimental evidence[81].

In general, for the cases presented, the agreement between the numerical simulations and the experimental data is quite good. For high confining pressures the model tends to underpredict the volumetric strains, Fig. 2.20(b). To improve the performance in this respect the form of plastic potential would have to be altered accordingly. The observed discrepancy, however, is not very significant to justify further complications in the formulation.

In concluding this Chapter, a relatively simple rate-independent plasticity model has been presented for predicting the behaviour of concrete under general three-dimensional state of stress. The model captures the most important trends of concrete behaviour under static loading, e.g. compaction-dilatancy transition, sensitivity of material characteristics to applied confining pressure, the phenomenon of a continuous brittle-ductile transition. In addition to elastic properties, only one material constants f_c' is required (or two constants f_c' and f_t' if the latter information is available) to completely define the material response in a hardening regime. An important feature of the model is the fact that both brittle and

ductile behaviour are described within the same phenomenological framework. This is certainly advantageous in the context of future numerical implementations.

It should be noted that the model does not predict plastic deformation for a hydrostatic loading path which is assumed to be a neutral one. This limitation is recognized. However, it is believed that such a path is unlikely to arise in the context of a boundary value problem.

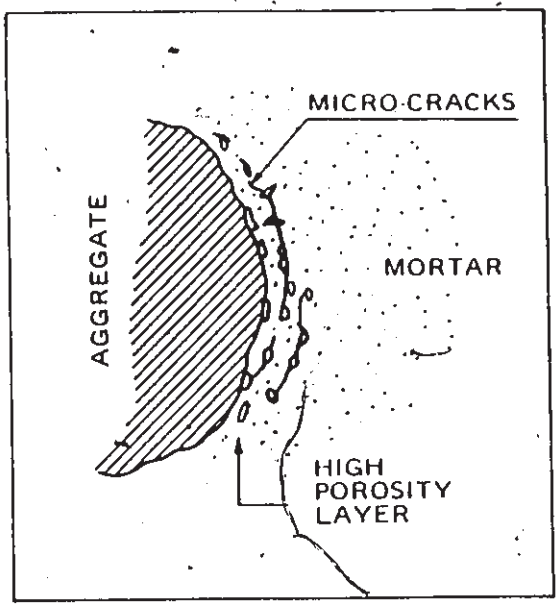

Fig. 2.1 Defects in the Transition Zone between Aggregate and Mortar.

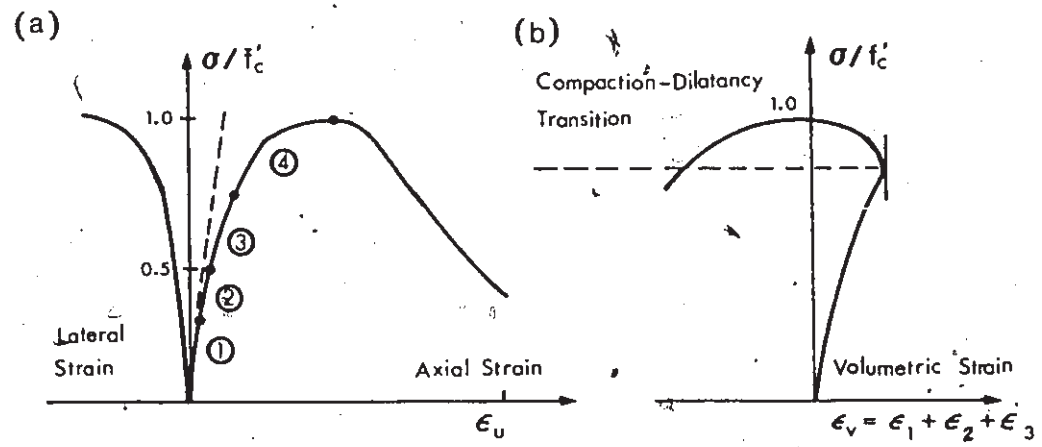

Fig. 2.2 Typical Plots of Compressive Stress Versus (a) Axial and Lateral Strains, and (b) Volumetric Strain(ref.[46]).

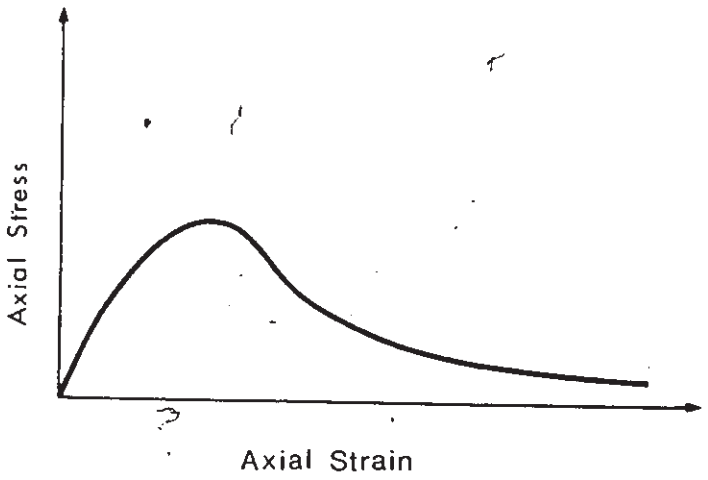

Fig. 2.3 Concrete Stress-Strain Curve under Uniaxial Tension (ref.[47]).

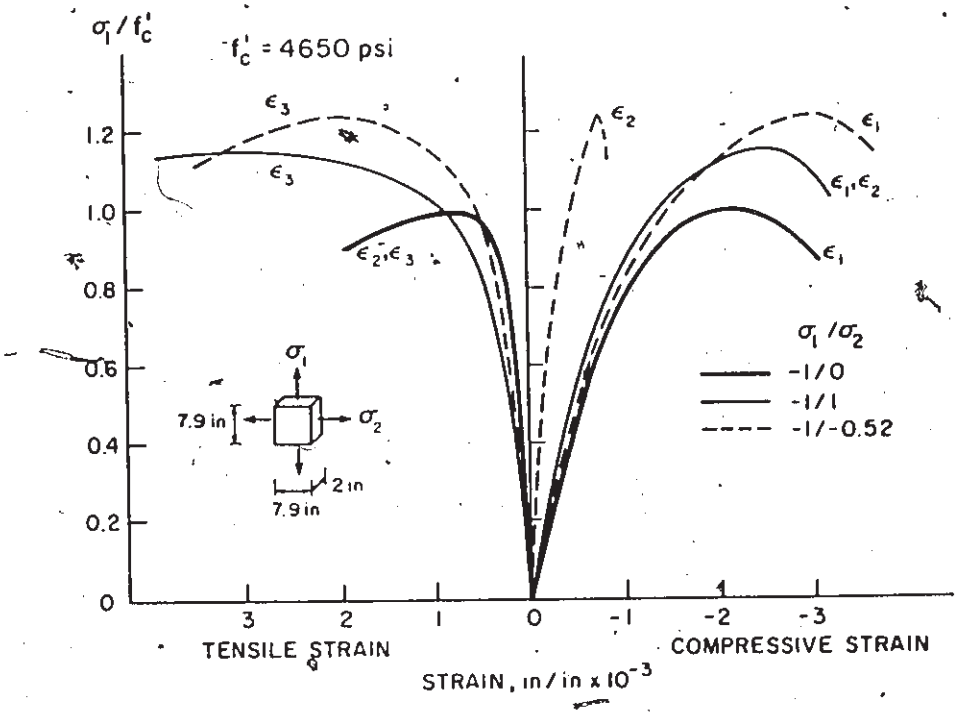

Fig. 2.4 Concrete Stress-Strain Curves under Biaxial Compression (ref.[50]).

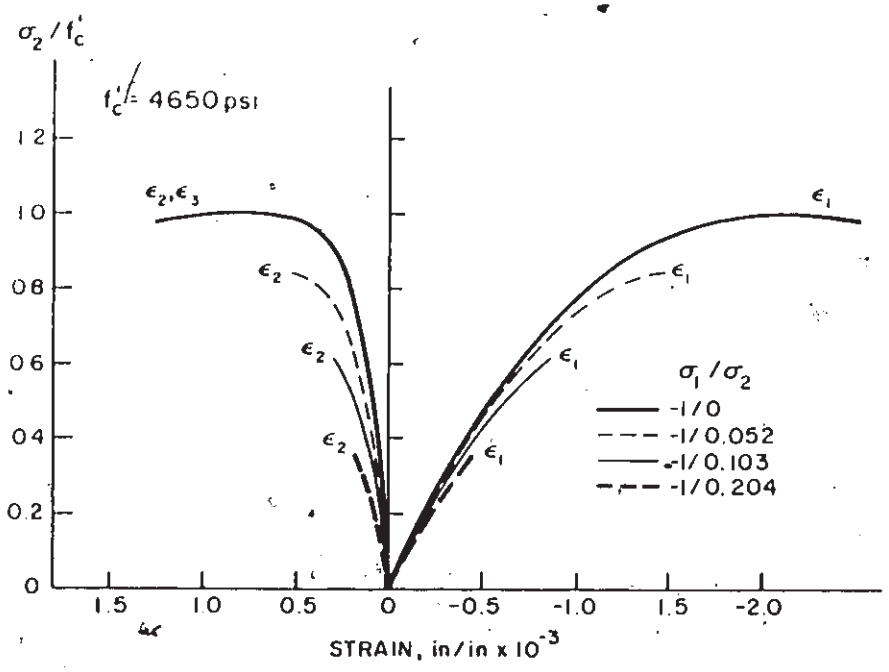

Fig. 2.5 Concrete Stress-Strain Curves under Combined tension and Compression(ref.[50]).

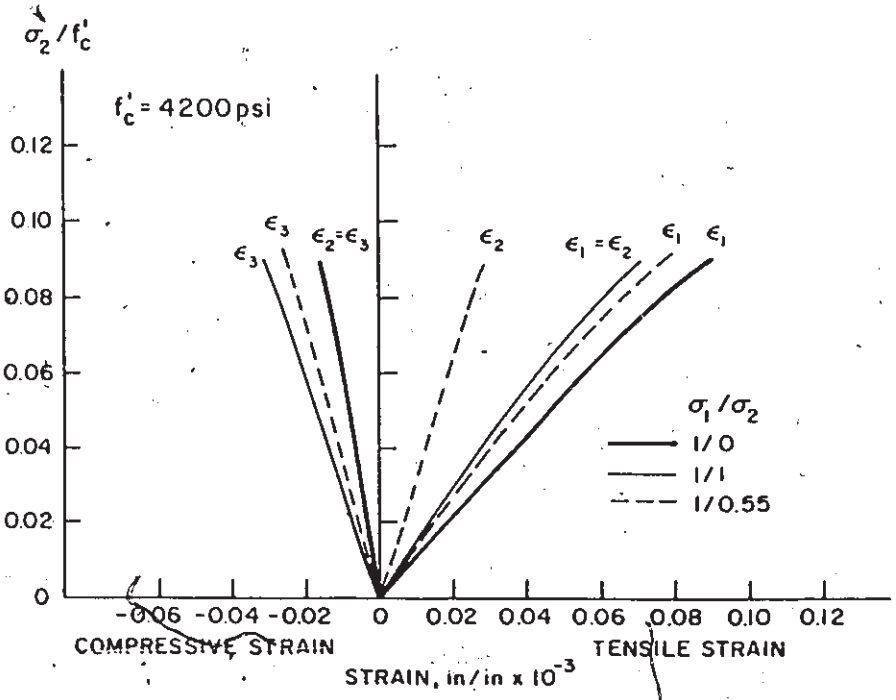

Fig. 2.6 Concrete Stress-Strain Curves under Biaxial Tension (ref.[50]).

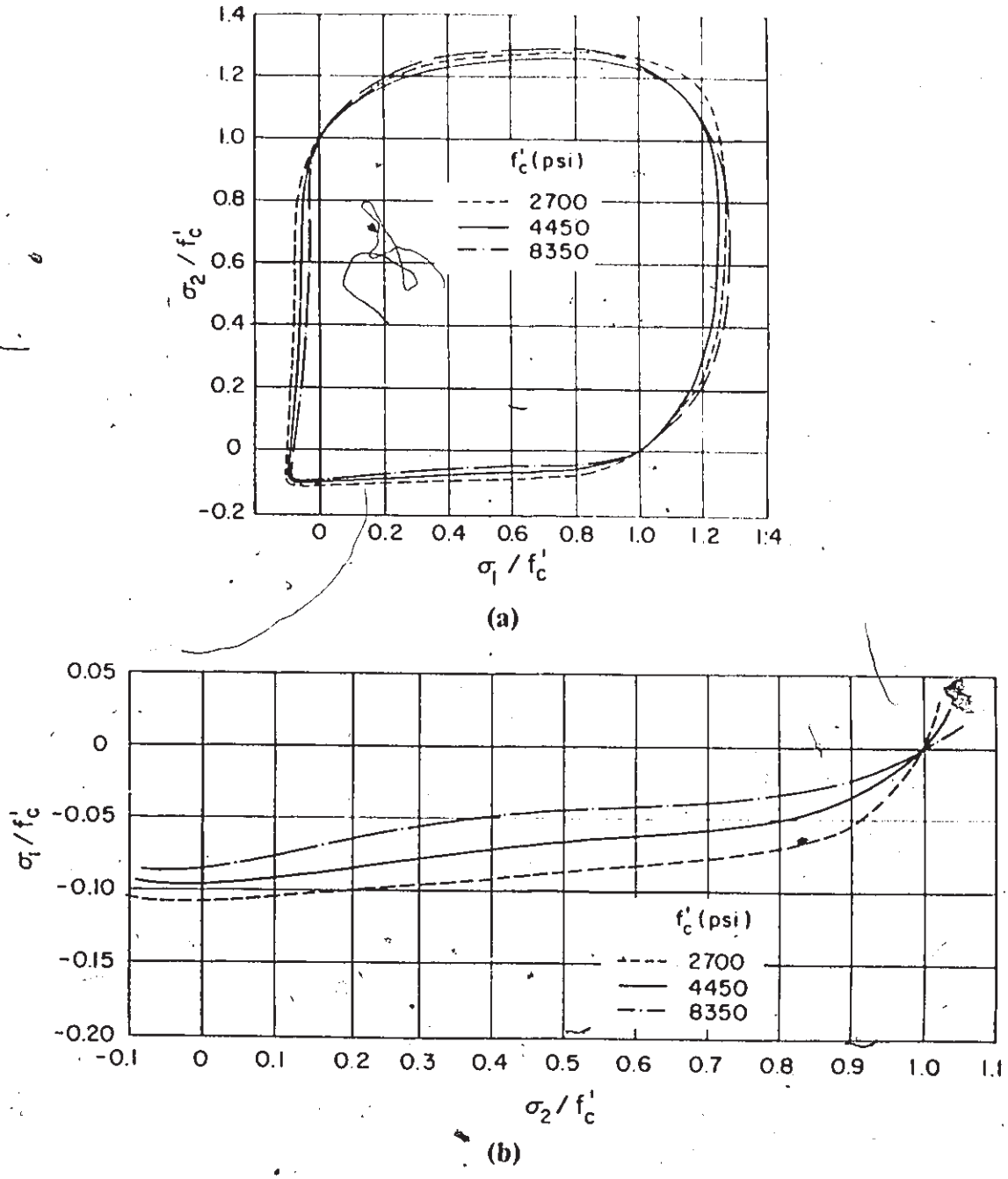

Fig. 2.7 Biaxial Stress Interaction Curves: (a) Strength Envelop; (b) Strength under Combined Tension and Compression (ref.[50]).

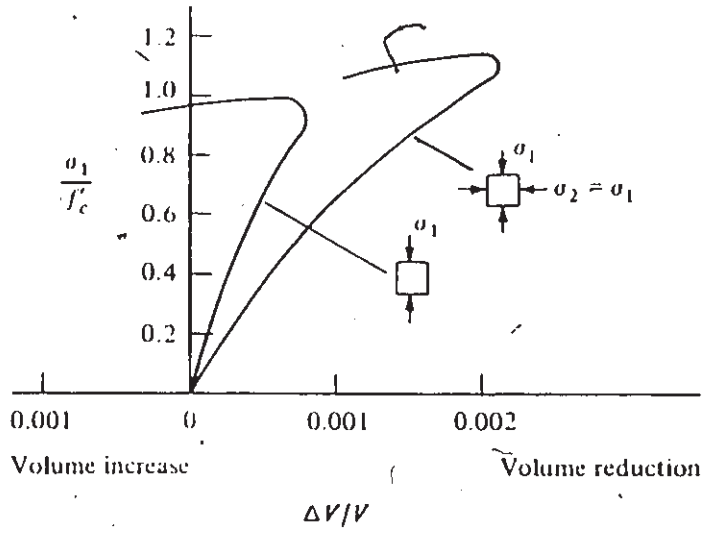

Fig. 2.8 Typical Stress-Strain Curve for Concrete Volume Change under Biaxial Compression(ref.[35]).

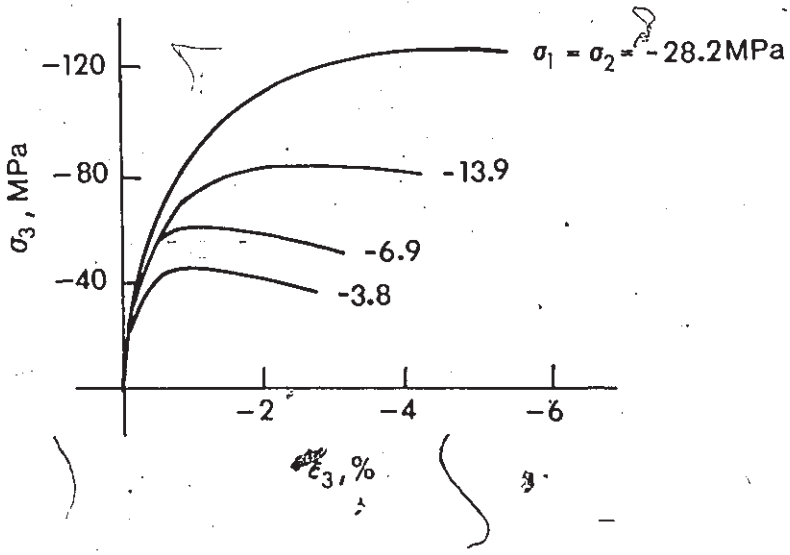

Fig. 2.9 Triaxial Compression Test of Concrete by Richart et al.[56].

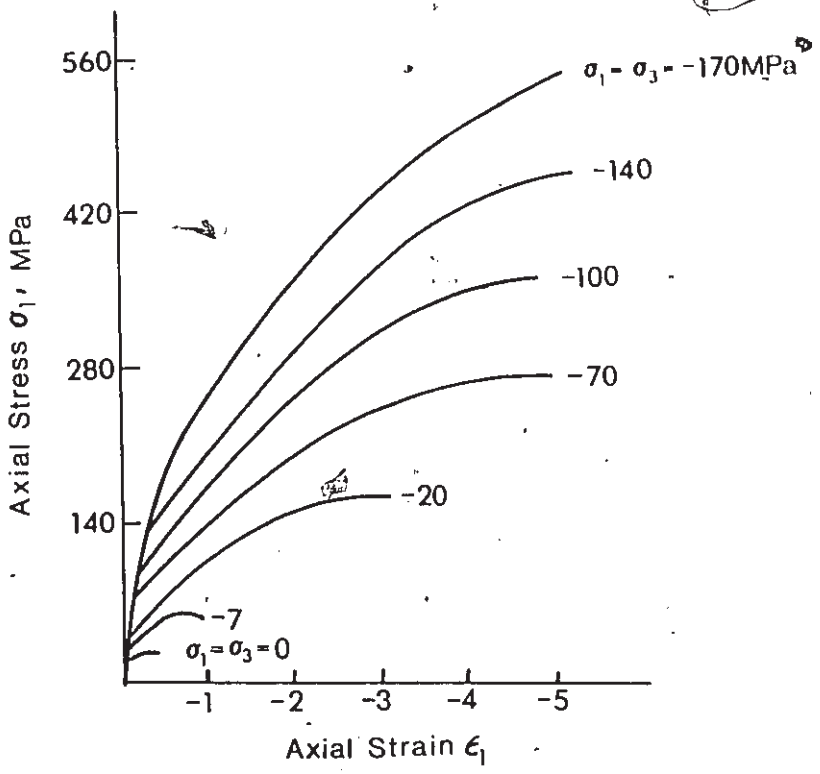

Fig. 2.10 Triaxial Stress-Strain Curves for Concrete(ref.[57]).

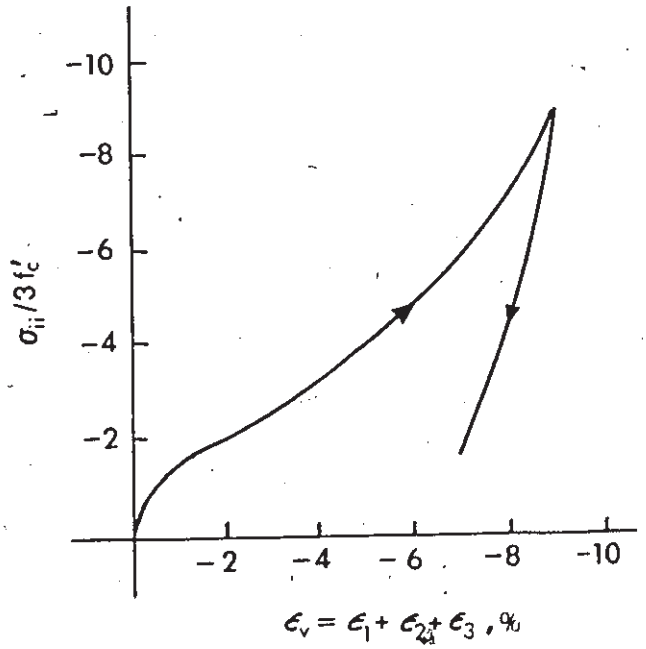

Fig. 2.11 Behaviour of Concrete under Hydrostatic Compression (ref.[35]).

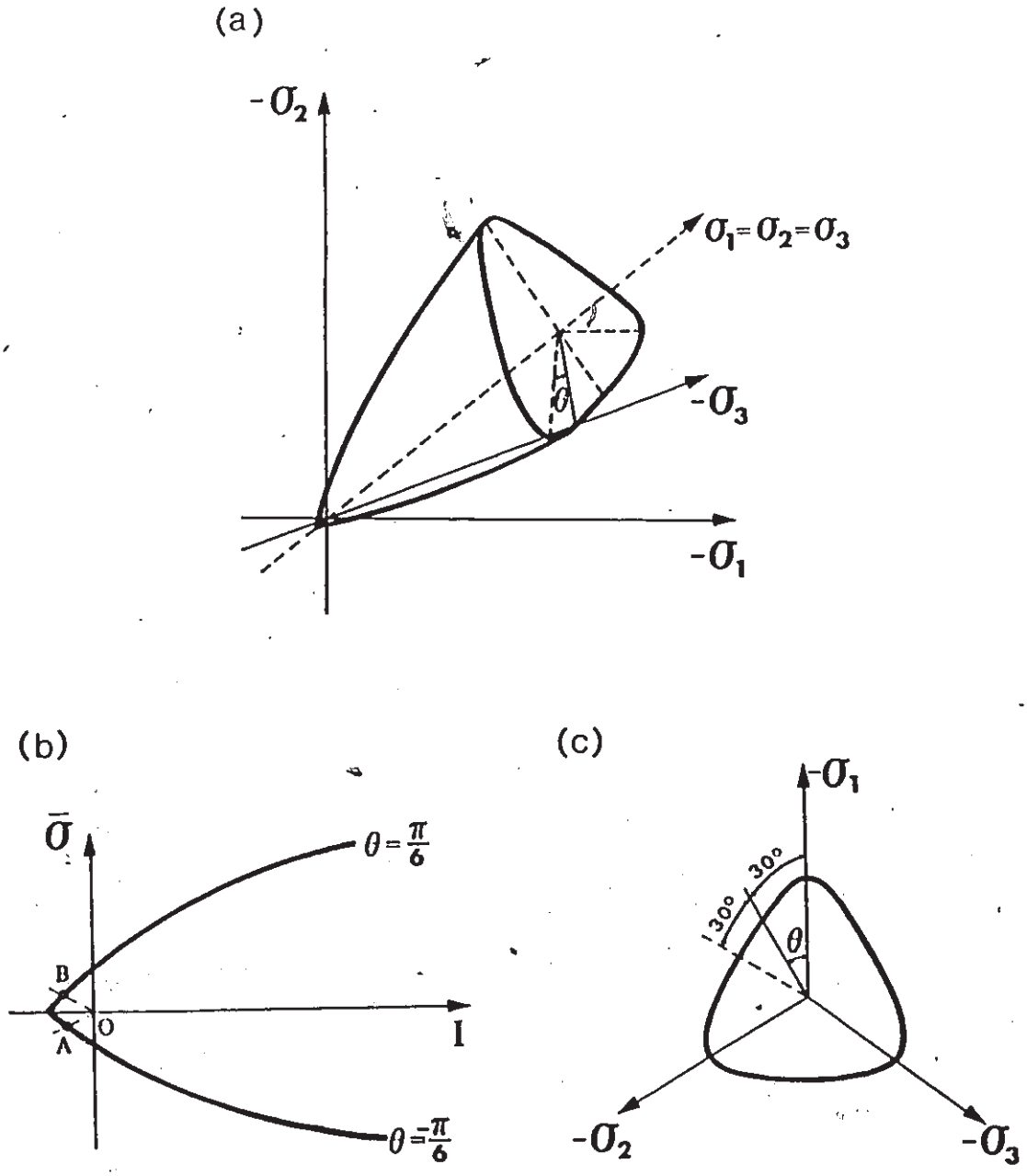

Fig. 2.12 Failure Surface in (a) Principal Stress Space; (b) Meridional Plane; (c) Deviatoric Plane.

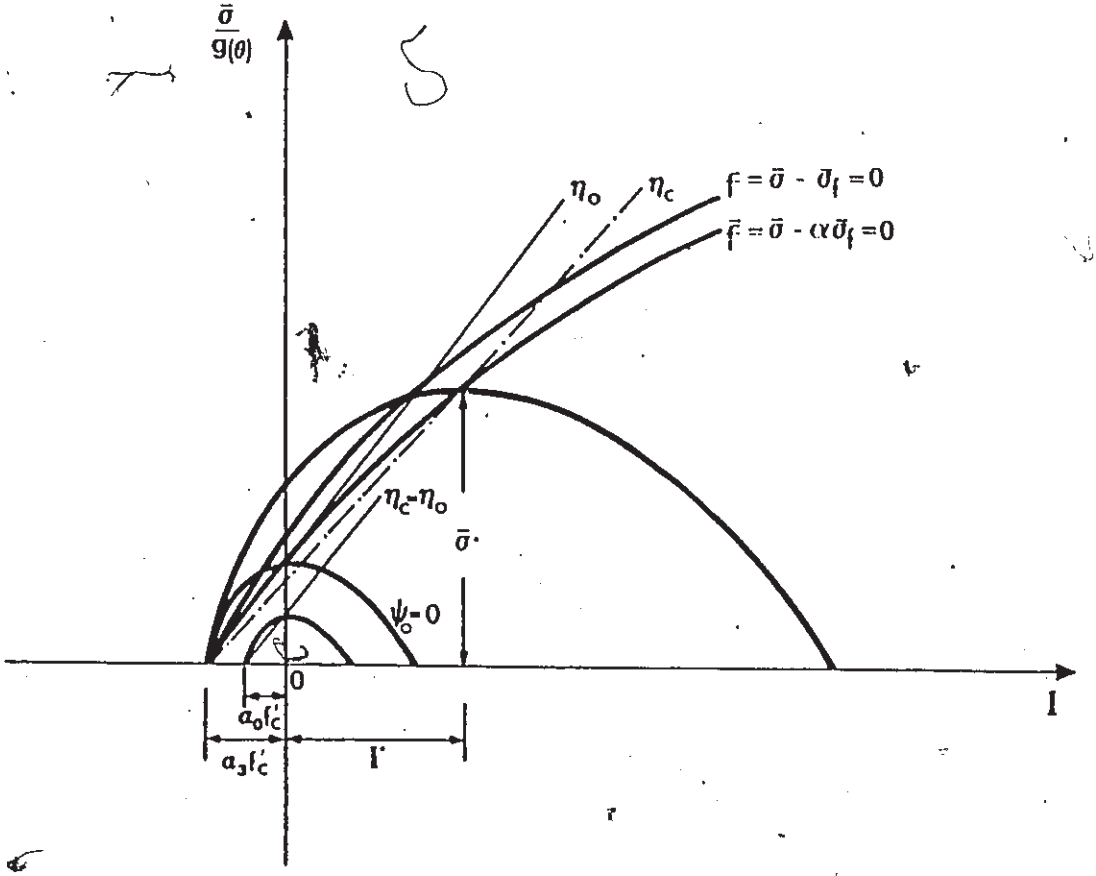

Fig. 2.13 Plastic Potential Surfaces in Meridional Plane.

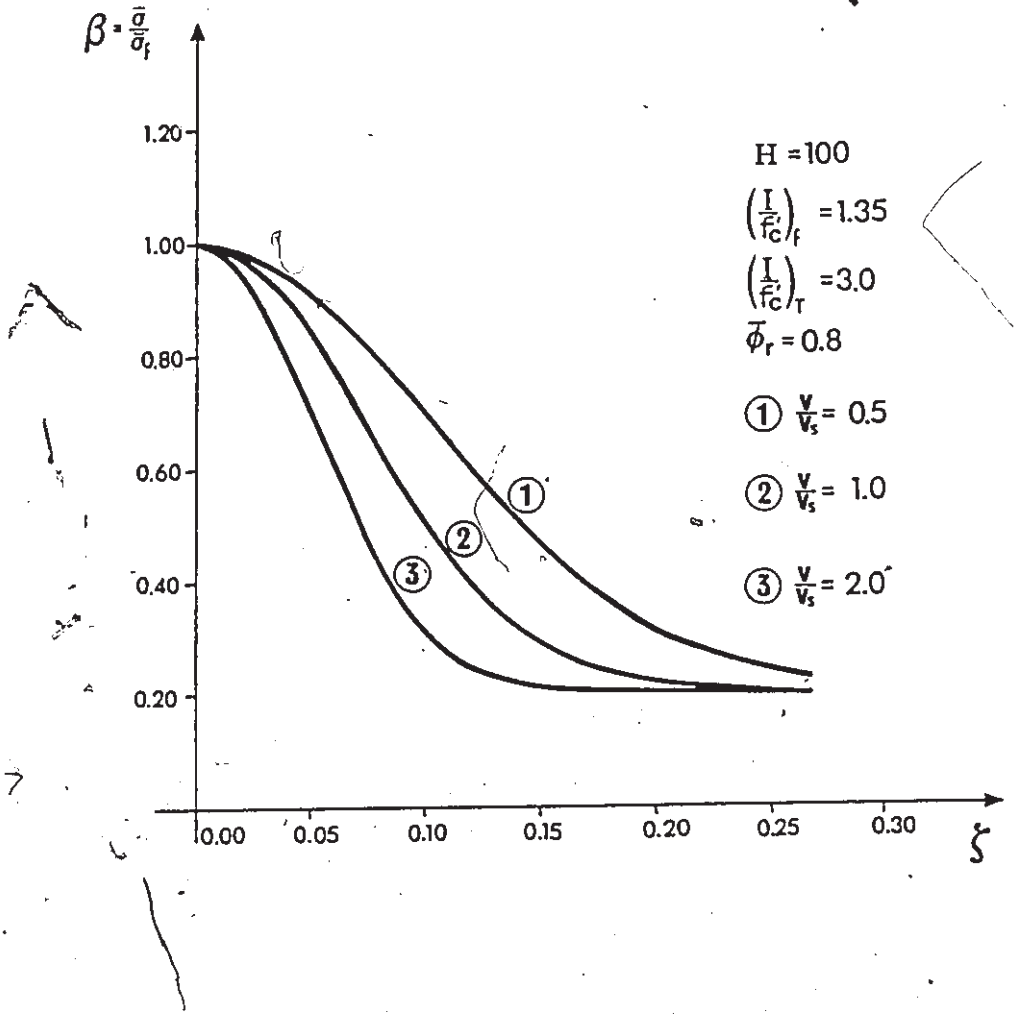

Fig. 2.14 Influence of Parameter $\bar{\phi}_s$ on the Rate of Strain Softening.

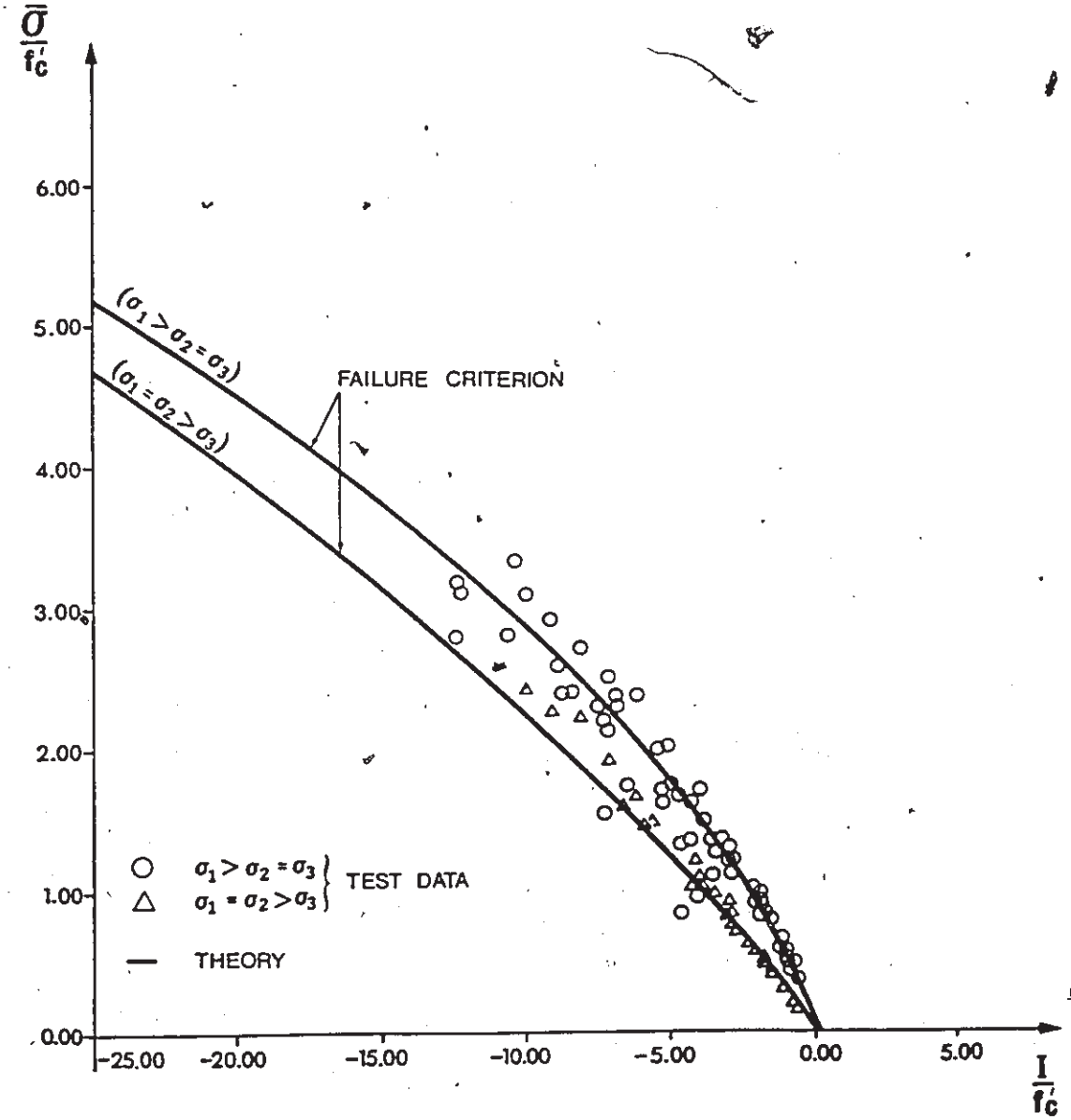

Fig. 2.15 Meridional Sections of the Failure Surface (for $\theta = \pm\pi/6$).

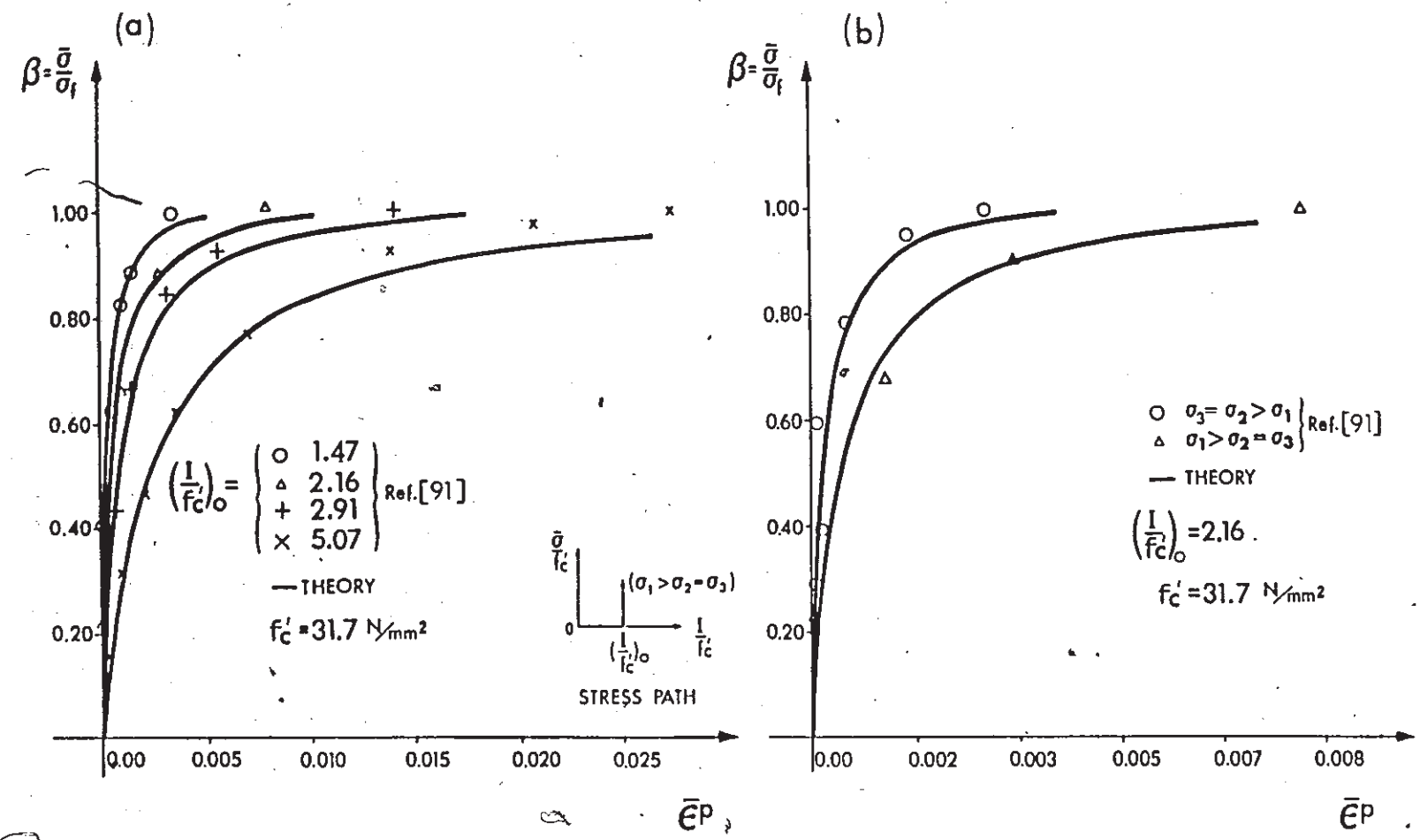

Fig. 2.16 Numerical Simulations of a Series of I=constant Tests.

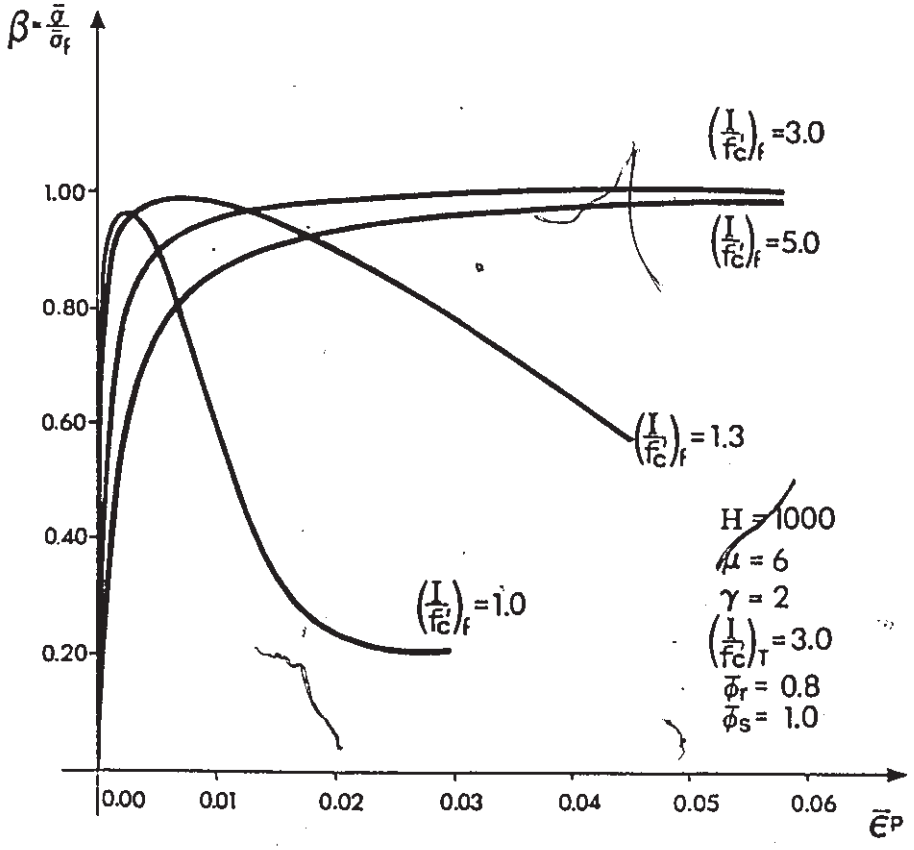

Fig. 2.17 Predicted Variations in Material Characteristics with Confining Pressure.

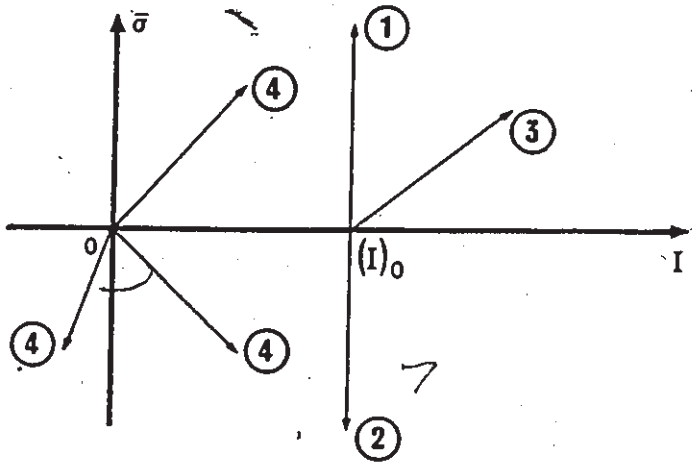

Fig. 2.18 Various Loading Paths Considered in Numerical Simulations.

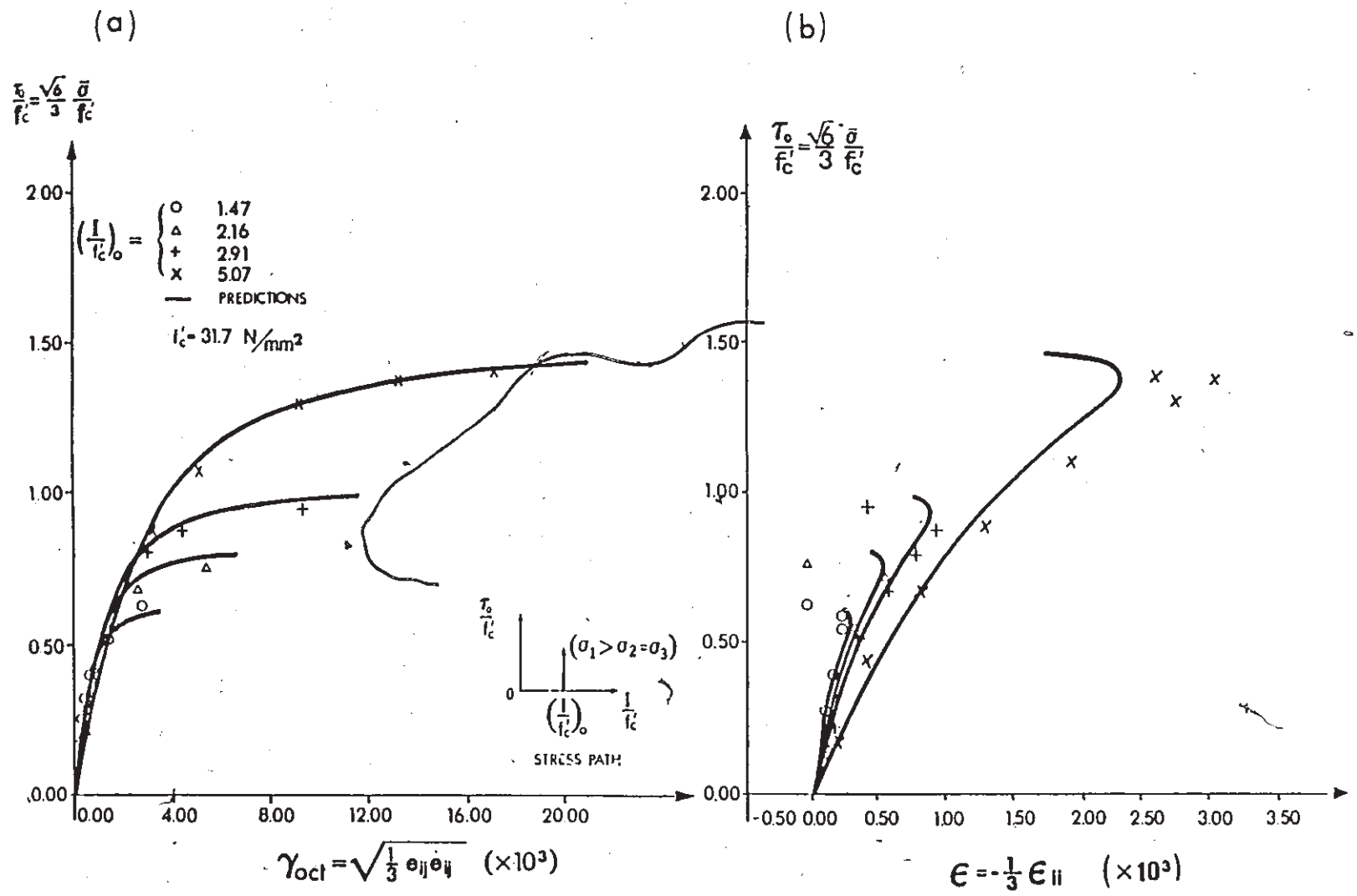

Fig. 2.19 Numerical Simulations of Various Compression Tests under I=constant (ref.[91]).

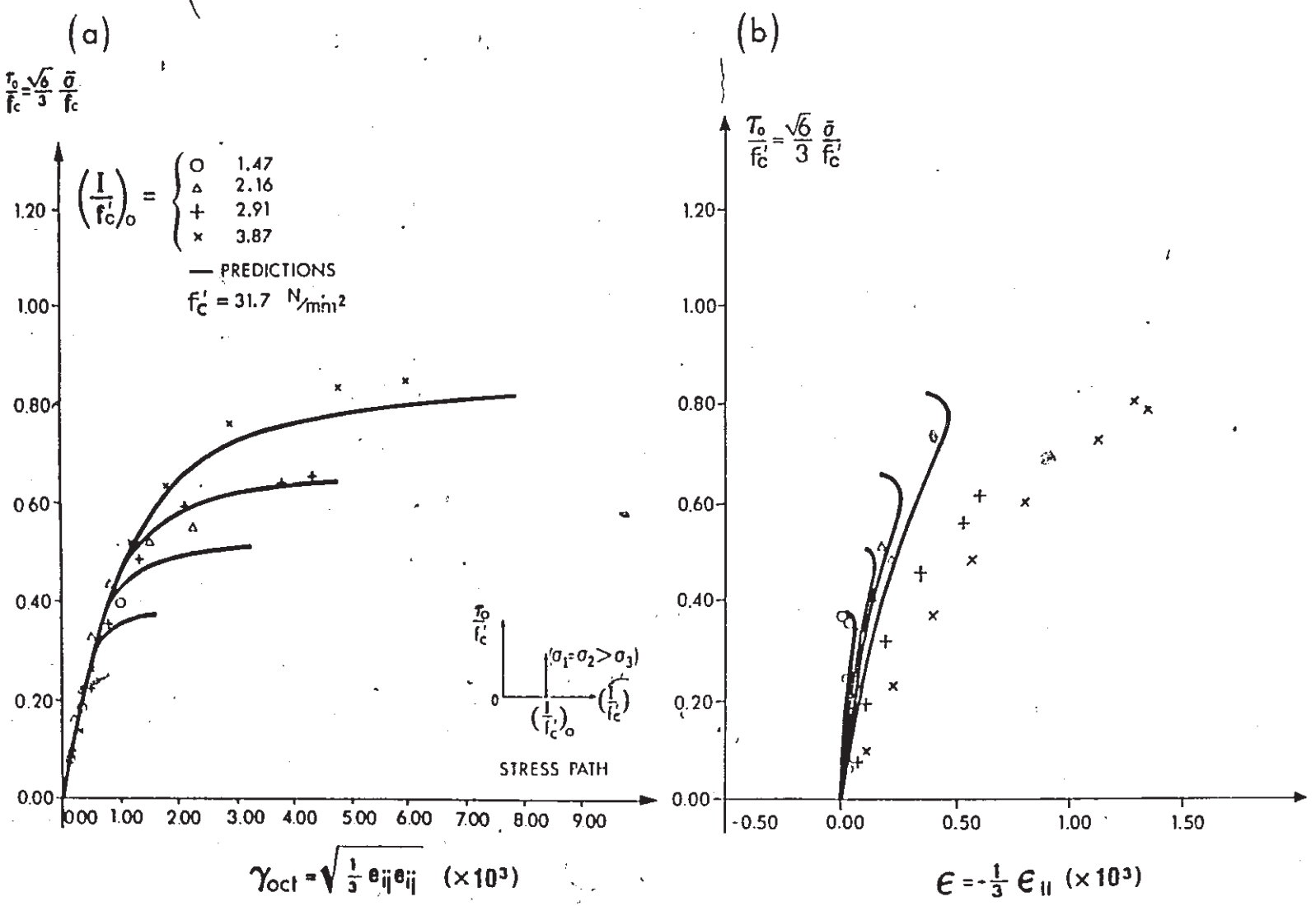

Fig. 2.20 Numerical Simulations of Various Extension Tests under I=constant (ref.[91]).

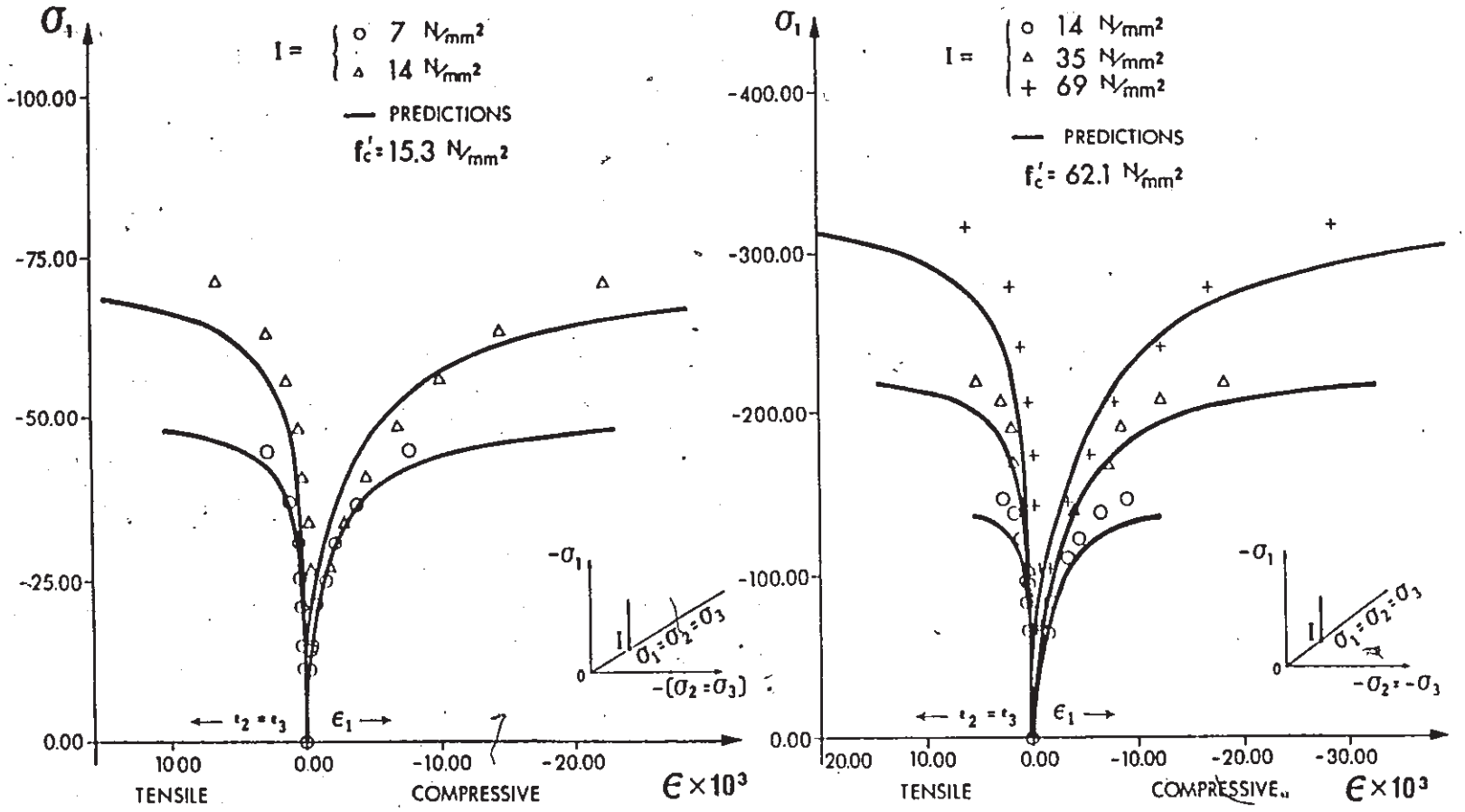

Fig. 2.21 Predictions for Various Uniaxial Compression Tests at Different Initial Confining Pressures(ref.[91]).

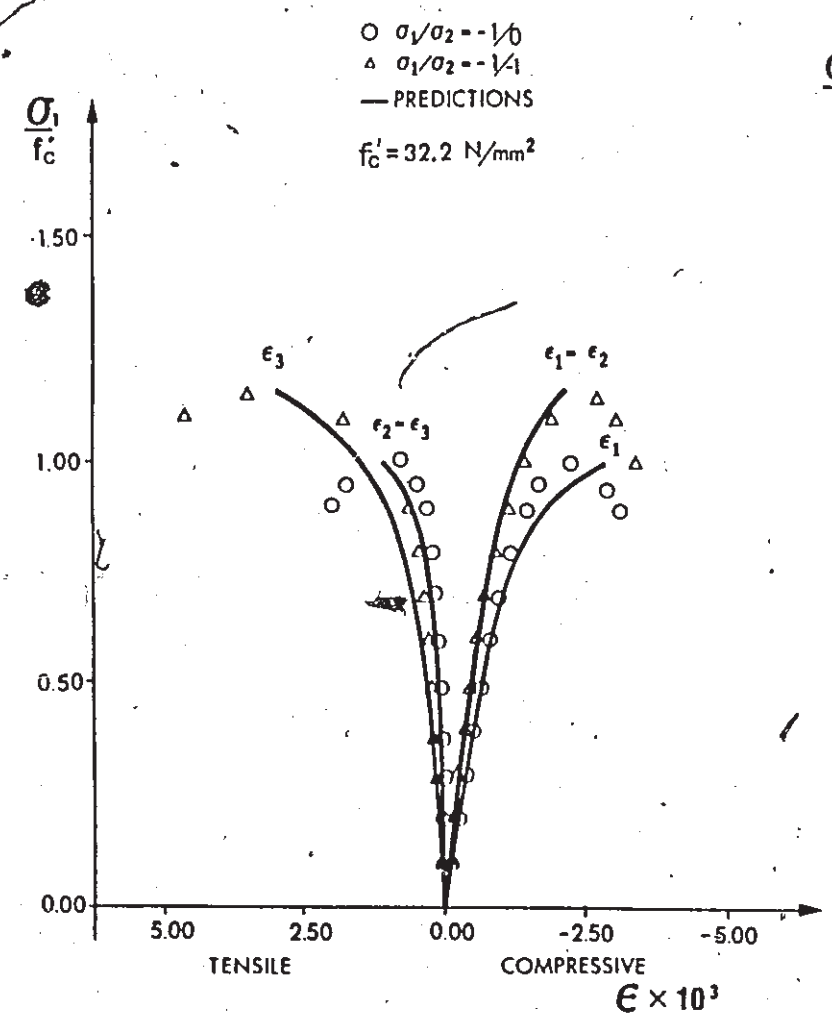

Fig. 2.22 Numerical Simulations of Uniaxial and Biaxial Compression Tests(ref.[50]).

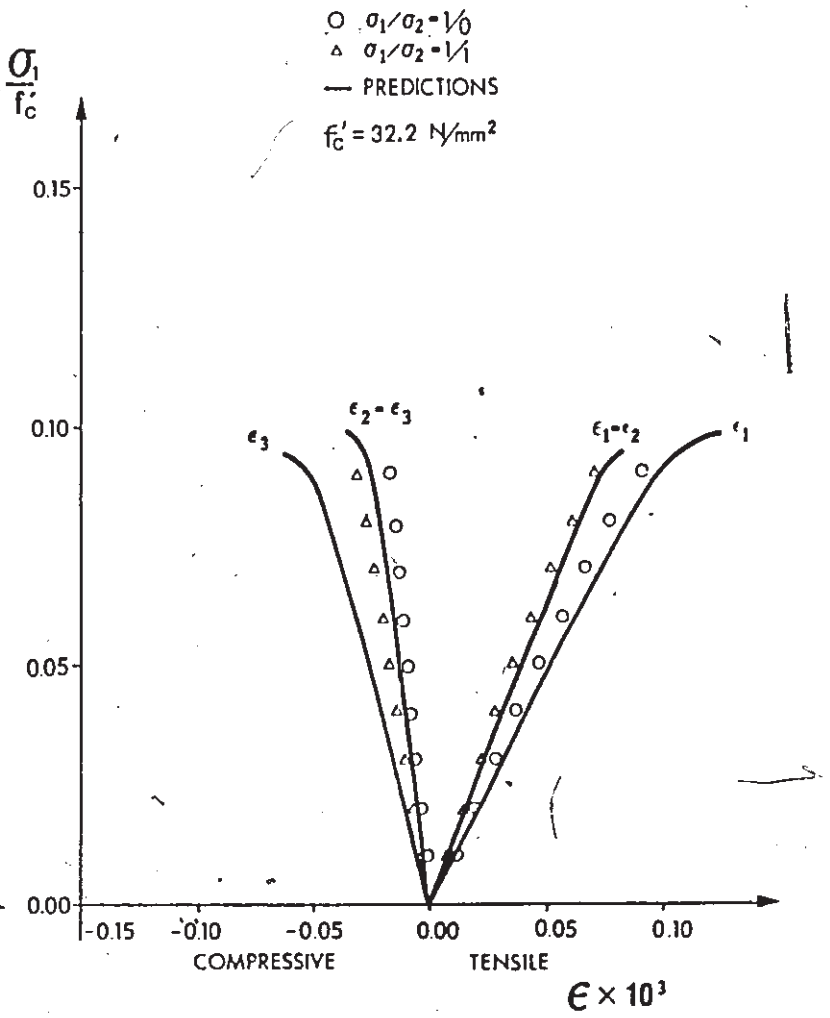

Fig. 2.23 Numerical Simulations of Uniaxial and Biaxial Extension Tests(ref.[50]).

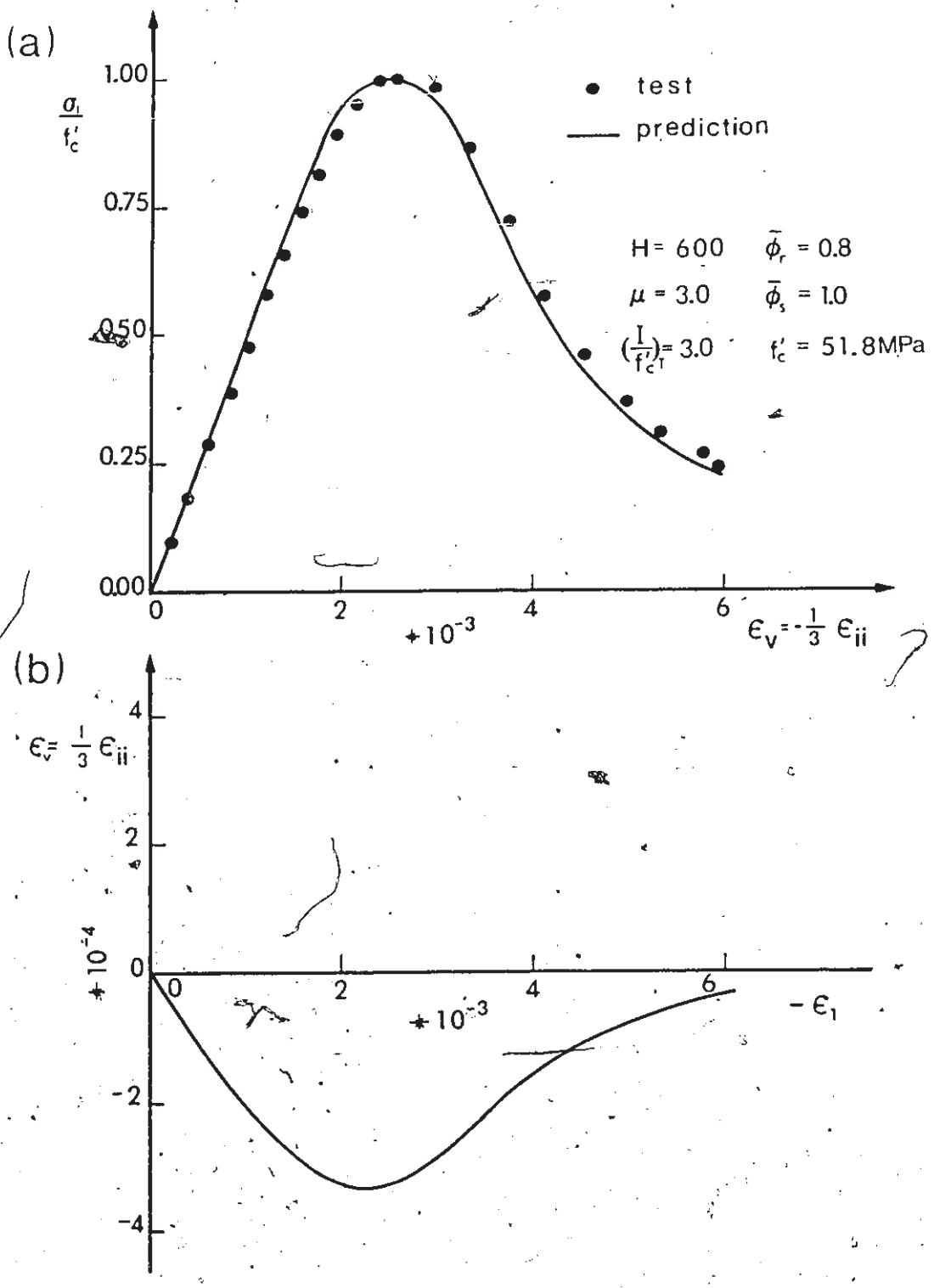

Fig. 2.24 Numerical Simulation of Unstable Response under Uniaxial Compression(ref.[95]).

CHAPTER 3

CONVEXITY OF YIELD LOCI FOR PRESSURE SENSITIVE MATERIALS

3.1 Introduction

In the mathematical formulation of elastoplastic constitutive relations, the convexity of yield surface or plastic potential is often considered as a necessary condition to ensure the positive rate of energy dissipation, refs.[96,97]. It can be easily shown, however, that convexity is not necessarily required for satisfying the condition of irreversibility. In other words, convexity is only a sufficient condition. The proof of this statement is provided in Appendix D.

The requirement of convexity for yield surface or loading surface was originally imposed by Drucker[98] in order to satisfy the so-called 'stability postulate'. This postulate can be expressed as follows

$$(\sigma^b_{ij} - \sigma^a_{ij})d\varepsilon^p_{ij} \geq 0 \quad \text{and} \quad d\sigma_{ij}d\varepsilon^p_{ij} \geq 0 \tag{3.1}$$

where σ^b_{ij} is the stress state on the yield surface, σ^a_{ij} is any other stress state in the interior or on this surface, $d\sigma_{ij}$ is stress increment at a given stress state which produces plastic strain increment $d\varepsilon^p_{ij}$. In Eq.(3.1), the first condition is called the

condition of 'stability in the large', whereas the second is referred to as 'stability in the small'. It has been shown in ref.[98] that if normality of the plastic strain vector to the yield surface is assumed and the convexity of the yield surface is maintained, this postulate is always satisfied. In fact, as shown by Drucker in ref.[99], only the stability in the small is required to prove the uniqueness of the solution to a boundary-value problem. Stability in the small does not require convexity. A sufficient condition to satisfy this postulate (in the context of strain hardening material) is the requirement of normality. Convexity is only required to maintain stability in the large. On the other hand, as stated by Drucker[100], the postulate of stability in the large is "more restrictive than reasonable on physical grounds for all paths of loading in all materials". In fact, Mroz[97] has also indicated that it is not necessary to satisfy this postulate in formulation of flow laws for elastic-plastic materials.

In view of the above considerations, neither the yield surface nor the plastic potential need to be convex. Despite of purely theoretical considerations, the convexity of the yield surface still should be maintained because experimental test data almost never show a concave shape of either yield or failure surface, e.g. concrete (ref.[46]). Furthermore, the neutral loading locus is also unlikely to be concave. Therefore, smooth and convex yield and failure surfaces should be used in the formulation of stress-strain relations.

It is known that the general characteristics of a yield or failure surface can be best described by its cross-sectional shape in the octahedral plane (π-plane) and its meridians in the meridional planes. The convexity in the meridional plane can be verified quite easily. In the octahedral plane, however, the cross-sectional shape is usually much more complex and the issue of convexity must be addressed explicitly. For example, for concrete the form of the failure envelope is significantly influenced by the value of the applied confining pressure. It is known that in the meridional sections this envelope can be well represented by a parabola. Whereas, in the π-plane the shape of the envelope varies from a curvilinear triangle for a low confining pressure to nearly a circular shape at high pressures. To reflect such complex variation of the shape in the proposed failure envelope, an appropriate π-plane generalization, through $g(\theta)$, must be formulated and its convexity must be examined explicitly.

In the recent years, various π-plane generalization, viz. the function $g(\theta)$, for isotropic yield/failure surfaces have been proposed, refs.[7,101-103]. As mentioned before, some of these generalizations do not assure convexity and those, which do, usually involve very complicated functional forms. In this chapter, the convexity of the various generalizations reported in the literature is examined using an appropriate analytical criterion. Moreover, some new simple forms, which remain convex in the entire physical range of deviatoric stress intensity ratios, are proposed.

In what follows, the general criterion for convexity is presented first. Then, this criterion is applied to examine convexity condition for various generalizations. Some comments on Lade[104] and Matsuoka's[105] formulations are also included. Finally, some newly proposed convex forms of function $g(\theta)$ in ref.[75] are discussed.

3.2 Criterion for Convexity in the Octahedral Plane

Consider an arbitrary function $\rho=\rho(\theta)$ in the polar coordinate system (ρ,θ). Using calculus[106], the curvature of this function is determined by

$$\kappa = \frac{\rho^2 + 2\rho'^2 - \rho\rho''}{(\rho^2 + \rho'^2)^{3/2}}, \tag{3.2}$$

in which $\rho'=\partial\rho/\partial\theta$, $\rho''=\partial^2\rho/\partial\theta^2$. It is obvious from Eq.(3.2) that the convexity of the function $\rho=\rho(\theta)$ is preserved if the condition

$$\rho^2 + 2\left(\frac{\partial\rho}{\partial\theta}\right)^2 - \rho\left(\frac{\partial^2\rho}{\partial\theta^2}\right) \geq 0 \tag{3.3}$$

is satisfied. Therefore, Inequality(3.3) represents the necessary and sufficient condition for convexity.

In plasticity the function $\rho=\rho(\theta)$ usually involves division of one function by another, in the form

$$\rho(\theta) = \rho_1(\theta)/\rho_2(\theta) \ . \tag{3.4}$$

Differentiating Eq.(3.4) with respect to θ

$$\frac{\partial \rho}{\partial \theta} = \rho\left(\frac{1}{\rho_1}\frac{\partial \rho_1}{\partial \theta} - \frac{1}{\rho_2}\frac{\partial \rho_2}{\partial \theta}\right)$$

$$\frac{\partial^2 \rho}{\partial \theta^2} = \rho\left[\left(\frac{1}{\rho_1}\frac{\partial \rho_1}{\partial \theta} - \frac{1}{\rho_2}\frac{\partial \rho_2}{\partial \theta}\right)^2 + \frac{1}{\rho_1}\frac{\partial^2 \rho_1}{\partial \theta^2} - \frac{1}{\rho_2}\frac{\partial^2 \rho_2}{\partial \theta^2} - \left(\frac{1}{\rho_1}\frac{\partial \rho_1}{\partial \theta}\right)^2 + \left(\frac{1}{\rho_2}\frac{\partial \rho_2}{\partial \theta}\right)^2\right] \tag{3.5}$$

and substituting the results into Inequality(3.3), an alternative condition to Inequality(3.3) is obtained

$$1 + \frac{2}{\rho_1}\frac{\partial \rho_1}{\partial \theta}\left(\frac{1}{\rho_1}\frac{\partial \rho_1}{\partial \theta} - \frac{1}{\rho_2}\frac{\partial \rho_2}{\partial \theta}\right) - \left(\frac{1}{\rho_1}\frac{\partial^2 \rho_1}{\partial \theta^2} - \frac{1}{\rho_2}\frac{\partial^2 \rho_2}{\partial \theta^2}\right) \geq 0 \ . \tag{3.6}$$

In the above inequality and Eq.(3.5), the functions ρ_1 and ρ_2 must be non-zero. In fact, ρ_1 and ρ_2 are never zero in the context of plasticity. Thus, Inequality(3.6) is used to examine various existing generalizations of the yield/plastic potential surfaces in the next section.

3.3 On Convexity of the Existing Formulations

The first expression defining a smooth deviatoric cross-section of the yield surface for frictional materials was proposed simultaneously by Gudehus[101] and Argyris, et al.[102]. Subsequently, a number of generalizations have been suggested by different researchers. A comprehensive review is provided in ref.[107]. Up until now, the question of convexity has not drawn enough attention and only recently Lin et al.[108] have addressed the problem to some extent. The major objective of this section is to fully examine the convexity of various formulations according to Inequality(3.6).

The existing generalizations, which have been frequently used in plasticity, may be listed as follows,

(i) Gudehus and Argyris'[101,102] formulation

$$g(\theta) = \frac{\bar{\sigma}}{\bar{\sigma}_c} = \frac{2K}{(1+K) - (1-K)\sin 3\theta} \tag{3.7}$$

(ii) Generalized Gudehus and Argyris'[108] formulation

$$g(\theta) = \frac{2K(C_1 - C_2 \sin 3\theta)}{(C_3 + K) - (C_3 - K)\sin 3\theta} \tag{3.8}$$

with

$$C_1 - C_2 = 1, \quad C_1 + C_2 = C_3$$

(iii) William and Warnke's[7] formulation

$$g(\theta) = \frac{(1-K^2)a + (2K-1)[(2+b)(1-K^2)+5K^2-4K]^{1/2}}{(2+b)(1-K^2)+(1-2K)^2} \tag{3.9}$$

where

$$a = \sqrt{3}\cos\theta - \sin\theta$$

$$b = \cos 2\theta - \sqrt{3}\sin 2\theta$$

(iv) Boswell and Chen's[103] formulation

$$g(\theta) = \frac{\sqrt{3}K}{[3-(1-K^2)(1+2\sin^2\theta+\sqrt{3}\sin 2\theta]^{1/2}} \tag{3.10}$$

In the equations above θ represents the angle measure of the third stress invariant $J_3=1/3s_{ij}s_{jk}s_{ki}$ as defined in Eq.(2.1), and K has the same definition as that in Eq.(2.3). It should be noted that an alternative definition of the angle θ, i.e.

$$\theta' = \frac{1}{3}\cos^{-1}\left(\frac{3\sqrt{3}}{2}\frac{J_3}{\bar{\sigma}^3}\right), \qquad 0 \leq \theta' \leq \frac{\pi}{3} \tag{3.11}$$

has also been used in the literature(see e.g. ref.[107]). When implementing the definition in Eq.(3.11), the functions in Eqs.(3.7) to (3.10) should be redefined by substituting the identity $\theta'=\theta+\pi/6$.

The expression in Eq.(3.9) proposed by William and Warnke was developed from an elliptical approximation, Fig. 3.1, which is unconditionally convex and smooth for $1/2 \leq K \leq 1$(see ref.[7]). Also, Boswell and Chen[103] have provided the proof of the convexity of their

formulation for $1/2 \leq K \leq 1$. Unfortunately, Eq.(3.10) does not describe a smooth surface because $\partial g/\partial\theta \neq 0$ at $\theta=\pi/6$. This leads to formation of corners at three apexes corresponding to "triaxial" compression states, see Fig. 3.2. It is also observed from Eq.(3.9) that William and Warnke's formulation involves very complex functions in both the numerator and the denominator, which may result in difficulties in calculations of the gradients $\partial f/\partial\sigma_{ij}$ and $\partial\Psi/\partial\sigma_{ij}$ in the case when $K=K(I)$.

Since the convexity of Eqs.(3.9) and (3.10) need not be examined here, the expression proposed by Gudehus and Argyris, Eq.(3.7), and its generalized form in Eq.(3.8) are dealt with. By taking the derivative (with respect to θ) of the numerator and denominator in both these equations, substituting the results into Inequality(3.6) and after some algebraic manipulations, the following results for Eq.(3.7)

$$\frac{1+K}{8(1-K)} \leq \sin 3\theta \qquad (3.12)$$

and for Eq.(3.8)

$$1 - \frac{9(1-K)(1+C_2)[C_2(1-\sin 3\theta+\cos^2 3\theta)-\sin 3\theta]}{[1+C_2(1-\sin 3\theta)]^2[(1+K)-(1-K)\sin 3\theta+2C_2(1-\sin 3\theta)]} \geq 0 . \qquad (3.13)$$

Since $-1 \leq \sin 3\theta \leq 1$, then Inequality(3.12) can be replaced by

$$\frac{1 + K}{8(1-K)} \leq -1 \tag{3.14}$$

which leads to the convexity criterion for Eq.(3.7) as

$$K \geq \frac{7}{9} \tag{3.15}$$

However, the close-form solution of Inequality(3.13) seems to be impossible for an arbitrary value of C_2 (except the case when the original Gudehus and Argyris' function is recovered). Hence the solution can only be obtained by numerical iteration techniques. The results of the numerical calculations for several values of C_2 are presented in Table 3.1. It can be seen from Table 3.1 that the limit value of K to guarantee convexity strongly depends on the choice of C_2. For C_2=0.34 the lowest limit value of K≥0.6603 is obtained, see Table 3.1. Figure 3.3 shows the deviatoric cross-sections, as described by Eq.(3.8), for various values of K. It is obvious that this generalization increases the range of the K-value within which the function is convex. But, in general, it does not assure convexity for the entire range 1/2≤K≤1. Therefore, it is concluded that this generalization by Eq.(3.8) as well as the original form in Eq.(3.7) are not applicable to concrete as the value of K for concrete may be as low as K=0.5658, but may be useful for soils, ref.[109].

3.4 Comments on Lade's and Matsuoka's Formulations

Lade et al.[104] have proposed a simple representation for the yield/failure surface expressed in terms of the first and the third invariants of the stress tensor, i.e.

$$I_1^3 - k_1 I_3 = 0 \tag{3.16}$$

in which $I_1=\sigma_{ii}$, $I_3=\det(\sigma_{ij})$ and k_1 is a constant which depends on the density of a material. Matsuoka et al.[105] suggested a similar form employing the second stress invariant I_2,

$$I_1 I_2 - k_1 I_3 = 0 \tag{3.17}$$

in which $I_2=1/2I_1^2-1/2\sigma_{ij}\sigma_{ij}$. It has been demonstrated in refs.[104,105] that in the principal stress space Eqs.(3.16) and (3.17) represent a conical surface with the apex at the stress space origin. Moreover, the cross sections in the octahedral plane are described by smooth non-circular shapes. The objective here is to derive appropriate expressions which defines function $g(\theta)$ for both formulations above and examine the range of convexity.

First, consider Lade's formulation. It can be shown that the following identities exist

$$\begin{aligned} I_2 &= (1/3)I_1^2 - J_2 \\ I_3 &= J_3 - (1/3)I_1 J_2 + (1/27)I_1^3 \end{aligned} \tag{3.18}$$

in which $J_2=1/2s_{ij}s_{ij}=\bar{\sigma}^2$. Substitute Eqs.(3.18) and (2.1) into Eq.(3.16) to obtain

$$\lambda^3 + p\lambda + q = 0 \tag{3.19}$$

where

$$\lambda = \left(\frac{\bar{\sigma}}{I_1}\right)^{-1}, \quad p = -\frac{9k_1}{k_1-27}, \quad q = -\frac{18k_1\sin3\theta}{\sqrt{3}(k_1-27)} . \tag{3.20}$$

For $k_1>27$, the real root of Eq.(3.19) is given by

$$\lambda=\begin{cases} 2\sqrt{\dfrac{3k_1}{k_1-27}}\cos\left[\dfrac{1}{3}\cos^{-1}\left(-\sqrt{\dfrac{k_1-2}{k_1}}\sin3\theta\right)\right], & \text{for } \sin3\theta<0 \\ 2\sqrt{\dfrac{3k_1}{k_1-27}}\cos\left[\dfrac{\pi}{3}-\dfrac{1}{3}\cos^{-1}\left(\sqrt{\dfrac{k_1-27}{k_1}}\sin3\theta\right)\right], & \text{for } \sin3\theta>0 . \end{cases} \tag{3.21}$$

Thus, for the definition of λ in Eq.(3.20), the function $g(\theta)$, defined as the ratio $(\bar{\sigma}/I_1)/(\bar{\sigma}/I_1)_{\theta=\pi/6}$, takes the following form

$$g(\theta)=\begin{cases} \dfrac{\cos[\pi/3-1/3\cos^{-1}A]}{\cos[1/3\cos^{-1}(-A\sin3\theta)]}, & \text{for } \sin3\theta<0 \qquad (3.22a) \\ \dfrac{\cos[\pi/3-1/3\cos^{-1}A]}{\cos[\pi/3-1/3\cos^{-1}(A\sin3\theta)]}, & \text{for } \sin3\theta>0 \qquad (3.22b) \end{cases}$$

where

$$A = \sqrt{\frac{k_1-27}{k_1}}, \qquad k_1 \geq 27 . \tag{3.22c}$$

Following the same procedure, the function $g(\theta)$ for Matsuoka's formulation can be obtained and has the same form as that of Eq.(3.22), except for parameter A which is now defined by

$$A = \sqrt{\frac{k_1^2(k_1-9)}{(k_1-3)^3}}, \qquad k_1 \geq 9 . \tag{3.23}$$

The function $g(\theta)$ in Eq.(3.22) must satisfy the conditions

$$g(-\pi/6)=K \quad \text{and} \quad g(\pi/6)=1 . \tag{3.24}$$

It can easily be verified that the second condition is always satisfied. Using the first condition, K can be expressed in terms of parameter A, i.e.

$$K = \frac{1}{2} + \frac{\sqrt{3}}{2} \tan\left(\frac{1}{3} \cos^{-1}A\right) . \tag{3.25}$$

According to Eqs.(3.22c) and (3.23) there is a range for A, $0 \leq A \leq 1$, which in view of Eq.(3.25) implies $1 \leq K \leq 1/2$.

In order to examine the convexity of Eq.(3.22), let take the derivatives (with respect to θ) of Eqs.(3.22a) and (3.22b).

Substitute them into inequality(3.5) to obtain the criteria for convexity

$$1-\frac{A\cos^2 3\theta\sqrt{1-(A\sin 3\theta)^2}-A[3(1-A^2)\sin 3\theta\tan[-\frac{\cos^{-1}(-A\sin 3\theta)}{3}]}{[1-(A\sin 3\theta)^2]^{3/2}}>0 \qquad (3.26a)$$

for $\sin 3\theta<0$, and

$$1-\frac{A\cos^2 3\theta\sqrt{1-(A\sin 3\theta)^2}-A[3(1-A^2)\sin 3\theta\tan[\frac{\pi-\cos^{-1}(A\sin 3\theta)}{3}]}{[1-(A\sin 3\theta)^2]^{3/2}}>0 \qquad (3.26b)$$

for $\sin 3\theta<0$.

Denote the left-hand sides of the above inequalities by $f_1(A)$ and $f_2(A)$, respectively. It can be shown (by verifying criteria $df_1/dA<0$ and $df_2/dA<0$) that both functions, $f_1(A)$ and $f_2(A)$, are monotonically decreasing in the range $0\leq A\leq 1$. Moreover, at $A=1$, both function reach the minimum, i.e. $f_1(1)=f_2(1)=0$. Therefore, Inequalities(3.26a) and (3.26b) are always satisfied. This leads to the conclusion that the function in Eq.(3.22) is convex in the entire range $0\leq A\leq 1$(or $1/2\leq K\leq 1$ by recalling Eq.(3.25)). Fig. 3.4 shows the cross sections in the deviatoric plane for different values of the parameter K. It can be seen from Fig. 3.4 that the shapes described by Eq.(3.22) are always smooth when $K>0.5$. This is a typical example of function $g(\theta)$ which is defined through two separate functions rather than just one function.

3.5 Proposed Alternative Formulations

Functions $g(\theta)$ as defined by Eqs.(3.9) and (3.22) are relatively complex. At the same time simpler functions, viz. Eqs.(3.7) and (3.8), do not assure convexity for low values of K. Hence, it may be useful to look for alternative expressions which are simple and satisfy convexity requirement.

Consider the following simple representation of the function $g(\theta)$ (already used in chapter 2, Eq.(2.3))

$$g(\theta)=\frac{(\sqrt{1+a}-\sqrt{1-a})K}{K\sqrt{1+a}-\sqrt{1-a}+(1-K)\sqrt{1-a\sin 3\theta}}; \quad a\to 1 . \tag{3.27}$$

This function satisfies $g(-\pi/6)=K$, $g(\pi/6)=1$ and when a approaches unity, it yields a smooth non-circular cross-section in the deviatoric plane. It should be noted that for $a=1$ the function $\partial g/\partial\theta$ becomes singular at $\theta=\pi/6$. But this singular point can be eliminated by selecting the value of a less than 1. In the following, the convexity of function in Eq.(3.27) is examined.

Based on inequality(3.6), the general criterion of convexity for Eq.(3.27) takes the following form

$$1-\frac{9a(1-K)[a/2(1+\sin^2 3\theta)-\sin 3\theta)]}{2(1-a\sin 3\theta)^{3/2}[K\sqrt{1+a}-\sqrt{1-a}+(1-K)\sqrt{1-a\sin 3\theta}]}\geq 0 . \tag{3.28}$$

The second term in Inequality(3.28) reaches its maximum value at $\sin 3\theta=-1$. This implies that Inequality(3.28) can be replaced by

$$1 - \frac{9a(1+a)(1-K)}{2(1+a)^{3/2}[K\sqrt{1+a} - \sqrt{1-a} + (1-K)\sqrt{1+a}]} \geq 0 . \tag{3.29}$$

From this inequality, after some algebraic manipulations, the following is obtained

$$K \geq \frac{7a - 2(1 - \sqrt{1-a^2})}{9a} . \tag{3.30}$$

As an example, if $a=0.9999$ then $K\geq 0.5587$ is a sufficient condition for convexity. Fig. 3.5 presents deviatoric cross sections generated by Eq.(3.27) for different values of parameter K.

An alternative to Eq.(3.22) is the simpler form presented below

$$g(\theta) = \begin{cases} (1-K)T+\sqrt{(1-K)^2T^2+4K-3}, & \text{for } g\geq\sqrt{4K^2-6K+3} \qquad (3.31a) \\ 2K/(\sqrt{3}\cos\theta-\sin\theta), & \text{for } g\leq\sqrt{4K^2-6K+3} \qquad (3.31b) \end{cases}$$

where $T=\sqrt{3}\cos\theta+\sin\theta$. According to this equation, the deviatoric cross-section is represented by a combination of a circular portion, Eq.(3.31a), and a straight-line portion defined by Eq.(3.31b). The straight-line branch is tangent to the circle with radius $r_0=2\bar{\sigma}_t-\bar{\sigma}_c$ at $\phi_0=\pi/3$, see Fig. 3.6. As $K=\bar{\sigma}_t/\bar{\sigma}_c$ varies from 1/2 to 1, the

shape of the deviatoric section changes from a triangle to a full circle. Figure 3.7 shows the cross-sections generated by Eq.(3.31) for various values of K. It is self-evident that the proposed function in Eq.(3.31) gives a smooth and convex surface in the entire range $1/2<K\leq 1$.

In concluding this Chapter, the convexity of various shape functions $g(\theta)$ has been examined according to the general criterion by Inequality(3.6). The expressions proposed by William and Warnke[7] as well as those employed by Lade[104] and Matsuoka[105] assure convexity for the entire range $1/2\leq K\leq 1$. The function proposed by Gudehus[101] and Argyris et al.[102] and its generalized form remain convex only for a certain range of K. It has been shown that the optimal selection of constants, C_1, C_2 and C_3 in Eq.(3.7) increases the convexity range from $K\geq 0.7778$ to $K\geq 0.6603$. In this study, some simple expressions defining the shape function $g(\theta)$ have been proposed and they ensure a smooth and convex surface for K values near 0.5. Hence, they are suitable for modelling of concrete behaviour.

TABLE 3.1 The Conditions of Convexity for Eq.(3.8)

C_1 =	C_2 =	C_3 =	K >
1.10	0.10	1.20	0.7333
1.20	0.20	1.40	0.6889
1.30	0.30	1.60	0.6622
1.32	0.32	1.64	0.6609
1.34	0.34	1.68	0.6603
1.36	0.36	1.72	0.6605
1.40	0.40	1.80	0.6626
1.50	0.50	2.00	0.6739
2.00	1.00	3.00	0.7491

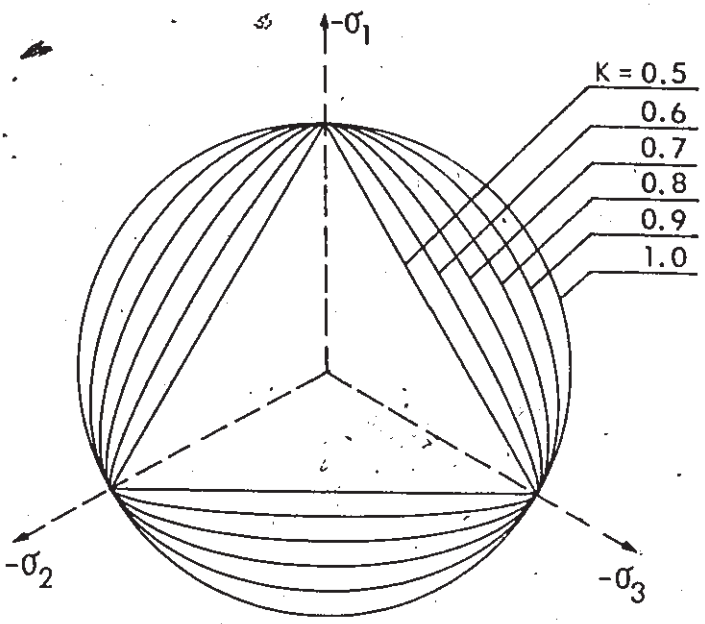

Fig. 3.1 π-Plane Cross Sections Generated by William and Warnke's Function, Eq.(3.9).

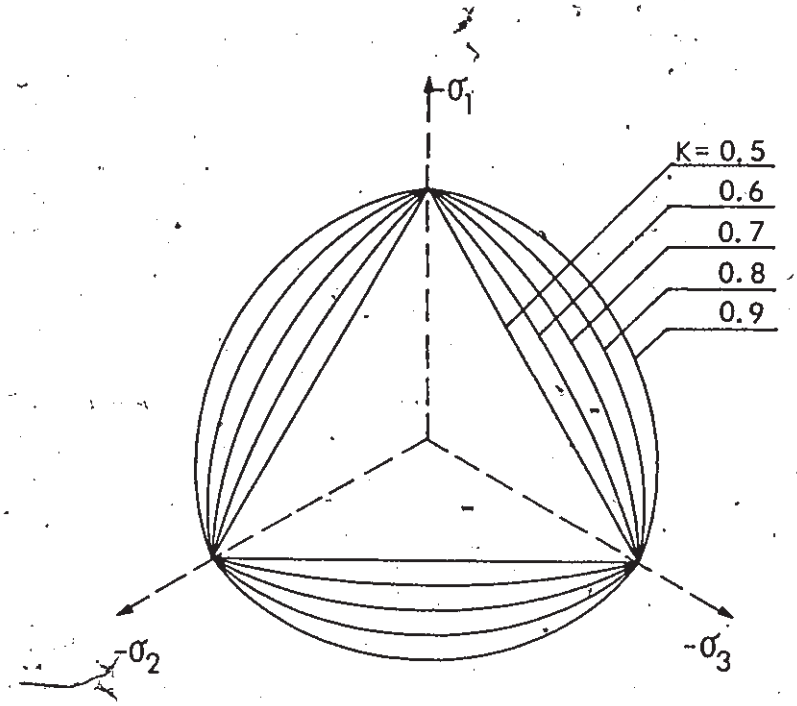

Fig. 3.2 π-Plane Cross Sections Obtained from Boswell and Chen's Function, Eq.(3.10).

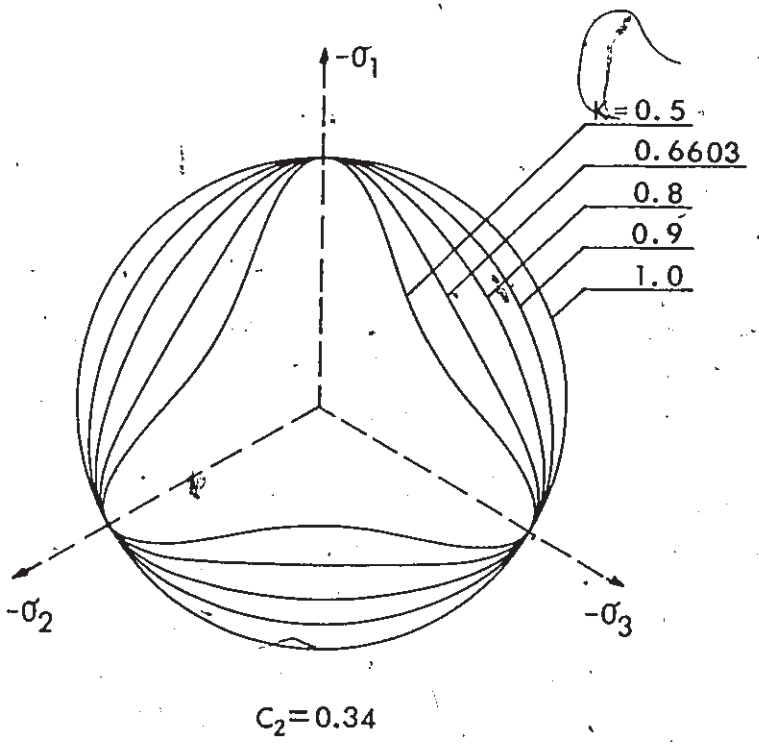

Fig. 3.3 *π-Plane Cross Sections for Generalized Gudehus and Argyris' Function, Eq.(3.8).*

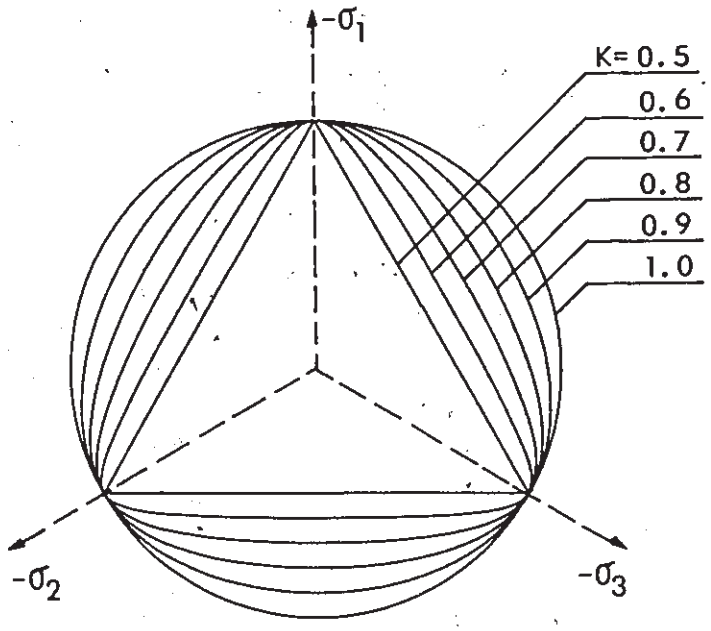

Fig. 3.4 *Deviatoric Cross Sections for Lade and Matsuoka's Formulations, Eq.(3.22).*

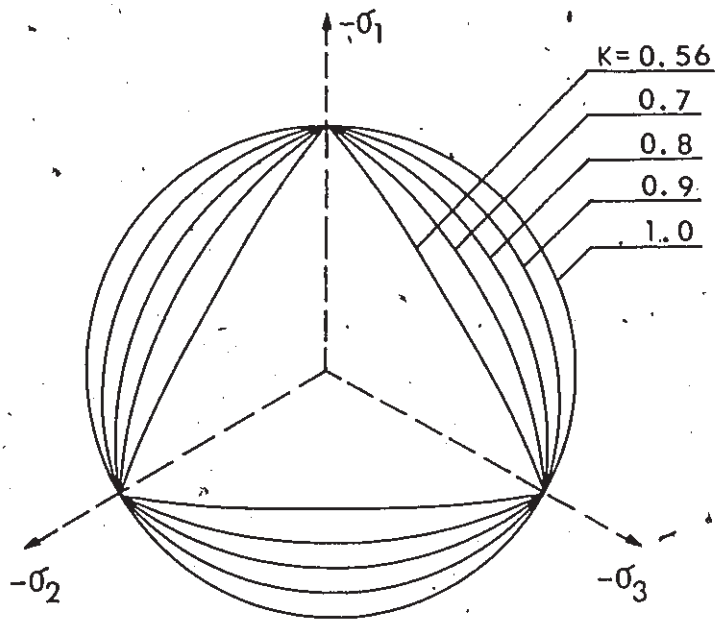

Fig. 3.5 Deviatoric Cross Sections Generated by Eq.(3.27).

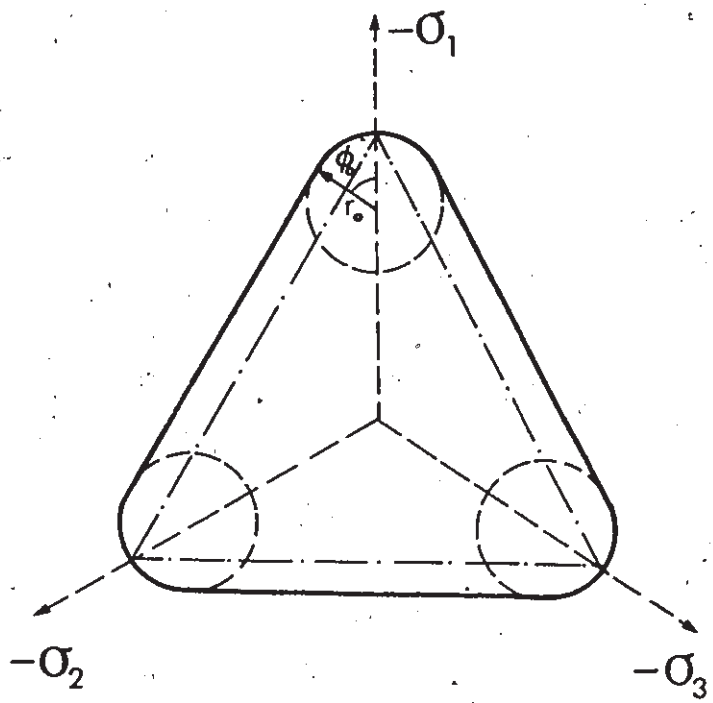

Fig. 3.6 Deviatoric Cross Section Composed of Circular and Straight-Line Portions, Eq.(3.31).

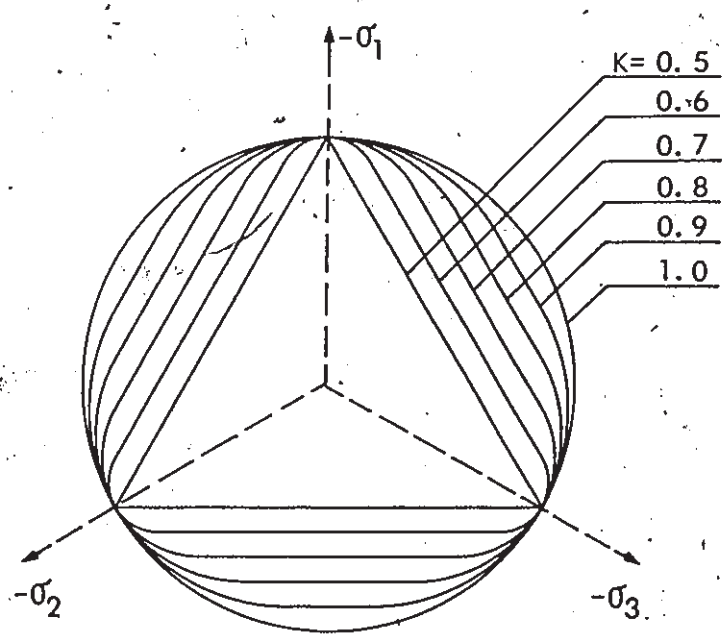

Fig. 3.7 Deviatoric Cross Sections Generated by Eq.(3.31) for Various Values of Parameter K.

CHAPTER 4

EXTENSION OF THE CONSTITUTIVE MODEL TO CYCLIC LOADING CONDITIONS

4.1 Introduction

This Chapter is concerned with an extension of constitutive model presented in Chapter 2 to cyclic behaviour of concrete. It is well known that the mechanical behaviour of concrete under cyclic loading is much more complex than that under monotonic loading. Consequently, most of the investigations reported in the literature have been restricted to the progressive failure of concrete under cyclic axial loading conditions(refs.[110-112]), and only a few dealt with the behaviour of concrete under cyclic biaxial or triaxial loading conditions, refs.[113,114]. It appears that at the present time there is a lack of experimental data on the cyclic behaviour of concrete subjected to general multiaxial loading conditions. In recognition of this fact, the present study is focused on the development of a rational constitutive framework which is applicable to general cyclic loading conditions. The proposed constitutive theory is then verified for some typical cyclic loading histories.

The concept proposed here represents an extension of the constitutive model already discussed in Chapter 2. As indicated in that chapter, the applicability of the model has been restricted to

monotonic loading histories since no irreversible deformation have been accounted for during stress-reversals. In this chapter, the model is modified to take stress-reversal histories into account. In what follows, the experimental observations on cyclic behaviour of concrete under uniaxial compressive loading are summarized first. Then, the constitutive description applicable to histories involving stress-reversals is presented. This employs the concept of neutral loading loci as presented in ref.[31] and an appropriate interpolation rule which defines the field of hardening moduli. Next, the procedure for identification of model parameters is outlined, followed by a series of numerical examples. In particular, the proposed constitutive model is used to simulate the effect of cyclic degradation of both stiffness and strength.

4.2 Experimental Observations

Under a low number of load cycles at relatively high stress levels, concrete undergoes high irreversible deformations which accumulate during each cycle. It is pointed out here that such deformation process is different from that of fatigue failure which occurs under a large number of load cycles at relatively low stress levels. For a low number of load cycles at high stress levels, the stress-strain response of concrete as observed from uniaxial compression tests is shown in Fig. 4.1. It can be seen from the figure that concrete stiffness and strength decreases with increasing number

of cycles. This cyclic degradation effect plays a major role in the course of progressive failure of concrete. It can also be observed that the stress-strain curve for monotonic loading serves as a reasonable envelope for the peak values of stresses for concrete under cyclic loading.

It should be noted that the observed degradation of stiffness in the course of cyclic loading is mainly due to continuous accumulation of plastic irreversible deformations resulting from microcracking instead of a progressive decay in elastic properties. Furthermore, the area of a hysteresis loop decreases with each successive cycle until the last loop when it increases just prior to complete failure of concrete specimen.

At the present time, the behaviour of concrete under a cyclic multiaxial loading condition is still unclear due to lack of experimental information and due to the difficulties in performing such experimental investigations. Although a few researchers have conducted some initial experimental studies, it is too early to draw any specific conclusions.

4.3 Constitutive Description for Stress-Reversal Histories

A general mathematical formulation of the constitutive model is presented in this section. As already mentioned, this formulation is based on the concept discussed in Chapter 2, and the emphasis here is placed on an adequate modelling of cyclic response of concrete.

According to the constitutive framework presented in the preceding chapters, during an initial active loading process the yield surface undergoes progressive expansion/contraction and its evolution is governed by an appropriately defined hardening/softening parameter. An incremental constitutive relation describing such deformation process has been derived in Section 2.3. Now, upon stress reversal, the functional form of the current yield locus is incorporated into the material memory. It is postulated, analogous to the bounding surface formulation in ref.[10], that this locus reflects the maximum load intensity attained during the past loading history. For the stress histories penetrating the interior of this surface, $f=0$, Eq.(2.7), the deformation process is described by employing a set of neutral loading loci, ref.[31]. For simplicity, the functional form of the neutral locus is proposed to be similar to that of the maximum load intensity surface, i.e.

$$f_n = \bar{\sigma} - \beta_n g(\theta) \bar{\sigma}_c = 0 \tag{4.1}$$

where β_n is a constant determined according to the current stress point. It should be noted that the neutral loading locus, Eq.(4.1),

defines the direction of stress rate for which the corresponding plastic strain rate vanishes instantaneously.

For the reverse loading process, the non-associated flow rule can now be conveniently expressed by

$$d\varepsilon^{p}_{ij} = h_p(n_{ij}d\sigma_{ij})\bar{n}_{ij} \tag{4.2}$$

where n_{ij} represents a unit tensor normal to the neutral surface,

$$n_{ij} = \frac{\partial f_n}{\partial \sigma_{ij}} / \left(\frac{\partial f_n}{\partial \sigma_{ij}} \frac{\partial f_n}{\partial \sigma_{ij}}\right)^{1/2} \tag{4.3}$$

and $\bar{n}_{ij}$ defines the direction of the plastic flow, i.e., represents a unit tensor normal to the plastic potential surface, Eq.(2.12).

Equation(4.2) holds for $n_{ij}d\sigma_{ij}$ both positive and negative, and h_p represents a scalar function depending on the position of the stress tensor relative to the maximum load intensity surface. According to Eq.(4.2), if $n_{ij}d\sigma_{ij}>0$ the plastic flow is directed along outward normal to the plastic potential; if $n_{ij}d\sigma_{ij}=0$ there is no plastic flow; and if $n_{ij}d\sigma_{ij}<0$ the plastic flow is along inward normal to the plastic potential. As suggested in ref.[116], the magnitude of the parameter h_p is assumed to vary between $h_p \to 0$ at the instant of stress reversal(i.e. instantaneous elastic response) and a prescribed value h_B at a so-called conjugate stress point σ^{c}_{ij} on the maximum load intensity surface, Fig. 4.2. In the present study, the following

interpolation rule for h_p is adopted, i.e.

$$h_p = [h_B^{-1} + k(\delta/\delta_0)^n]^{-1} \tag{4.4}$$

where δ and δ_0 represent spatial angles between the stress tensor σ_{ij} and the conjugate stress tensor $\sigma^c{}_{ij}$, and between $\sigma^c{}_{ij}$ and the so-called datum stress tensor $\sigma^d{}_{ij}$, respectively. They are calculated according to

$$\delta = \cos^{-1}\frac{\sigma^c{}_{ij}\sigma_{ij}}{(\sigma^c{}_{ij}\sigma^c{}_{ij})^{1/2}(\sigma_{ij}\sigma_{ij})^{1/2}};$$

$$\delta_0 = \cos^{-1}\frac{\sigma^c{}_{ij}\sigma^d{}_{ij}}{(\sigma^c{}_{ij}\sigma^c{}_{ij})^{1/2}(\sigma^d{}_{ij}\sigma^d{}_{ij})^{1/2}} \tag{4.5}$$

with $\sigma^c{}_{ij}$ and $\sigma^d{}_{ij}$ given by

$$\sigma^c{}_{ij} = r_c s_{ij} + \frac{1}{3}\sigma_{kk}\delta_{ij}; \qquad \sigma^d{}_{ij} = r_d s_{ij} + \frac{1}{3}\sigma_{kk}\delta_{ij} \tag{4.6}$$

Here r_c and r_d represent radii of the conjugate and datum stress point as measured in the π-plane, respectively, i.e.

$$r_c = \frac{\beta(\xi)g(\theta)\bar{\sigma}_c}{\bar{\sigma}}; \qquad r_d = \frac{\beta(\xi)g(-\theta)\bar{\sigma}_c}{\bar{\sigma}}; \quad \text{for } n_{ij}d\sigma_{ij} \geq 0 . \tag{4.7}$$

For $n_{ij}d\sigma_{ij} < 0$, the definitions of r_c and r_d are interchanged with

each other. According to Eqs.(4.6) and (4.7) both the conjugate and the datum stress points are located on the maximum load intensity surface and σ^d_{ij} is coplanar with both σ_{ij} and σ^c_{ij}, Fig. 4.2. In Eq.(4.4) h_B is defined by

$$h_B = \left(\frac{\partial f}{\partial \sigma_{ij}} \frac{\partial f}{\partial \sigma_{ij}}\right)^{1/2} \left(\frac{\partial \Psi}{\partial \sigma_{ij}} \frac{\partial \Psi}{\partial \sigma_{ij}}\right)^{1/2} / H_p \tag{4.8}$$

where H_p is specified by Eq.(2.29). It should be emphasized here that the gradient tensors as well as H_p are all evaluated at the conjugate stress point. In order to account for the effect of stiffness degradation during cyclic loading and to avoid the ratchetting effect, the parameters k and Λ are selected in the following form

$$k = k_0 \exp(-\rho(\delta/\delta_0) \tag{4.9a}$$

and

$$\Lambda = \Lambda_0 + \bar{A}\xi \; ; \quad \rho = \rho_0 + \bar{A}\xi \tag{4.9b}$$

where k_0, Λ_0, ρ_0 and $\bar{A}$ are material constants. The value of k, Eq.(4.9a), is evaluated only at each stress reversal point and it remains constant during the subsequent loading history.

Instead of Eq.(4.4), an alternative expression for h_p is frequently used in plasticity, i.e.

$$h_p = h_B[1 - (\delta/\delta_0)]^{\Lambda} . \tag{4.10}$$

It should be pointed out here that Eq.(4.10) may cause premature failure of concrete in the course of cyclic loading. Therefore, implementation of the interpolation rule by Eq.(4.4) is strongly recommended.

In general, during a stress reversal process, the size of the maximum load intensity surface undergoes evolution determined by the incremental damage parameter given by

$$d\xi = \pm(d\bar{\varepsilon}^p/\bar{\Phi}_n) \quad . \tag{4.11}$$

It is postulated that the positive sign is associated with the condition $e_{ij}de^p_{ij}>0$, and $\bar{\Phi}_n$ is related to $\bar{\Phi}$, Eq.(2.10), through the following relation,

$$\bar{\Phi}_n = 1 - (1 - \bar{\Phi}) \frac{\langle \alpha' - \delta/\delta_0 \rangle}{\alpha'} \tag{4.12}$$

in which α' is a small positive number with the value in the range 0.05 to 0.1 determined through numerical simulations, and the symbol $\langle\ \rangle$ is defined by Eq.(2.18). Incorporation of Eq.(4.12), rather than Eq.(2.10), in the evolution law for the damage parameter ξ is based on the observation that for stress histories penetrating the interior of the maximum load intensity surface, Eq.(2.10) overestimates the influence of confining pressure on mechanical behaviour of concrete.

Finally, to complete the present formulation, assume the additivity between the elastic and plastic strain increments,

Eq.(2.25). Substitution of the flow rule, Eq.(4.2), into Eq.(2.25) yields

$$d\varepsilon_{ij} = (D^{e}_{ijkl})^{-1} d\sigma_{kl} + h_p \bar{n}_{ij} n_{kl} d\sigma_{kl} \quad . \tag{4.13}$$

Thus, the general constitutive relation is given by

$$d\varepsilon_{ij} = C_{ijkl} d\sigma_{kl} \tag{4.14}$$

where

$$C_{ijkl} = (D^{e}_{ijkl})^{-1} + h_p \bar{n}_{ij} n_{kl} \quad . \tag{4.15}$$

The inverse relation to Eq.(4.14) takes the following form

$$d\sigma_{ij} = (C_{ijkl})^{-1} d\varepsilon_{kl} \quad . \tag{4.16}$$

Equation (4.16) or (4.14) represents the constitutive relation that governs the response of concrete during stress reverse process, i.e. $df<0$.

4.4 Determination of Model Parameters

In this section the procedure for identification of model parameters is described. A detailed discussion on the identification procedure for the parameters defining the constitutive relation for initial monotonic loading history has been provided in Section 2.4. Here, emphasis is placed on the determination of the parameters

associated with the interpolation rule, Eqs.(4.4) and (4.9), for modelling the cyclic behaviour of concrete.

Equation(4.9), describing the evolution of parameter k, requires the specification of four constants, k_0, Λ_0, ρ_0 and $\bar{A}$. In general, the combination of the values of k_0, Λ_0 and ρ_0 controls the shape of hysteresis loops, whereas the value of constant $\bar{A}$ governs the progressive deterioration of stiffness during consecutive stress reversals. The parameters k_0, Λ_0 and ρ_0 should be determined numerically (e.g. trial and error procedure) by fitting the experimental data for a complete unloading-reloading program. Consider, for example, a typical uniaxial compression test involving a full stress cycle. At the instant of stress reversal the response of the material is elastic. To satisfy this requirement the parameter k_0 should be assigned a large value, $k_0 >> h_\beta$, so that at $\delta=\delta_0$ there is $h_p \to k^{-1} \to 0$. Given the value of k_0 (say between 10^9 to 10^{10} N/mm^2) the constant Λ_0 should be selected by fitting the unloading branch of hysteresis loop. At the next stress reversal point the parameter k is recalculated using Eq.(4.9a). An appropriate value of ρ_0 should now be chosen (typically $3\Lambda_0 \leq \rho_0 \leq 5\Lambda_0$) to have a proper simulation of the reloading branch (via initial reloading modulus and the width of hysteresis loop).

The value of parameter $\bar{A}$ can be obtained by simulating several stress-strain cycles up to a stage at which the stiffness degradation effect become pronounced. The number of cycles required to reach this

stage is determined by numerical simulations. It should be pointed out that the present approach to model stiffness degradation is more rational than that suggested in ref.[10] which attributes this effect to a progressive decay in elastic properties.

The number of parameters involved in the interpolation rule can be reduced by introducing some simplifications. As an example, the following equations may be used

$$k = k_0 10^{-\Lambda(\delta/\delta_0)} , \qquad \Lambda = \Lambda_0 + \bar{A}\xi \tag{4.17}$$

In this case the shape of hysteresis loop is determined by the values of two parameters only, i.e. k_0 and Λ_0. The effectiveness of Eq.(4.17) as compared to Eq.(4.9) is discussed in the next section.

4.5 Numerical Modelling of Cyclic Degradation Phenomenon

The proposed constitutive model has been applied to simulate the stress-strain response of concrete in typical uniaxial compression tests involving cyclic loading. For comparison purposes, the experimental results from ref.[112] are shown in Figs. 4.3(a) and 4.4(a), whereas the predictions from the proposed model are presented in Figs. 4.3(b) and 4.4(b), respectively. In these figures all stress and strain measures are normalized with respect to the uniaxial compressive strength, f_c', and the axial strain, ε_0 corresponding to

$\sigma_{l=f_c'}$, respectively. Fig. 4.3(b) shows the predictions for a strain-controlled test. The model reflects adequately a gradual decay in the resulting axial stress amplitude and a progressive degradation of the material stiffness in the course of cyclic loading. The numerical results are in very close agreement with the experimental data in Fig.4.3(a). In a stress-controlled loading program(Figs. 4.4(a) and 4.4(b)), a continuous accumulation of axial strain takes place leading eventually to failure of concrete. The predicted number of cycles to induce failure, for loadings between $\sigma_{max}=0.92f_c'$ and $\sigma_{min}=0.42f_c'$, is identical to that obtained experimentally.

The predictions presented in Figs. 4.3(b) and 4.4(b) are based on the interpolation rule defined by Eq.(4.9), whereas Figures 4.5(a) and 4.5(b) provide the predictions obtained using a simplified form, Eq.(4.17). As expected, Eq.(4.9) allows one to model more adequately the shape of individual hysteresis loops. In general, however, both series of predictions are qualitatively similar and remain in a fairly close agreement with experimental data.

In conclusion, a rate-independent constitutive model for concrete subjected to cyclic load conditions has been presented. An initial active loading process has been described using the conceptual framework outlined in Chapter 2. For subsequent stress reversals, a simple and numerically efficient formulation, which accounts for progressive degradation of concrete stiffness, has been proposed. It

has been shown that the model is capable of simulating various salient characteristics of concrete response in a wide range of initial confining pressures (in Chapter 2). It should be noted that in the present study the numerical verification of cyclic response has been restricted to typical uniaxial stress and strain-controlled cyclic loading histories due to lack of experimental data on general multiaxial cyclic loading conditions. However, the present formulation is developed based on most general loading conditions. It is expected that the proposed model will be equally applicable to other loading conditions.

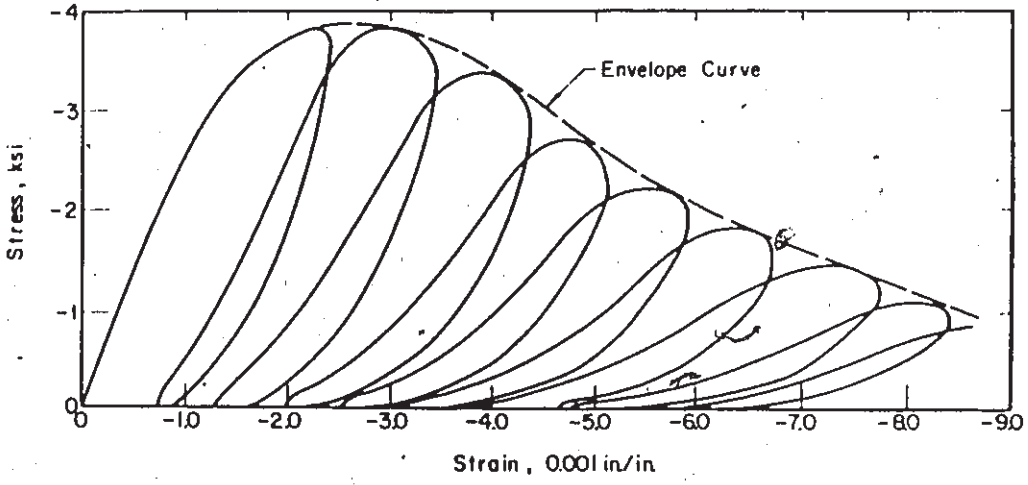

Fig. 4.1 Behaviour of Concrete under Cycles of Compressive Loading (ref.[110]).

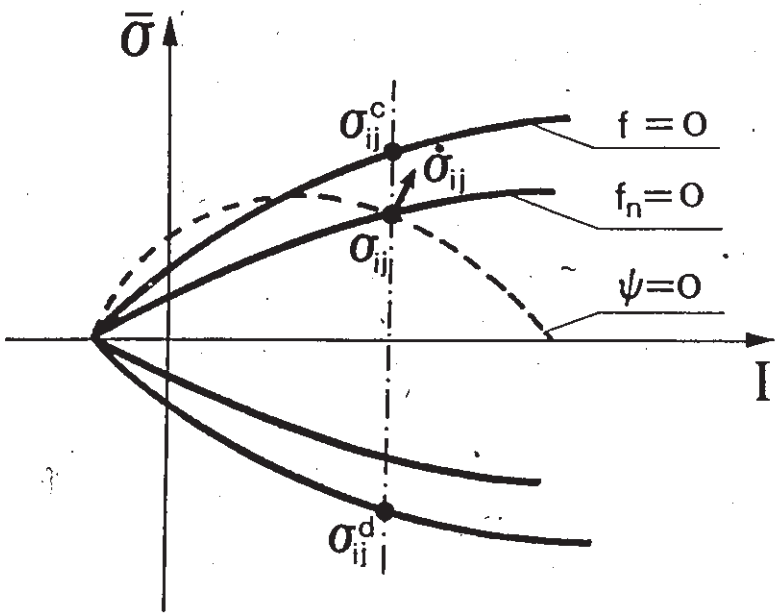

Fig. 4.2 , Meridional Section of Maximum Load Intensity Surface f=0 and Neutral Locus f_n=0.

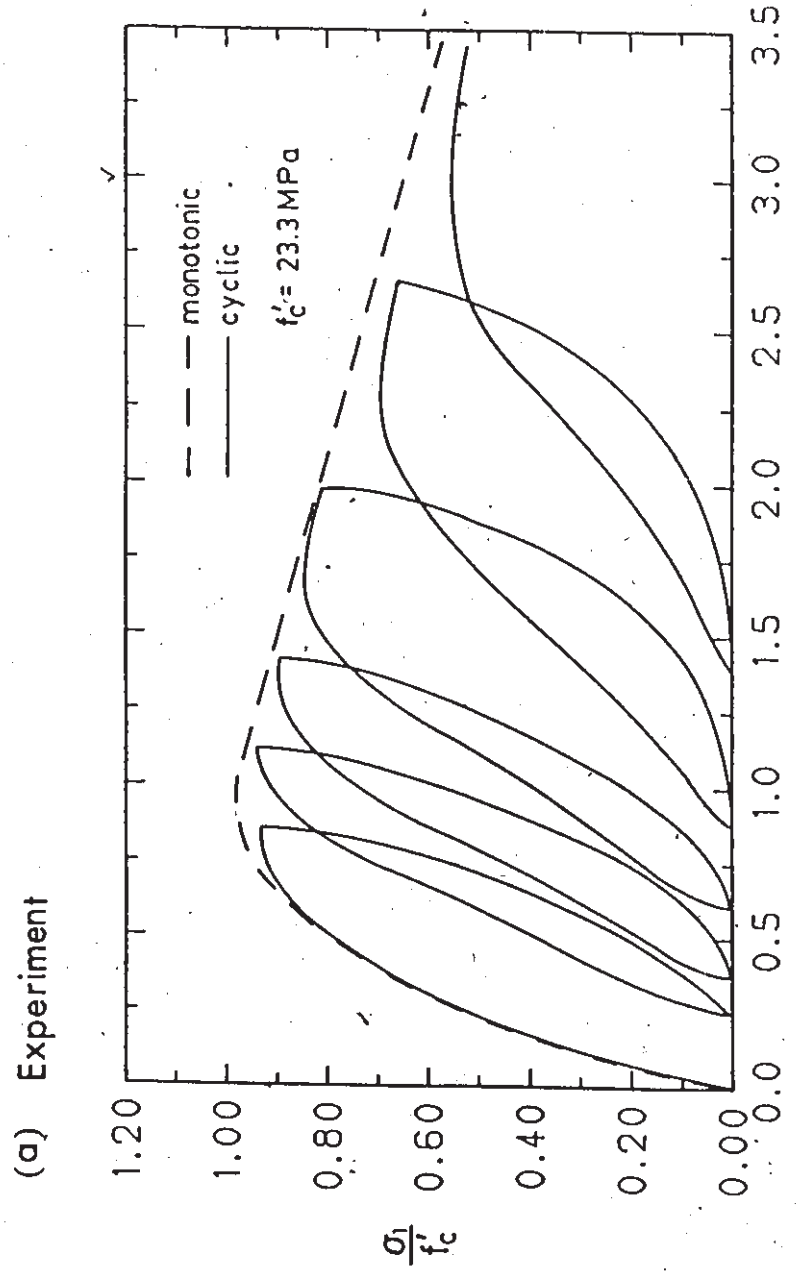
(a) Experiment
monotonic
cyclic
f'_c= 23.3 MPa
$\frac{\sigma_1}{f'_c}$
ϵ_1/ϵ_0
0.00
0.20
0.40
0.60
0.80
1.00
1.20
0.0
0.5
1.0
1.5
2.0
2.5
3.0
3.5

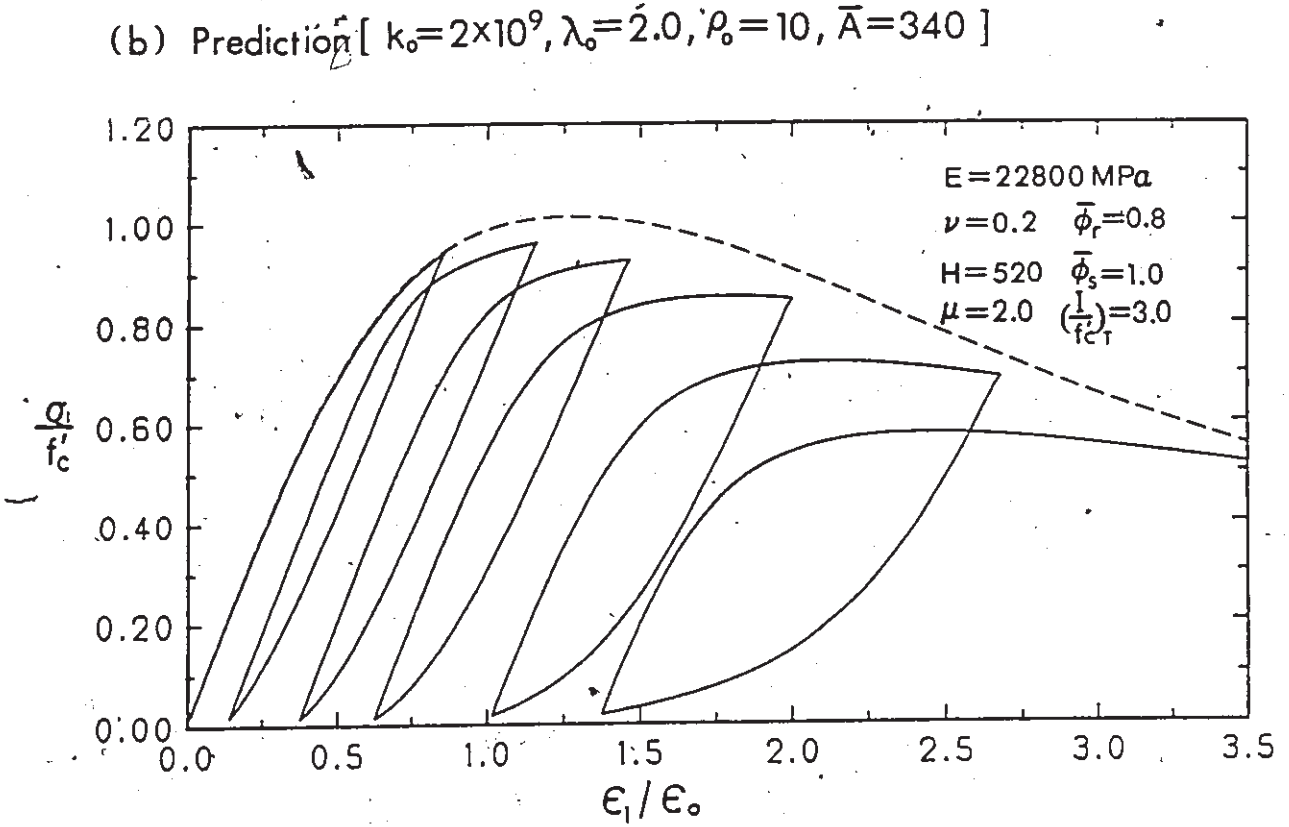

Fig. 4.3 *Concrete Stress-Strain Curve for a Strain-Controlled Uniaxial CompressionTest: (a) Experimental result; (b) Numerical Prediction.*

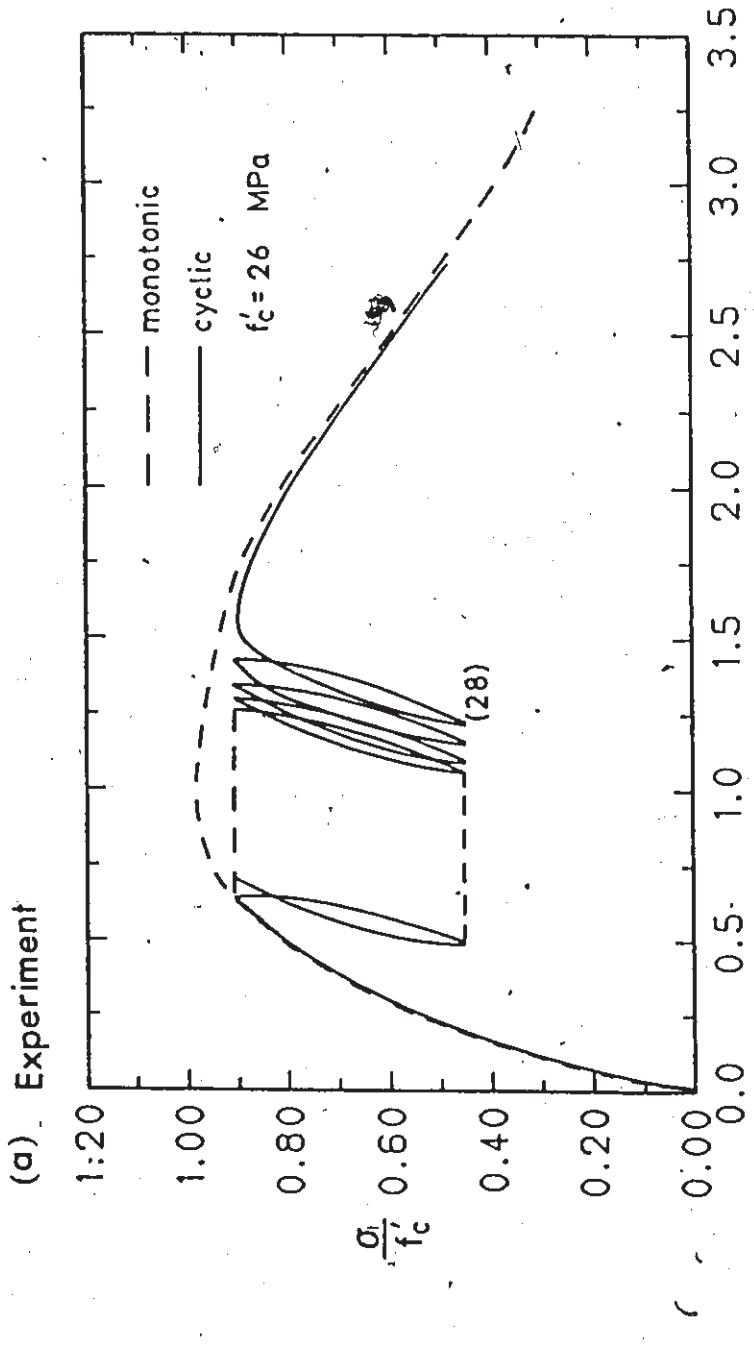
(a) Experiment
monotonic
cyclic
f'_c = 26 MPa
(28)
$\frac{\sigma_1}{f'_c}$
ϵ_1/ϵ_o
1:20
1.00
0.80
0.60
0.40
0.20
0.00
0.0
0.5
1.0
1.5
2.0
2.5
3.0
3.5

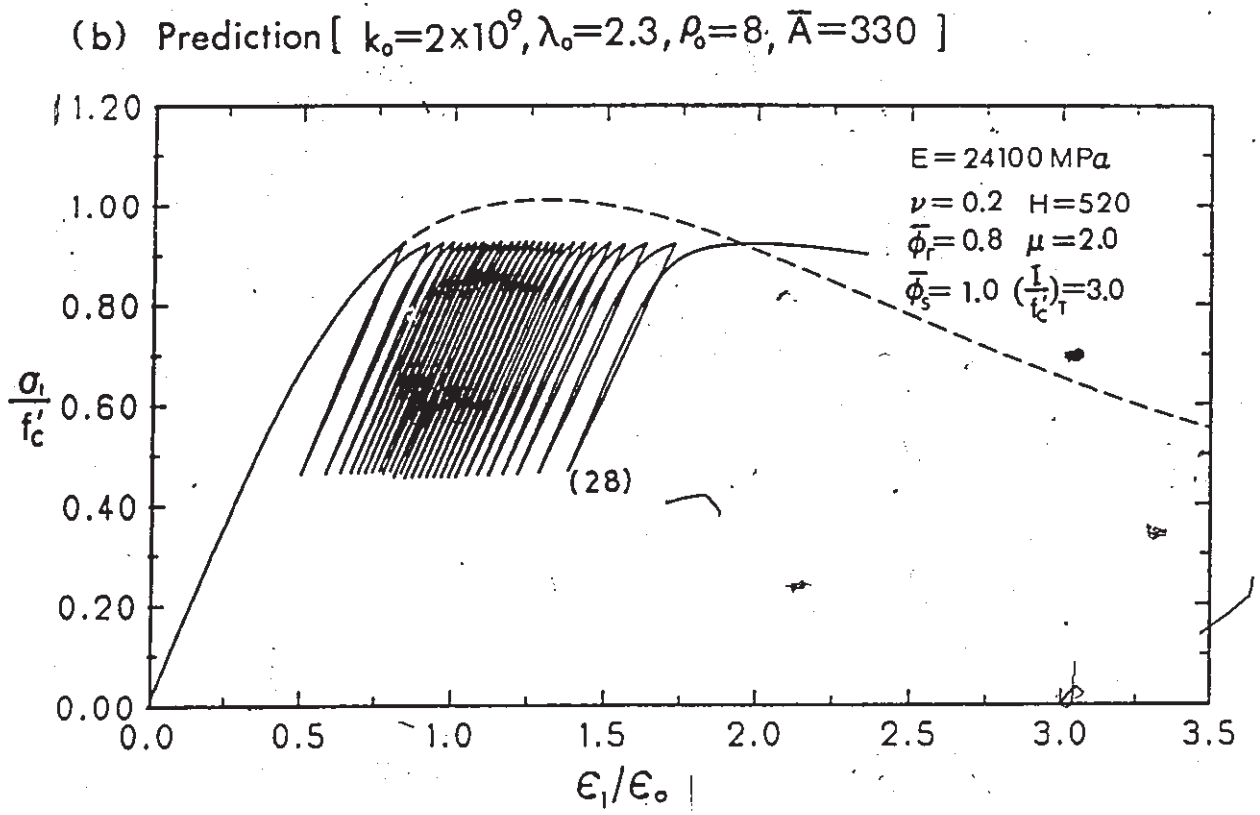

Fig. 4.4 Concrete Stress-Strain Curve for a Stress-Controlled Uniaxial Compression Test: (a) Experimental Result; (b) Numerical Prediction.

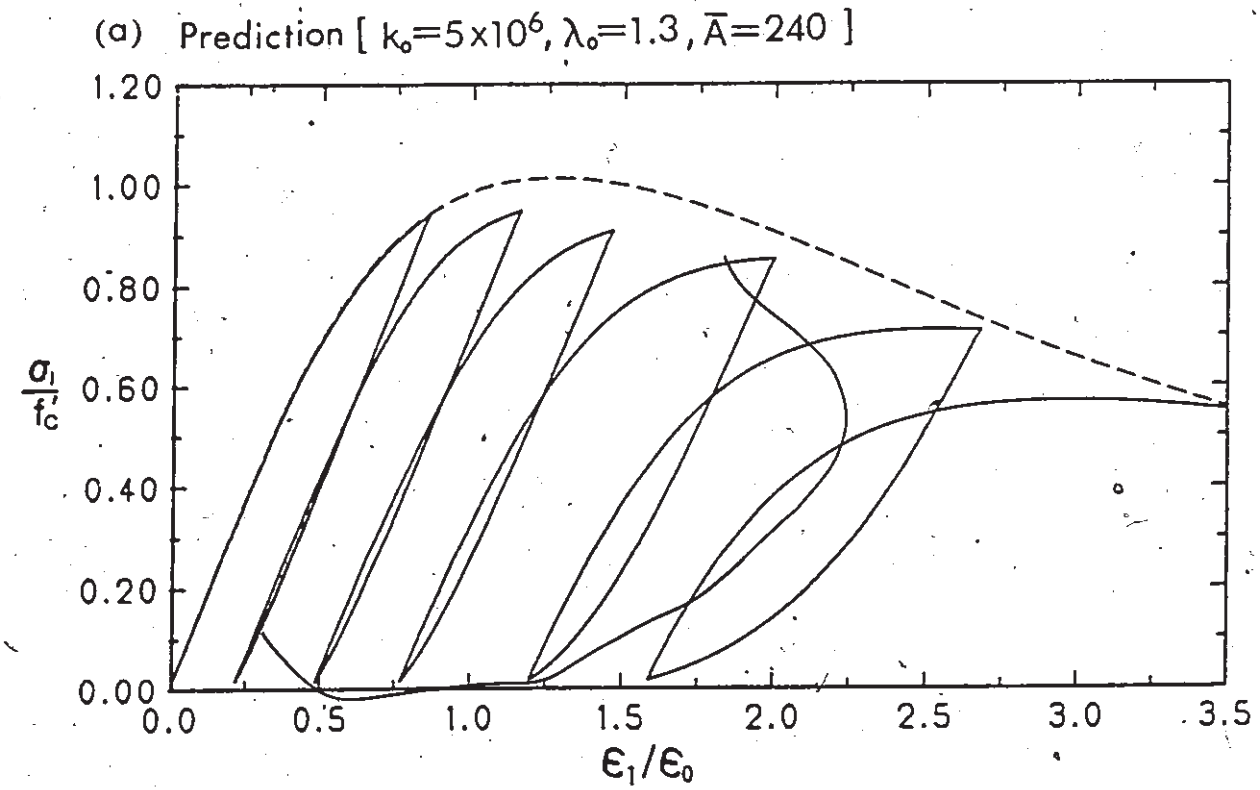
(a) Prediction [$k_o=5\times10^6$, $\lambda_o=1.3$, $\bar{A}=240$]
1.20
1.00
0.80
0.60
0.40
0.20
0.00
$\frac{\sigma_1}{f_c'}$
0.0
0.5
1.0
1.5
2.0
2.5
3.0
3.5
ϵ_1/ϵ_0

(b) Prediction [$k_o=5\times10^6$, $\lambda_o=1.2$, $\bar{A}=180$]

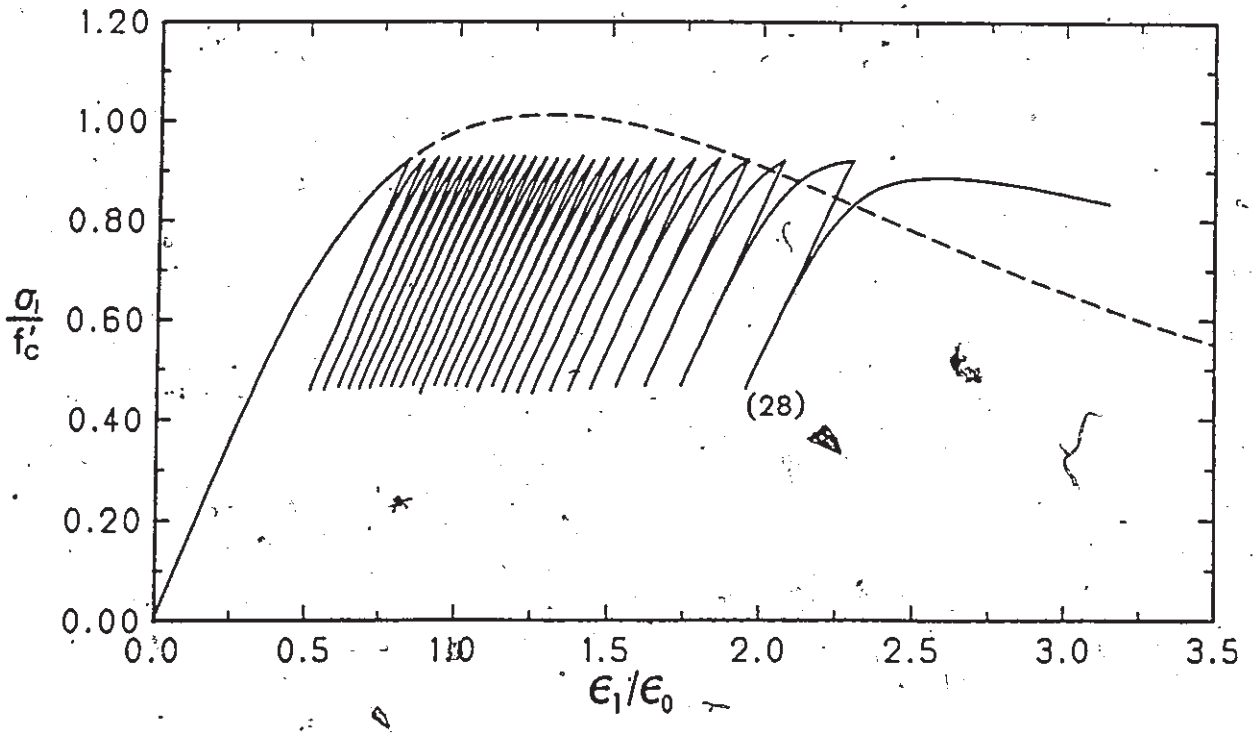

Fig. 4.5 Numerical Predictions for both the strain and Stress-Controlled Tests Using Simplified Interpopiation Rule, Eq.(4.13).

CHAPTER 5

BRITTLE-DUCTILE TRANSITION IN CONCRETE AS A BIFURCATION PROBLEM

5.1 Introduction

It was mentioned in Chapter 2 that the mechanical behaviour of concrete is largely influenced by the confining pressure. At high pressures the material displays a stable behaviour, as the confining pressure decreases a gradual transition from stable (ductile) to unstable (brittle) behaviour takes place. In Chapter 2 the onset of such unstable response was determined by a path-independent criterion. Although this approach can reasonably well simulate the strain softening response and the ductile-brittle transition, it is not a rigorous approach and further improvement is necessary.

In this chapter the initiation of strain softening response is considered as a bifurcation problem. Consequently, the ductile-brittle transition is determined from considerations of stability of the constitutive relations. In what follows, necessary conditions for bifurcation corresponding to strain localization are first derived. To examine whether the bifurcation is physically feasible, an additional condition for localization is postulated according to the concept of maximum second rate ($dW^p = d\sigma_{ij} d\varepsilon^p_{ij}$ or $\dot{\sigma}_{ij}\dot{\varepsilon}_{ij}$) of energy dissipation. Subsequently, some numerical examples are presented and

numerical prediction of ductile-brittle transition are discussed.

5.2 Necessary Condition for Strain Localization

The strain softening phenomenon in plain concrete is observed essentially in uniaxial compression/tension test under zero (or very low) confining pressures. It appears that the strain softening behaviour can be attributed to nonhomogeneous deformation resulting from macroscopic fracturing and sliding along asperities. In the present study, it is postulated that the strain softening phenomenon is the result of localization of deformation into a shear band. The initiation of such localization can be considered as a bifurcation problem, i.e. instability in the macroscopic constitutive description which admits inception of an alternative nonhomogeneous deformation mechanism. The theoretical background on the shear band localization was provided in refs.[117,118]. In the following, the necessary condition for strain localization in three dimensional configuration is derived. Both the compliance(ref.[119]) and the stiffness(ref.[120]) approaches are followed to predict the onset of strain localization. The resulting formulation is restricted to problems involving infinitesimal deformations which are relevant to many boundary value problems of practical interest.

Consider an isotropic and homogeneous sample with geometry defined in a rectangular Cartesian coordinate system $\{x_1, x_2, x_3\}$,

such that x_1, x_2 and x_3 directions coincide with the σ_1, σ_2 and σ_3 (principal stresses), respectively, as shown in Fig. 5.1. Next, consider another rectangular Cartesian coordinate system $\{x_1', x_2', x_3'\}$ along a hypothetical shear band within which the localization of deformation takes place. The transformation between the two sets of axes is given by

$$\begin{bmatrix} \hat{e}_1' \\ \hat{e}_2' \\ \hat{e}_3' \end{bmatrix} = \begin{bmatrix} t_1 & t_2 & t_3 \\ s_1 & s_2 & s_3 \\ n_1 & n_2 & n_3 \end{bmatrix} \begin{bmatrix} \hat{e}_1 \\ \hat{e}_2 \\ \hat{e}_3 \end{bmatrix} \tag{5.1}$$

where $\hat{e}_i'$ and $\hat{e}_i$ $(i=1,2,3)$ denote the unit vectors along the corresponding coordinate axes (Fig. 5.1); t_i, s_i and n_i $(i=1,2,3)$ represent the direction cosines of the x_1', x_2' and x_3' axes, respectively. According to the transformation law for second-order Cartesian tensors, the stress tensors in the two systems are related by

$$\begin{bmatrix} \sigma_1 & 0 & 0 \\ 0 & \sigma_2 & 0 \\ 0 & 0 & \sigma_3 \end{bmatrix} = \begin{bmatrix} t_1 & s_1 & n_1 \\ t_2 & s_2 & n_2 \\ t_3 & s_3 & n_3 \end{bmatrix} \begin{bmatrix} \sigma_{tt} & \sigma_{ts} & \sigma_{tn} \\ \sigma_{st} & \sigma_{ss} & \sigma_{sn} \\ \sigma_{nt} & \sigma_{ns} & \sigma_{nn} \end{bmatrix} \begin{bmatrix} t_1 & t_2 & t_3 \\ s_1 & s_2 & s_3 \\ n_1 & n_2 & n_3 \end{bmatrix}. \tag{5.2}$$

In matrix form, the transformation law is written as

$$\{\sigma\} = [T]\ \{\sigma^*\} \tag{5.3}$$

where $\{\sigma\}=\{\sigma_1,\sigma_2,\sigma_3\}^T$, $\{\sigma^*\}=\{\sigma_{tt},\sigma_{ss},\sigma_{nn},\ \sigma_{ts},\sigma_{ns},\sigma_{nt}\}^T$ and $[T]$ represents the transformation matrix

$$[T] = \begin{bmatrix} t_1^2 & s_1^2 & n_1^2 & 2t_1s_1 & 2n_1s_1 & 2n_1t_1 \\ t_2^2 & s_2^2 & n_2^2 & 2t_2s_2 & 2n_2s_2 & 2n_2t_2 \\ t_3^2 & s_3^2 & n_3^2 & 2t_3s_3 & 2n_3s_3 & 2n_3t_3 \end{bmatrix} \tag{5.4}$$

Likewise, the transformation law for strain rate vector is given by

$$\{\dot{\varepsilon}^*\} = [T]^T\ \{\dot{\varepsilon}\} \tag{5.5}$$

where $\{\dot{\varepsilon}\}=\{\dot{\varepsilon}_1,\dot{\varepsilon}_2,\dot{\varepsilon}_3\}^T$ and $\{\dot{\varepsilon}^*\}=\{\dot{\varepsilon}_{tt},\dot{\varepsilon}_{ss},\dot{\varepsilon}_{nn},\ \dot{\gamma}_{ts},\dot{\gamma}_{ns},\dot{\gamma}_{nt}\}^T$.

It is assumed that the initially uniform deformation field of the sample is described by an elastoplastic constitutive relation

$$\{\dot{\varepsilon}\} = [C]\ \{\dot{\sigma}\} \tag{5.6}$$

where $[C]$ represents the compliance matrix defined as

$$[C] = [C^e] + \frac{1}{H_p}\,[\bar{C}]\ . \tag{5.7}$$

In Eq.(5.7), $[C^e]$ is the elastic compliance, H_p denotes the hardening modulus, and $[\bar{C}]=\{\partial\Psi/\partial\sigma\}\{\partial f/\partial\sigma\}^T$ in which Ψ=constant and f=0

represent the plastic potential and the yield surface, respectively. Relative to $\{x_1', x_2', x_3'\}$ coordinate system, the constitutive relation, i.e. Eq.(5.6), takes the form

$$\{\dot{\varepsilon}^*\} = [C^*]\,\{\dot{\sigma}^*\} \tag{5.8}$$

where

$$[C^*] = [T]^T\,[C]\,[T]\ . \tag{5.9}$$

To seek conditions for which continued deformation of the material may result in the inception of a shear band, write the constitutive law in terms of differences between the stress and strain rates inside and outside the band (under the assumption of continuous bifurcation)

$$\{\Delta\dot{\varepsilon}^*\} = [C^*]\,\{\Delta\dot{\sigma}^*\} \tag{5.10}$$

where $\Delta\dot{\varepsilon}^*_{ij}=(\dot{\varepsilon}^*_{ij})_{inside}-(\dot{\varepsilon}^*_{ij})_{outside}$ and $\Delta\dot{\sigma}^*_{ij}=(\dot{\sigma}^*_{ij})_{inside}-(\dot{\sigma}^*_{ij})_{outside}$. The non-uniformities in the strain rate field are kinematically restricted to the form

$$\Delta\dot{\varepsilon}_{tt}=0, \qquad \Delta\dot{\varepsilon}_{ss}=0, \qquad \Delta\dot{\gamma}_{ts}=0\ . \tag{5.11}$$

At the same time stress equilibrium should continue to be satisfied at the onset of bifurcation. The equilibrium statement admits stress discontinuity only for the stress rates corresponding to the strain rates in Eq.(5.11), i.e. $\Delta\dot{\sigma}_{tt}\neq 0$, $\Delta\dot{\sigma}_{ss}\neq 0$ and $\Delta\dot{\sigma}_{ts}\neq 0$, otherwise

$$\Delta\dot{\sigma}_{nn}=0, \qquad \Delta\dot{\sigma}_{nt}=0, \qquad \Delta\dot{\sigma}_{ns}=0 \ . \tag{5.12}$$

Substituting constrains in Eqs.(5.11) and (5.12) into Eq.(5.10) yields

$$\begin{aligned}
\Delta\dot{\varepsilon}_{tt} &= C^{*}_{11}\Delta\dot{\sigma}_{tt} + C^{*}_{12}\Delta\dot{\sigma}_{ss} + C^{*}_{14}\Delta\dot{\sigma}_{ts} = 0 \\
\Delta\dot{\varepsilon}_{ss} &= C^{*}_{21}\Delta\dot{\sigma}_{tt} + C^{*}_{22}\Delta\dot{\sigma}_{ss} + C^{*}_{24}\Delta\dot{\sigma}_{ts} = 0 \\
\Delta\dot{\gamma}_{ts} &= C^{*}_{41}\Delta\dot{\sigma}_{tt} + C^{*}_{42}\Delta\dot{\sigma}_{ss} + C^{*}_{44}\Delta\dot{\sigma}_{ts} = 0 \ .
\end{aligned} \tag{5.13}$$

Since Eq.(5.13) is a set of linear, homogeneous equations in stress rates $\Delta\dot{\sigma}_{tt}$, $\Delta\dot{\sigma}_{ss}$ and $\Delta\dot{\sigma}_{ts}$, a non-trivial solution exists only if

$$\det \begin{bmatrix} C^{*}_{11} & C^{*}_{12} & C^{*}_{14} \\ C^{*}_{21} & C^{*}_{22} & C^{*}_{24} \\ C^{*}_{41} & C^{*}_{42} & C^{*}_{44} \end{bmatrix} = 0 \tag{5.14}$$

which is a necessary condition for bifurcation. According to Eq.(5.9), the coefficients of the transformed compliance matrix, appearing in Eq.(5.14), can be expressed as

$$C^{*}_{ij} = \{T_i\}^{T}\,[C]\,\{T_j\}, \quad (i,j=1,2,4) \ . \tag{5.15}$$

Here, $\{T_i\}$ and $\{T_j\}$ are vectors corresponding to the i^{th} and j^{th} columns of the transformation matrix [T] given by Eq.(5.4). Now introduce Eq.(5.7) into Eq.(5.15) to obtain

$$C^{*}_{ij} = \alpha^{e}_{ij} + \bar{\alpha}_{ij}/H_p \qquad (i,j=1,2,4) \tag{5.16}$$

where

$$\alpha^{e}_{ij} = \{T_i\}^T [C^e] \{T_j\} = \alpha^{e}_{ji}$$
$$\bar{\alpha}_{ij} = \{T_i\}^T [\bar{C}] \{T_j\} . \tag{5.17}$$

It should be noted that in Eq.(5.17) α^{e}_{ij} is different from the corresponding element C^{e}_{ij} in the matrix $[C^e]$ because α^{e}_{ij} and C^{e}_{ij} are referred to different stress spaces, i.e. α^{e}_{ij} is related to the $\{\sigma^*\}$ (six-dimensional) space while C^{e}_{ij} to the $\{\sigma\}$ (three-dimensional) space.

By expanding the determinant in Eq.(5.14), utilizing Eq.(5.16), and after some algebraic manipulations, the following cubic equation for the hardening modulus H_p is obtained

$$B_1 H_p^3 + B_2 H_p^2 + B_3 H_p + B_4 = 0 \tag{5.18}$$

where coefficients B_1, B_2, B_3 and B_4, which depend on the values of α^{e}_{ij} and $\bar{\alpha}_{ij}$, are provided in Appendix E.

Equation(5.18) relates the hardening modulus at the inception of strain localization to the elastic compliance, the prevailing stress-state and the orientation of the shear band. For an assumed

orientation of the shear band, the following conditions of orthonormality are always satisfied

(i) normality conditions

$$t_i t_i = 1, \quad s_i s_i = 1, \quad n_i n_i = 1 \tag{5.19}$$

(ii) orthogonality conditions

$$t_i s_i = 0, \quad t_i n_i = 0, \quad s_i n_i = 0 \ . \tag{5.20}$$

To seek the critical value of H_p at which the strain localization takes place, the above conditions have to be incorporated into Eq.(5.18). As a result, the critical (or maximum) value of H_p depends only on the two variables t_1 and t_2. The closed-form solution to this type of problem seems to be impossible due to nonlinearity of Eq.(5.18). Hence, the solution can only be obtained by numerical techniques, e.g. ref.[121]. In fact, this solution explicitly provides the necessary condition for strain localization. This comprises the orientation of the critical plane of localization and the critical value of the hardening modulus. If the actual value of H_p from Eq.(2.29) becomes less than or equal to the critical value of H_p, the bifurcation to a non-uniform mode involving the inception of a shear band is said to be possible. It should be noted that components of the unit normal to the plane of localization (n_1, n_2, n_3) can be evaluated by the cross product of $\hat{e}_1'$ and $\hat{e}_2'$, i.e. $\hat{e}_3' = e_1' \times \hat{e}_2'$, leading to the following

$$n_1 = t_2 s_3 - t_3 s_2, \quad n_2 = t_3 s_1 - t_1 s_3, \quad n_3 = t_1 s_2 - t_2 s_1 \ . \tag{5.21}$$

Next, Consider briefly an alternative way of formulating the necessary condition for bifurcation, i.e. using the stiffness approach. Adopting Eq.(5.2), one can write the inverse transformation of the stress vector as

$$\{\sigma^*\} = [\bar{T}]\ \{\sigma\} \tag{5.22}$$

where $\{\sigma\}$ and $\{\sigma^*\}$ are the same as defined in Eq.(5.3), and $[\bar{T}]$ represents the transpose of the matrix $[T]$ in Eq.(5.4) as

$$[\bar{T}] = \begin{bmatrix} t_1^2 & t_2^2 & t_3^2 \\ s_1^2 & s_2^2 & s_3^2 \\ n_1^2 & n_2^2 & n_3^2 \\ t_1 s_1 & t_2 s_2 & t_3 s_3 \\ n_1 s_1 & n_2 s_2 & n_3 s_3 \\ n_1 t_1 & n_2 t_2 & n_3 t_3 \end{bmatrix} \tag{5.23}$$

The constitutive relation in $\{x_1', x_2', x_3'\}$ system can be written as

$$\{\dot{\Delta\sigma}^*\} = [D^*]\ \{\dot{\Delta\varepsilon}^*\} \tag{5.24}$$

where

$$[D^*] = [\bar{T}]\ [D]\ [\bar{T}]^T \tag{5.25}$$

In Eq.(5.25), $[D]$ represents the stiffness matrix as defined in Eq.(2.31). At the inception of shear band, the equilibrium condition, Eq.(5.11), and the strain compatibility, Eq.(5.12), must be satisfied.

This leads to the following equations

$$\begin{aligned}
\Delta\dot{\sigma}_{nn} &= D^{*}_{33}\Delta\dot{\varepsilon}_{nn} + D^{*}_{35}\Delta\dot{\gamma}_{ns} + D^{*}_{36}\Delta\dot{\gamma}_{nt} = 0 \\
\Delta\dot{\sigma}_{nt} &= D^{*}_{53}\Delta\dot{\varepsilon}_{nn} + D^{*}_{55}\Delta\dot{\gamma}_{ns} + D^{*}_{56}\Delta\dot{\gamma}_{nt} = 0 \\
\Delta\dot{\sigma}_{ns} &= D^{*}_{63}\Delta\dot{\varepsilon}_{nn} + D^{*}_{65}\Delta\dot{\gamma}_{ns} + D^{*}_{66}\Delta\dot{\gamma}_{nt} = 0
\end{aligned} \tag{5.26}$$

Using the same argument as adopted for Eq.(5.13), the necessary condition for bifurcation is now given by

$$\det \begin{bmatrix} D^{*}_{33} & D^{*}_{35} & D^{*}_{36} \\ D^{*}_{53} & D^{*}_{55} & D^{*}_{56} \\ D^{*}_{63} & D^{*}_{65} & D^{*}_{66} \end{bmatrix} = 0 \tag{5.27}$$

The procedure for solving this equation in terms of the orientation of the critical plane of localization and the critical value of the hardening modulus is essentially the same as that used for Eq.(5.14). However, it is expected that the numerical solution to Eq.(5.27) will be more time-consuming than that for Eq.(5.14).

5.3 Condition for Determination of Bifurcation Paths

As already mentioned, the criterion (5.14) or (5.27) represents only the necessary condition for the inception of strain localization. In general, at a bifurcation point, two deformation mechanisms, i.e. continued homogeneous or nonhomogeneous mode of deformation, are possible. To determine which of the deformation modes is feasible, an additional condition for strain localization should be provided. In the following, such a condition is formulated based on comparison of second rates of energy dissipation in the two alternate modes.

Consider the case when the condition in Eq.(5.14) or Eq.(5.27) is satisfied, i.e. the material is at the potential inception of strain localization. Now calculate the second rate of energy dissipation for the two possible modes as shown in Fig. 5.2, i.e.

$$\dot{dW}^p = \dot{\sigma}_{ij}\dot{\varepsilon}^p_{ij} \tag{5.28}$$

After substituting the constitutive relations, Eq.(2.31), and the flow rule, Eq.(2.12), into Eq.(5.28), the following is obtained

$$\dot{dW}^p = \frac{\dot{\omega}_1}{H_e+H_p}\left(\omega_2 - \frac{\omega_1\omega_3}{H_e+H_p}\right) \tag{5.29}$$

where

$$\omega_1 = (\partial f/\partial\sigma_{ij})D^e_{ijkl}d\varepsilon_{kl}$$

$$\omega_2 = (\partial\Psi/\partial\sigma_{ij})D^e_{ijkl}d\varepsilon_{kl}$$

$$\omega_3 = (\partial\Psi/\partial\sigma_{ij})D^e_{ijkl}(\partial\Psi/\partial\sigma_{kl}) \qquad (5.30)$$

and H_e, H_p are given in Eq.(2.29); D^e_{ijkl} represents the elastic constitutive tensor.

Let $(d\dot{W}^p)_H$ & $(d\dot{W}^p)_S$ represent the second rate of energy dissipation along the homogeneous deformation path (i.e. hardening path) and the non-homogeneous deformation path (i.e. softening path), respectively. It is now postulated that if the absolute value of $(d\dot{W}^p)_H$ is greater than that of $(d\dot{W}^p)_S$, the material maintains its stable response (i.e. associated with homogeneous deformation); otherwise the strain localization takes place (i.e. deformation of the material is no longer uniform). To express this postulate mathematically, the following inequality is obtained

$$\left|(d\dot{W}^p)_H\right| - \left|(d\dot{W}^p)_S\right| > 0 \; . \qquad (5.31)$$

It is known that for the hardening path, $H_p>0$ and $(d\dot{W}^p)_H>0$; whereas for the softening path, $H_p<0$ and $(d\dot{W}^p)_S<0$. As a consequence, Inequality (5.31) can be replaced by

$$(d\dot{W}^p)_H + (d\dot{W}^p)_S > 0 \qquad (5.32)$$

In this study, the above inequality is considered as the additional condition for strain localization. In the next section, this condition is used (in conjunction with the necessary condition (5.14)) to describe the brittle-ductile transition in concrete as a bifurcation problem.

5.4 Description of Brittle-Ductile Transition as a Bifurcation Problem

It has been indicated in Chapter 2 that the mechanical response of concrete is largely influenced by the value of confining pressure. At relatively high pressures, concrete displays a stable behaviour. As the confining pressure decreases, a gradual transition from ductile to brittle behaviour takes place. Where in the brittle regime, concrete exhibits an unstable response, i.e. strain softening phenomenon. In the previous discussion in this chapter, onset of this phenomenon has been considered as a bifurcation problem. Now, by employing both the necessary and additional condition for strain localization, the brittle-ductile transition can also be treated as a bifurcation problem.

Consider the mechanical response of concrete during an active loading process. Initially, concrete deforms in a homogeneous manner. As the deformation progresses, the plastic deformation accumulates and the hardening modulus H_p decreases. When the value of H_p reduces to its critical value $(H_p)_{cr}$ obtained from condition in Eq.(5.14), concrete is

at the potential inception of unstable (brittle) response. If the condition in Eq.(5.32) is also satisfied, the stable response continues. However, if Inequality(5.32) is violated, the unstable deformation commences.

Following Eq.(2.29), the hardening modulus H_p can be written in the following form

$$H_p = \bar{H}_p \frac{d\beta}{d\xi} \tag{5.33}$$

where

$$\bar{H}_p = -\frac{\partial f}{\partial \beta}\left(\text{dev}\frac{\partial \Psi}{\partial \sigma_{ij}}\right)\text{dev}\frac{\partial \Psi}{\partial \sigma_{ij}}\Big)/\bar{\Phi} \,. \tag{5.34}$$

Assume that the current state of stress is at the bifurcation point, i.e. the necessary condition (5.14) has been satisfied. At this point, the value of $\bar{H}_p$ is fixed while the value of $d\beta/d\xi$ depends on the path selected,

$$\left(\frac{d\beta}{d\xi}\right)_{\xi=\xi_f} = \begin{cases} \dfrac{A}{(A+B\xi_f)^2} & \text{for hardening path} \\ -C\beta_f\bar{\Phi}_r & \text{for softening path} \,. \end{cases} \tag{5.35}$$

Introducing Eqs.(5.34) and (5.35) directly into Eq.(5.29) yields

$$(dW^p)_H = \frac{\omega_1}{H_e + \dfrac{A\bar{H}_p}{(A+B\xi_f)^2}}\left[\omega_2 - \frac{\omega_1\omega_3}{H_e + \dfrac{A\bar{H}_p}{(A+B\xi_f)^2}}\right]$$

and (5.36)

$$(dW^p)_S = \frac{\omega_1'}{H_e + C\beta_f\bar{\phi}_r\bar{H}_p}\left[\omega_1' - \frac{\omega_1'\omega_3}{H_e + C\beta_f\bar{\phi}_r\bar{H}_p}\right] .$$

After substitution of the above results into Inequality(5.32), the following inequality is obtained

$$\lambda^2 - \frac{\omega_2'}{\omega_1'\omega_3}\lambda - \frac{(dW^p)_H}{(\omega_1')^2\omega_3} < 0 \qquad (5.37)$$

where

$$\lambda = \frac{1}{(H_e - C\beta_f\bar{\phi}_r\bar{H}_p)} . \qquad (5.38)$$

It is clear from the inequality above that a stable response requires

$$\lambda < \lambda_c \qquad (5.39)$$

where

$$\lambda_c = \frac{1}{2}\left[\frac{\omega_2'}{\omega_1'\omega_3} + \sqrt{\left(\frac{\omega_2'}{\omega_1'\omega_3}\right)^2 + \frac{4(dW^p)_H}{(\omega_1')^2\omega_3}}\right] . \qquad (5.40)$$

In view of the definition of λ, Eq.(5.38), Inequality(5.39) implies that

$$C < C_{cr} = \frac{\lambda_c H_e - 1}{\lambda_c \beta_f \bar{\phi}_r \bar{H}_p} \tag{5.41}$$

where C is a constant which controls the rate of strain softening and is evaluated by

$$C = \bar{\phi}_3 H/[a_3+(I/f_c')_f]^u \ . \tag{5.42}$$

It should be noted that the equation above is just a simplification of Eq.(2.17) and all the definitions for the parameters involved here are exactly the same as those for Eq.(2.17).

Now, that Inequality(5.41) is an explicit condition for a stable response, an unstable response must take place if it is violated in such a way that $C>C_{cr}$. Then, it is obvious that the brittle-ductile transition is reached when the condition of $C=C_{cr}$ is satisfied. In other words, the brittle-ductile transition can be determined simply by comparing the value of C from Eq.(2.17) with that of C_{cr}. When the brittle-ductile transition stage is reached (i.e. $C=C_{cr}$), the value of $(I/f_c')_f$ obtained at this instant represents the normalized transition pressure. It should be noted that although, the transition pressure is obtained as part of the numerical solution, it can also be treated as a material parameter when such information is available.

5.5 Numerical Examples

The proposed bifurcation concept is now applied to simulate the response of concrete subjected to uniaxial compression under constant confining pressure. For this 'triaxial' loading configuration, the necessary condition for bifurcation, as defined by Eq.(5.14), can now be simplified. This is because the bifurcation analysis becomes a two dimensional problem, Fig. 5.3. Generally, at the inception of a shear band in a two dimensional case, the following conditions must be satisfied in order to maintain equilibrium and strain compatibility,

$$\Delta\dot{\sigma}_{nn} = 0, \quad \Delta\dot{\sigma}_{nt} = 0$$

$$\Delta\dot{\varepsilon}_{tt} = 0, \quad \Delta\dot{\varepsilon}_{ss} = 0 \tag{5.43}$$

But, for the uniaxial compression test under constant confining pressure, it has been found that the critical value of H_p obtained from the conditions in Eq.(5.43) is less than zero. This implies that the bifurcation mode associated with Eq.(5.43) is unlikely. An alternative mode, which should be considered, is that associated with the following additional constraint

$$\Delta\dot{\sigma}_{ss} = 0 \ . \tag{5.44}$$

Now, using the conditions in Eqs.(5.43) and (5.44), and following the same procedure as adopted for the three dimensional formulation, an explicit criterion for strain localization is obtained, i.e.

$$H_p \leq (H_p)_{cr} = \frac{E}{2(1-\upsilon^2)} \left[-a + \sqrt{a^2 - (1-\upsilon^2)b}\right] \tag{5.45}$$

where

$$a = \frac{\partial \Psi}{\partial \sigma_1}\frac{\partial f}{\partial \sigma_1} + \frac{\partial \Psi}{\partial \sigma_3}\frac{\partial f}{\partial \sigma_3} + \upsilon\left(\frac{\partial \Psi}{\partial \sigma_1}\frac{\partial f}{\partial \sigma_3} + \frac{\partial \Psi}{\partial \sigma_3}\frac{\partial f}{\partial \sigma_1}\right)$$

$$b \leq 4\left(\frac{\partial \Psi}{\partial \sigma_1}\frac{\partial f}{\partial \sigma_1}\right)\left(\frac{\partial \Psi}{\partial \sigma_3}\frac{\partial f}{\partial \sigma_3}\right) - \left(\frac{\partial \Psi}{\partial \sigma_1}\frac{\partial f}{\partial \sigma_3} + \frac{\partial \Psi}{\partial \sigma_3}\frac{\partial f}{\partial \sigma_1}\right)^2 . \tag{5.46}$$

The inclination of two potential shear bands with respect to the σ_3-axis is determined by

$$\theta_0 = \pm \tan^{-1}\sqrt{\frac{2\upsilon(H_p)_{cr} - E\left(\frac{\partial \Psi}{\partial \sigma_1}\frac{\partial f}{\partial \sigma_3} + \frac{\partial \Psi}{\partial \sigma_3}\frac{\partial f}{\partial \sigma_1}\right)}{2\left[(H_p)_{cr} + E\frac{\partial \Psi}{\partial \sigma_1}\frac{\partial f}{\partial \sigma_1}\right]}} . \tag{5.47}$$

It should be emphasized here that the criterion above is only valid for the uniaxial compression test under constant confining pressure. A similar formulation applicable to plane strain uniaxial compression test, which corresponds to Eq.(5.43) alone, is presented in Appendix E.

Consider a concrete sample, with the set of material parameters specified in Fig. 5.4, subjected to uniaxial compression under various

initial confining pressures. As mentioned before, at the low confining pressure, the element may exhibit a brittle response as induced by the strain localization. But, if the confining pressure is relatively high, the strain localization may not occur at all. This pressure-dependent behaviour is now numerically simulated by the proposed concept. The inception of strain localization (or strain softening response) is determined by the conditions in Eqs.(5.45) and (5.41). The numerical results are presented in Figs. 5.4 and 5.5 and the corresponding values of $(H_p)_{cr}$, θ_0 and C_{cr} for different initial confining pressures are summarized in Table 5.1. It should be noted that Fig. 5.4(a) shows the deviatoric characteristics by plotting β vs. $\bar{\varepsilon}^p$ while Fig. 5.4(b) presents the uniaxial stress vs. uniaxial strain diagrams.

For the material parameters selected, it is clear from Fig. 5.4 (a) or (b) that the brittle-ductile transition takes place at the initial pressure between -20MPa and -30MPa. In order to locate this transition point, the trial and error technique has been applied to search for the case when the condition of $C=C_{cr}$ is satisfied. The numerical analysis shows that the transition occurs when the concrete sample is loaded from the initial pressure of -20.845MPa. The predicted brittle-ductile transition pressure is -162.13MPa. It appears that this transition is a function of the initial confining pressure.

Figs. 5.5(a) and 5.5(b) present the numerical results corresponding to two possible deformation modes in the post-bifurcation regime. In these figures, the solid lines represent the response for a

continued homogeneous deformation mode while the dash lines are associated with a shear band localization mechanism. As can be seen from Fig. 5.5(a), at the bifurcation point, the rate of hardening is more or less equal to the rate of softening. This implies that the proposed condition for localization, i.e. Inequality(5.32) can be approximated by

$$(\partial\beta/\partial\bar{\varepsilon}^p)_H > (\partial\beta/\partial\bar{\varepsilon}^p)_S \tag{5.48}$$

where the subscripts H and S denote the strain hardening and softening paths, respectively. The adoption of this inequality means that the contribution of hydrostatic stress to the second rate of energy dissipation in this case is negligible. It can also be seen from Fig. 5.5(b) that the brittle-ductile transition takes place in the compaction domain. Theoretically, however, the transition may occur in the dilation domain as well. At the present time, there is a lack of experimental information concerning the value of transition pressure and the corresponding volumetric deformation characteristics. It is certain that such information is very important for completely understanding the bifurcation behaviour of concrete.

TABLE 5.1 Values of Various Parameters at the Bifurcation

$P_0=\sigma_{ii}/3$ (MPa)	$(H_p^*)_{cr}$ (MPa)	θ_0 (Deg.)	C_{cr}	ξ_f (10^{-4})	$(I/f_c')_f$
0.0	2766.04	46.75	-1846.62	6.44	0.789
-10.0	2013.41	44.27	44.59	4.74	2.025
-20.0	1664.34	42.86	272.71	4.03	3.040
-30.0	1442.63	41.9	419.33	3.65	3.970

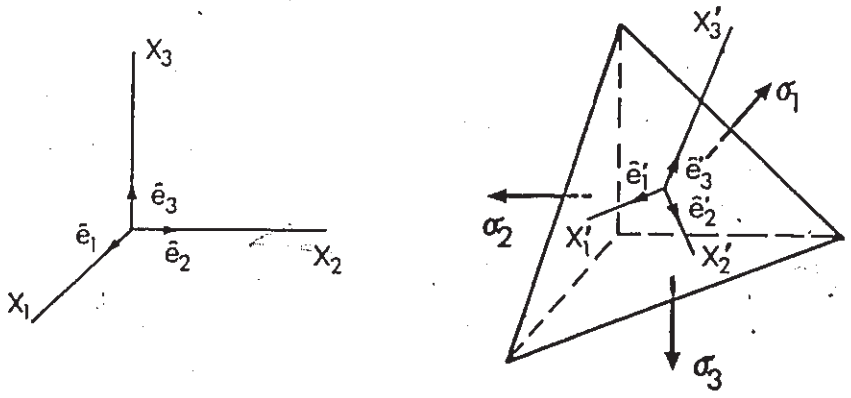

Fig. 5.1 Two Cartesian Coordinate Systems.

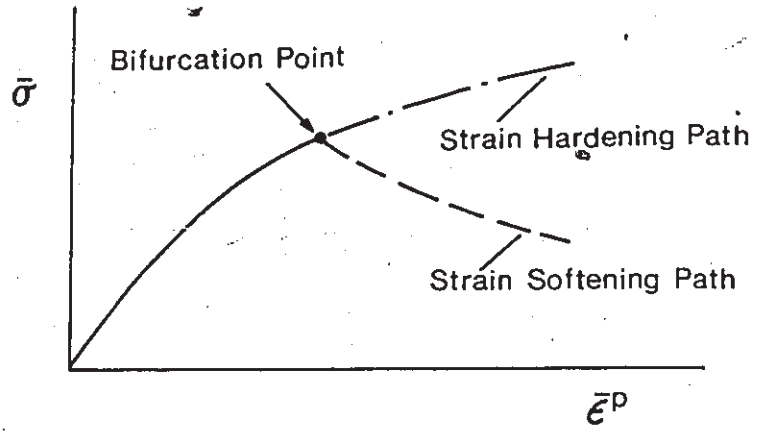

Fig. 5.2 Two Possible Deformation Modes at a Bifurcation Point.

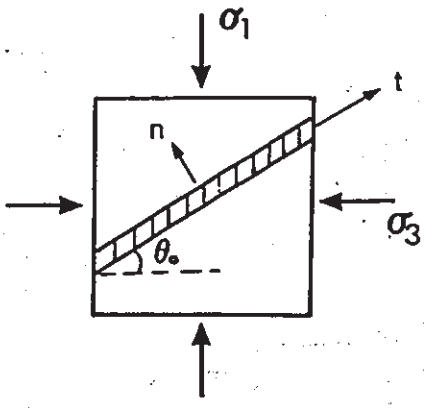

Fig. 5.3 Shear Band Orientation with Respect to Global Frame of Reference in Two Dimensional Situation.

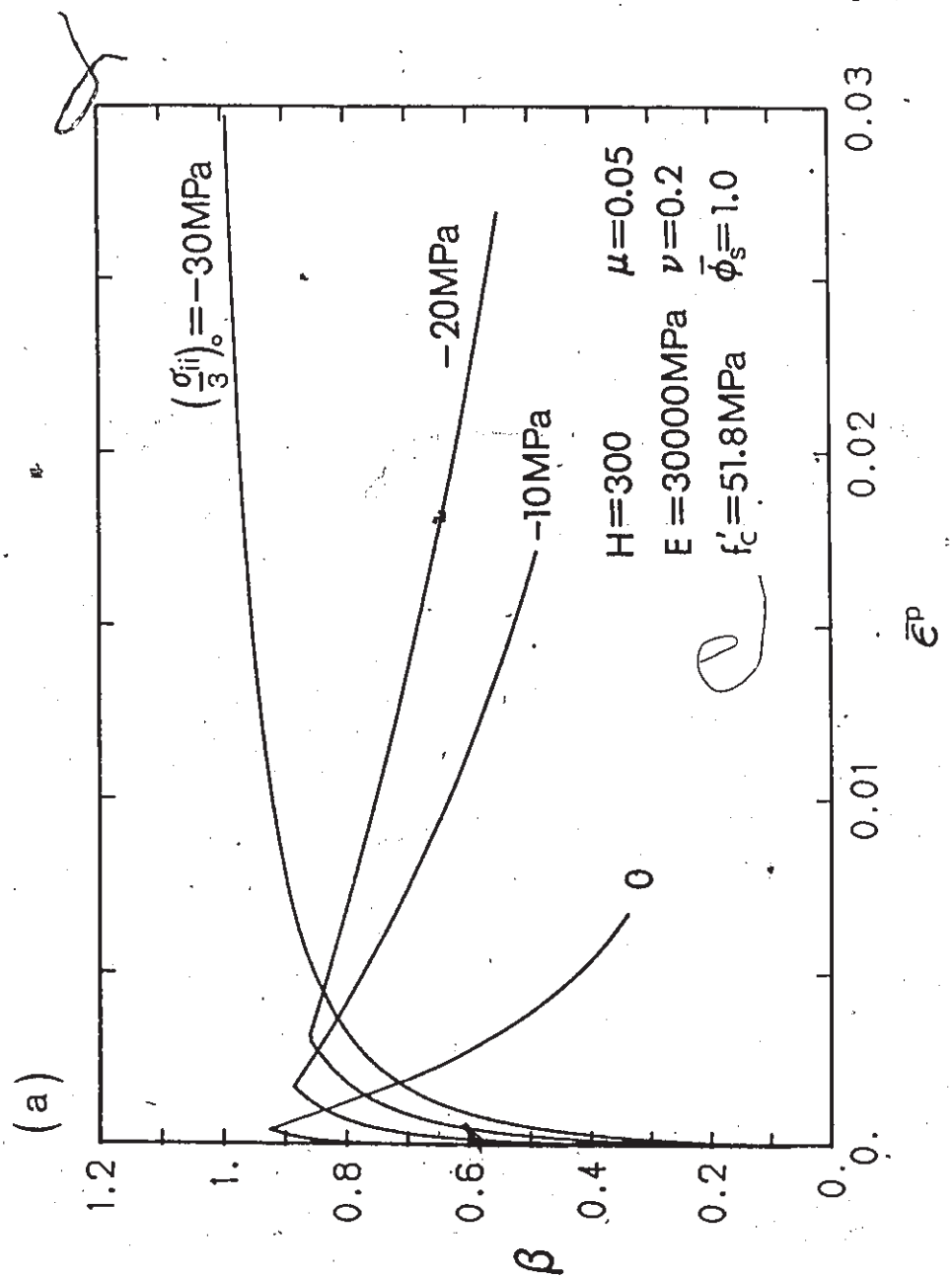
(a)
$(\frac{\sigma_{ii}}{3})_o$=−30MPa
−20MPa
−10MPa
0
H=300
E=30000MPa
f'_c=51.8MPa
μ=0.05
ν=0.2
$\bar{\phi}_s$=1.0
β
$\bar{\epsilon}^p$
1.2
1.
0.8
0.6
0.4
0.2
0.
0.01
0.02
0.03

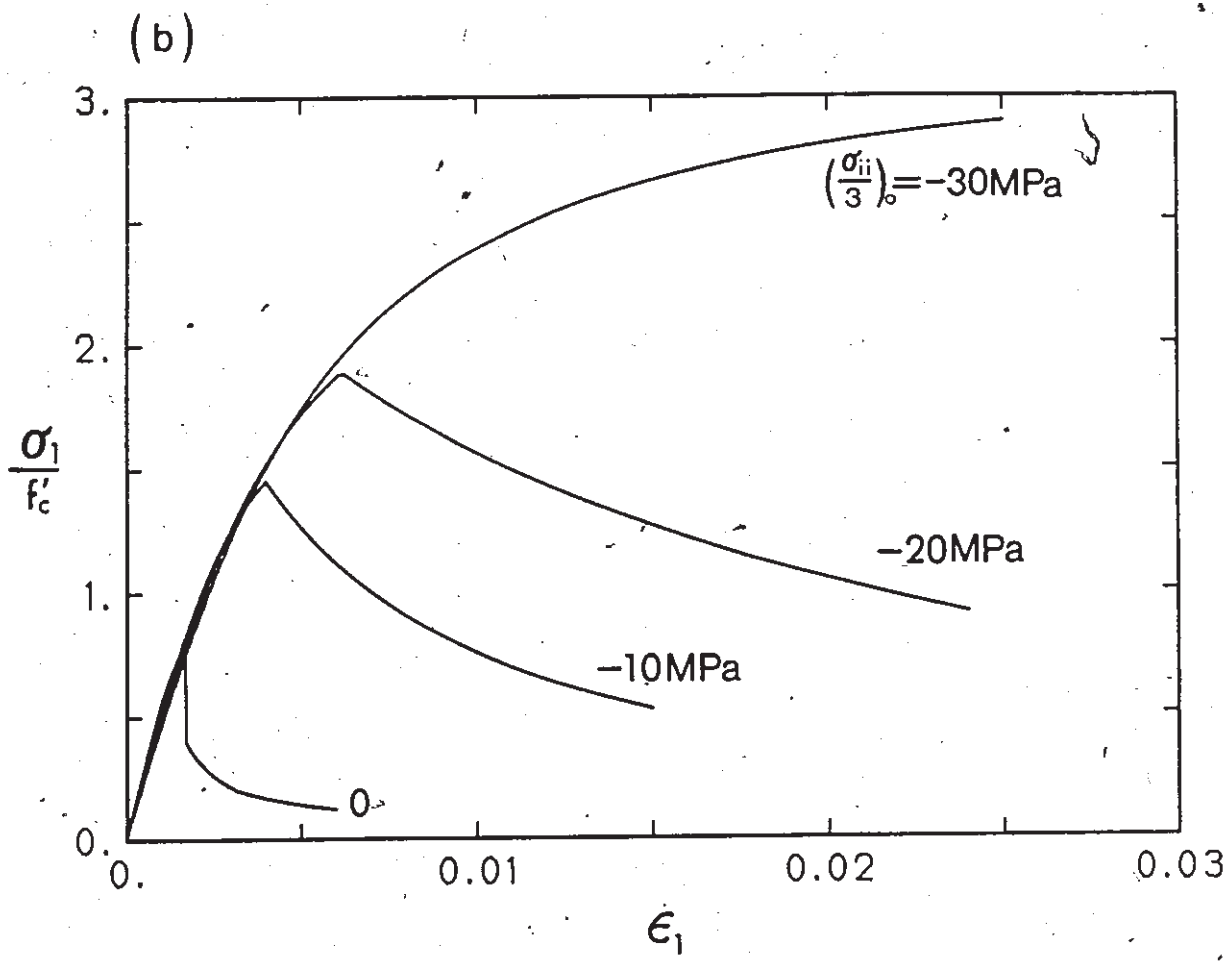

Fig. 5.4 *Numerical Results of Bifurcation Analysis for Concrete under Uniaxial Compressions at Various Initial Confining Pressures: (a) Plotted in β Vs. $\bar{\varepsilon}^p$ Diagram; (b) Plotted in σ_1 Vs. ε_1 Diagram.*

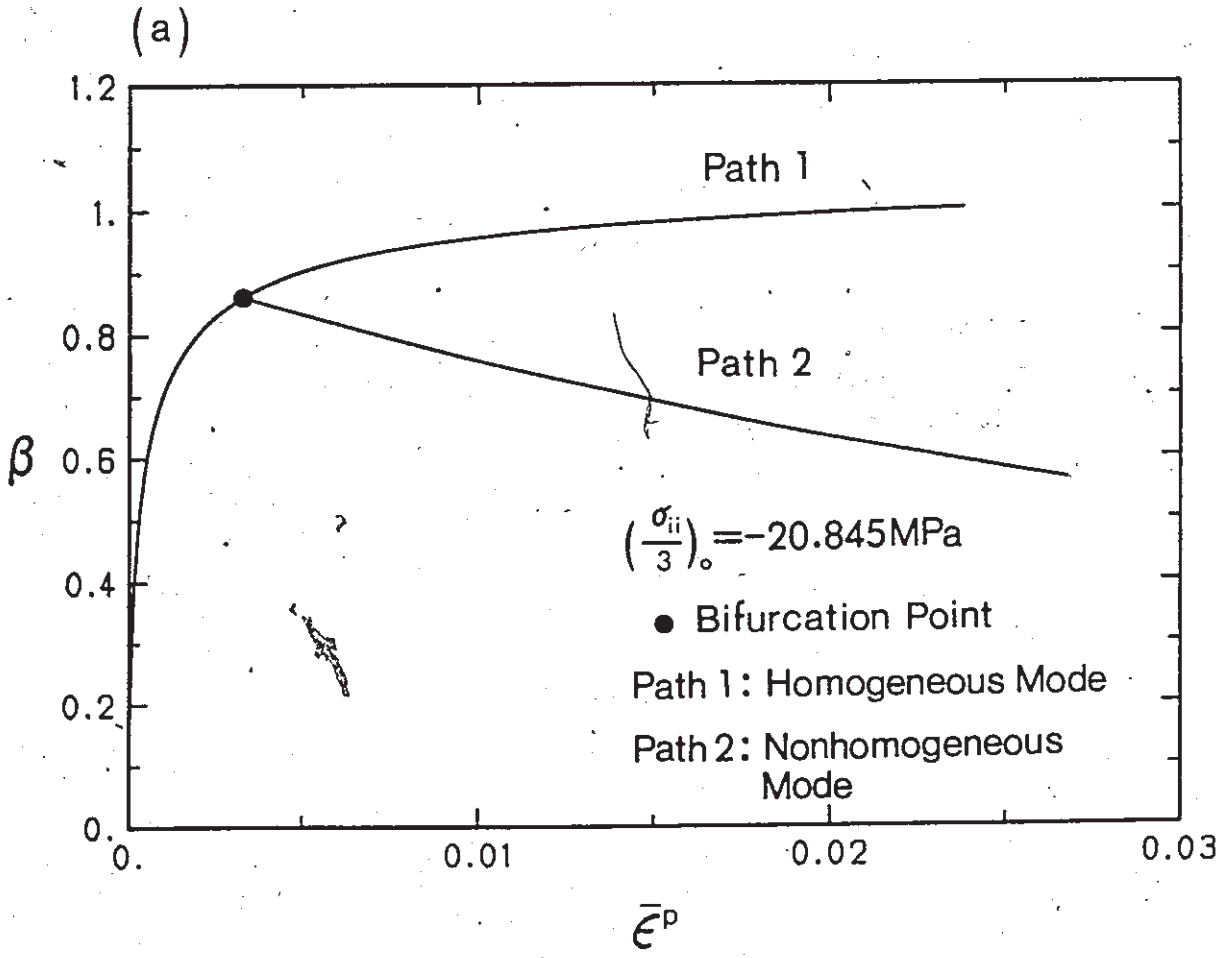
(a)
1.2
1.
0.8
0.6
0.4
0.2
0.
β
0.
0.01
0.02
0.03
$\bar{\epsilon}^p$
Path 1
Path 2
$\left(\frac{\sigma_{ii}}{3}\right)_o$ =-20.845MPa
● Bifurcation Point
Path 1: Homogeneous Mode
Path 2: Nonhomogeneous Mode

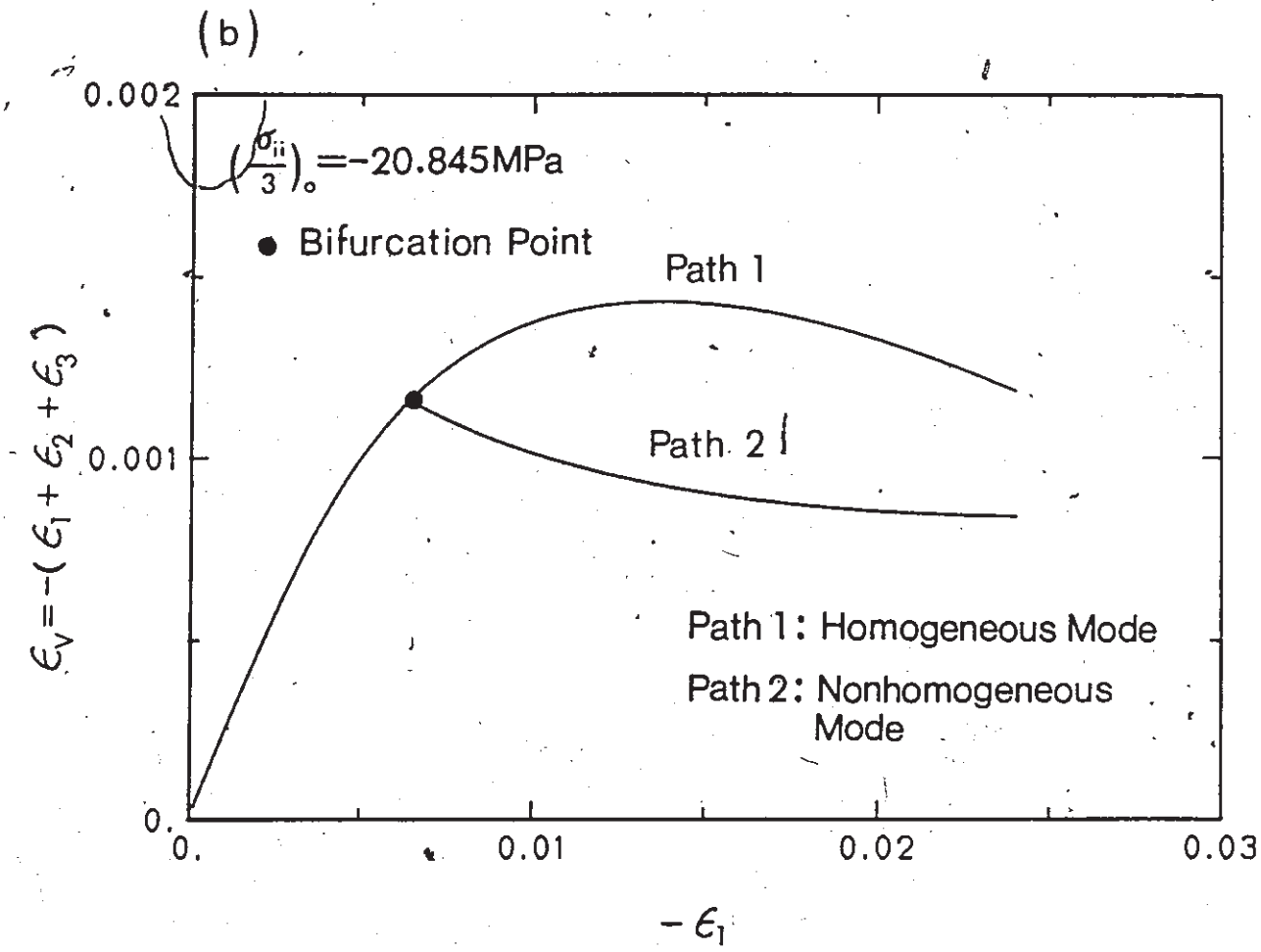

Fig. 5.5 *Numerical Simulations of Brittle-Ductile Transition Behaviour: (a) Plotted in β Vs. $\bar{\varepsilon}^p$ Diagram; (b) Plotted in ε_v Vs. ε_1 Diagram.*

CHAPTER 6

FINITE ELEMENT MODELLING OF CONCRETE STRUCTURES

6.1 Introduction

This Chapter deals with the finite element analysis of mechanical behaviour of concrete structures including analysis of reinforced concrete slabs and plain concrete beams. The proposed constitutive relations based on the theory of plasticity as presented in Chapter 2 are now incorporated into formulation of a finite element model for nonlinear analysis of plain or reinforced concrete structures. In the previous discussions, the effectiveness of the proposed constitutive relations was verified for a number of loading paths regarding pure concrete. The agreement between the numerical simulations and the experimental data was found to be very satisfactory. In the present discussion, the proposed model is further verified through finite element analysis of a boundary-value problem, i.e. simply supported reinforced concrete slab.

In order to achieve the above, two different structural members are selected to be analyzed numerically, i.e. reinforced concrete slab and plain concrete beam. The main objective of the analysis of reinforced concrete slabs is to see whether the proposed constitutive theory can adequately model both cracking and crushing of concrete in a real structural member with reinforcement during an increasing load

process. It is also necessary to check whether it can improve numerical predictions in terms of load-deflection characteristic. Since the proposed model also incorporates appropriate 'size parameter' which relates the rate of strain softening to the relative volume of the sample and the applied confining pressure, it is worthwhile to investigate the finite element solutions which involve unstable material response. In fact, the numerical analysis of plain concrete beams to be presented is mainly for this purpose.

This Chapter is divided into three parts. The first part describes general procedure for nonlinear finite element analysis, which includes basic formulation of the finite element model, general solution algorithm for the nonlinear system and numerical implementation of elastoplastic constitutive models. The second part presents the finite element modelling of reinforced concrete slabs together with extensive discussions on the numerical results. In the third part, the finite element analysis of strain softening response of concrete is provided. The results of the present approach incorporating the size parameter are compared with those obtained using the conventional finite element modelling approach.

6.2 General Description of Nonlinear Finite Element Analysis

The finite element method has been considered as one of the most powerful numerical methods of structural analysis over the last three decades. The method has provided researchers as well as engineers with a tool of very wide applicability. A comprehensive discussion of the theory and application of the method to various engineering problems has been given by Zienkiewicz[122]. With regard to its application to reinforced concrete members and structures, a state-of-art report on this subject has been prepared by ASCE Committee on Concrete and Masonry Structures[1] and some more recent developments are provided in ref.[123].

It is well known that concrete structures usually exhibit nonlinear behaviour due to material nonlinearities and/or cracking of concrete. In order to develop a realistic finite element model, these nonlinearities must be taken into account and appropriately modelled. As a consequence, the finite element solution to a real concrete structural problem usually involves very complicated nonlinear analysis. This section provides a general background on such analysis. In what follows, the mathematical formulation of finite element method is first described, and then the general solution technique for nonlinear analysis of non-symmetric system with strain softening response is discussed. Finally, the procedure for numerical implementation of the elastoplatic constitutive model is presented.

6.2.1 Formulation of Finite Element Method

In the finite element method the continuum (or structure) is divided into a number of finite elements. Within each element the continuum behaviour is approximated by simple interpolation functions. The formulation of the element behaviour such as element stiffness matrix and load vector is arrived at using an energy principle, in particular, the principle of virtual work for nonlinear system. The assembly of the force-displacement relationships for all of the elements then leads to a finite number of simultaneous algebraic equations from which the solution can be obtained.

Consider an element from a discretized system of a continuum and assume a displacement field {u} within this element which satisfies certain continuity requirement. This displacement field can be expressed in the following manner(see ref.[122] for details),

$$\{u\} = [N]\{a\} \tag{6.1}$$

in which matrix [N] contains the interpolation polynomials and {a} is a vector containing the nodal displacements. By taking appropriate derivatives of Eq.(6.1), the strain-displacement relationship is obtained, i.e.

$$\{\varepsilon\} = [B]\{a\} \tag{6.2}$$

in which

$$[B] = [L]\,[N] \,. \tag{6.3}$$

In Eq.(6.3) $[L]$ represents a matrix differential operator. Writing Eq.(6.2) in an incremental form

$$\{d\varepsilon\} = [B]\,\{da\} \tag{6.4}$$

and substituting the result into an appropriate constitutive relation, e.g. Eq.(2.31), yields

$$\{d\sigma\} = [D][B]\{da\} \,. \tag{6.5}$$

In case of linear analysis, the total stress then can be obtained from total strain as

$$\{\sigma\} = [D][B]\{a\} \tag{6.6}$$

where $[D]$ is the constitutive matrix.

The principle of virtual work is now used to obtain the following integral equation, also referred to as weak form,

$$\int_V \{\delta\varepsilon\}^T\{\sigma\}dV - \{\delta a\}^T\{r\} = 0 \tag{6.7}$$

where $\{\delta\varepsilon\}^T$ and $\{\delta a\}^T$ represent the virtual strain and virtual

displacement vectors, respectively; {r} is the vector of nodal forces. Substituting Eqs.(6.4) and (6.6) into Eq.(6.7) and after some rearrangement, the following discretized equations of equilibrium are obtained

$$[k]\{a\} - \{r\} = 0 \tag{6.8}$$

where

$$[k] = \int_V ([B]^T[D][B])dV \tag{6.9}$$

$$\{r\} = \int_S [N]^T\{t\}dS + \int_V [N]^T\{b\}dV \ . \tag{6.10}$$

In the above equations, [k] is the desired element stiffness matrix, and {t}, {b} denote the surface traction and body force vectors, respectively.

Once the element stiffness matrices and load vectors have been calculated and transformed from local to the global coordinates, the total stiffness matrix [K] is obtained by the systematic assemblage of all element stiffness, similarly the total load vector [R] is formed by systematic addition of all element load vectors. The final equilibrium equations can be expressed in the following simple form

$$[K]\{\Delta\} = \{R\} \ . \tag{6.11}$$

The incremental form of Eq.(6.11) can also be derived from Eq.(6.7) by considering {dσ} and {dr}, in the incremental form, leading to

$$[K]\{d\Delta\} = \{dR\} \tag{6.12}$$

where [K] can also include the initial stress matrix and/or initial geometric matrix. When the external load-increment vector {dR} is known, the unknown nodal-displacement vector {dΔ} is then found by solving Eq.(6.12). It should be noted that since the material nonlinearities are incorporated in the model, Eq.(6.12) represents a set of nonlinear algebraic equations.

6.2.2 Solution Procedures for Nonlinear Analysis

As mentioned before, the nonlinearity arises solely from the nonlinear form of the constitutive relations of concrete, Eq.(2.31). A solution to such nonlinear problem is usually obtained by applying the load incrementally and performing a number of iterations until the constitutive equations and the conditions of equilibrium are satisfied within an specified tolerance. Therefore, the focal point of this type of solution algorithm is to combine the incremental method with an iterative technique within each load increment.

For the strain softening elastoplastic behaviour with non-associated flow rule, the most suitable approach seems to be the

initial stress method first proposed by Zienkiewicz et al.[124,125]. According to this method, the stiffness matrix remains constant, i.e. the initially elastic one. The advantages of using such a constant positive definite matrix throughout subsequent computations are not only for economic reasons but also to enable computations into the strain softening range described by the non-associated constitutive laws. Therefore, this method has been adopted in the present study.

The essence of this method is that at any load increment the nodal force system due to internal stresses developed is evaluated and compared with the applied nodal force system. The difference between the two force systems results in a set of residual forces that can be interpreted as a measure of lack of equilibrium. To restore equilibrium the residuals are then applied to the structure and the problem is resolved. This process is repeated until the residuals are reasonably small, then leading to the satisfaction of equilibrium within a specified tolerance.

The following computational steps are carried out for a typical load increment in the finite element modelling.

(i) Apply the i^{th} load increment to the structure and determine increments of elastic strain $\{\Delta\varepsilon'\}_1$ and corresponding elastic stress $\{\Delta\sigma'\}_1$ using the elasticity matrix $[D^e]$.

(ii) Add the stress and strain increments to the initial stresses and strains, respectively, to obtain the updated values

$$\{\sigma'_i\} = \{\sigma_{i-1}\} + \{\Delta\sigma'\}_1 \tag{6.13}$$

and

$$\{\varepsilon'_i\} = \{\varepsilon_{i-1}\} + \{\Delta\varepsilon'\}_1 \tag{6.14}$$

where $\{\sigma_{i-1}\}$ and $\{\varepsilon_{i-1}\}$ are the initial stresses and strains at the beginning of the current load increment.

(iii) Check the yield condition using the updated stresses and strains. Three cases should be considered:

(a) If $f(\{\sigma'_i\},\xi_{i-1})<0$ (ξ_{i-1} refers to the initial value of hardening/softening parameter at the start of the increment), only the elastic deformations occur and process is ended without further calculations for plastic deformations. Then, apply the next load increment (if any) and proceed with step (i).

(b) If $f(\{\sigma'_i\},\xi_{i-1})>0$ and $f(\{\sigma_{i-1}\},\xi_{i-1})=0$ (i.e. the material had yielded at start of the increment), find the correct stress increment $\{\Delta\sigma\}_1$ from Eq.(2.31), namely

$$\{\Delta\sigma\}_1 = [D^{ep}]\{\Delta\varepsilon'\}_1 \tag{6.15}$$

and then evaluate the initial stress for corrections as the difference between the stress increment computed using $[D^e]$ and stress increment computed above, i.e.

$$\{\Delta\sigma''\}_1 = \{\Delta\sigma'\}_1 - \{\Delta\sigma\}_1 \ . \tag{6.16}$$

(c) If $f(\{\sigma'_i\},\xi_{i-1})>0$ but $f(\{\sigma_{i-1}\},\xi_{i-1})<0$, find the

intermediate stress and strain values at which the material yields. The difference between the updated and the intermediate values results in the stress and strain increments beyond the yield point and has to be adjusted according to Eqs.(6.15) and (6.16). Then proceed as in (b) above. Regarding determination of the intermediate stress, the mathematical procedure will be described in the next subsection.

(iv) Evaluate the current values of stresses and strains

$$\{\sigma_i\} = \{\sigma'_i\} - \{\Delta\sigma''\}_l \tag{4.17}$$

$$\{\varepsilon_i\} = \{\varepsilon'_i\} \ . \tag{4.18}$$

(v) Find the current value of the hardening parameter ξ_i and check the consistency condition, Eq.(2.26). If it is not satisfied by the current state of stress, scale the stress back to the yield surface. This will be discussed in detail later.

(vi) Compute the residual nodal force vector corresponding to the initial stresses in Eq.(6.16)

$$\{\Delta P\}_l = -\int_V [B]^T \{\Delta\sigma''\}_l dV \ . \tag{6.19}$$

(vii) Apply the residual load vector to the structure and resolve the problem to find a new elastic solution, $\{\Delta\sigma'\}_2$ and $\{\Delta\varepsilon'\}_2$.

(viii) Repeat steps (ii) to (vii) until the residual load vector is reasonably small as described below.

The iterative process is terminated if the convergence criterion is satisfied. In the present study the norm of displacement changes $\|d\Delta'_i\| = \{d\Delta'_i\}^T\{d\Delta'_i\}$ is adopted as the convergence criterion. It is specified that when this norm $\|d\Delta'_i\|$ is less than or equal to 10^{-2} percent of the norm of the actual displacements, the convergence is assumed to be reached. If this is not achieved in a reasonable number of iterations, a collapse state is reached and the whole process is stopped.

It should be noted that the above calculations for stress and strain increments are performed at each integration point. Perhaps the numerical scheme for acceleration of the iteration process can be incorporated as described in ref.[126]. But, for simplicity, this scheme will not be implemented in this study.

6.2.3 Numerical Implementation of Elastoplastic Constitutive Model

When using an elastoplastic constitutive model in the finite element formulation, attention must be paid to ensuring the condition of consistency, df=0. In order to achieve this requirement at any stage of loading, special attention must be paid to computational procedure for adequately estimating the current state of stress. These include the procedure for finding the intermediate stress at which yield begins and for scaling of stress to the yield surface, etc. In what follows, these procedures are briefly discussed. See refs.[125,127] for more

detailed information.

(i) *Scaling Factor for Determination of the Intermediate Stress*

During a transition from elastic to plastic behaviour the scaling factor r at which yield begins must be appropriately determined. A simple approach to estimate this factor r has been suggested by Nayak and Zienkiewicz[125]. The following is a brief outline of the approach.

If $\{\sigma_0\}$ represents the initial elastic state of stress, $\{\Delta\varepsilon\}$ is the strain increment corresponding to elastic stress change

$$\{\Delta\sigma_e\} = [D^e]\{\Delta\varepsilon\} \tag{6.20}$$

then the following conditions must be met

$$f(\{\sigma_0\},\xi_0) = f_0 < 0 \tag{6.21}$$

$$f(\{\sigma_0\}+\{\Delta\sigma_e\},\xi_0) = f_1 > 0 \tag{6.22}$$

for plastic deformations to occur in this increment. The scaling factor r is determined on the basis such that the following condition is satisfied

$$f(\{\sigma_0\}+r\{\Delta\sigma_e\},\xi_0) = 0 \ . \tag{6.23}$$

In some cases, explicit expressions for r can be derived if the yield functions are very simple. For most of the yield functions, however, the factor r has to be determined numerically. The simplest approximate value of $r=r_1$ from Eq.(6.23) is found by a linear interpolation in f, i.e.

$$r_1 = - f_0/(f_1 - f_0) \ . \tag{6.24}$$

This, of cause, will not satisfy Eq.(6.23) if f is a complex nonlinear function. Therefore, substituting r_1 for Eq.(6.24) in Eq.(6.23) will fail the required condition, i.e.

$$f(\{\sigma_0\}+r_1\{\Delta\sigma_e\},\xi_0) = f_2 \neq 0 \ . \tag{6.25}$$

A improved estimation of r can be obtained by utilizing the consistency condition, Eq.(2.26). For an instantaneous position of yield surface (i.e. for a constant ξ_0), the change in the yield function can be expressed as

$$df = \{\partial f/\partial\sigma\}^T\{d\sigma\} \ . \tag{6.26}$$

Assuming the following for now

$$\{d\sigma\} = \Delta r_1\{\Delta\sigma_e\} \tag{6.27}$$

and also for small changes

$$df = -f_1 \tag{6.28}$$

then after substitution of Eqs.(6.27) and (6.28) into Eq.(6.26) leads to

$$f_1 = -\Delta r_1 \{\partial f/\partial \sigma\}^T \{\Delta \sigma_e\} \tag{6.29}$$

with an improved estimation of r given by

$$r = r_1 - \frac{f_1}{\{\partial f/\partial \sigma\}^T \{\Delta \sigma_e\}} . \tag{6.30}$$

(ii) Subincrements of Strain

It is noted that the computation of $\{\Delta\sigma\}_1$ in Eq.(6.16) requires integration of Eq.(6.15) since $[D^{ep}]$ changes with the state of stress. Numerically, this can be done by dividing $\{\Delta\varepsilon'\}_1$ into a number of smaller steps which are referred to as subincrements. However, the computed stresses during the subincrements may still be inaccurate, depending on the size of strain subincrement. This means that the computed stresses may lie outside the yield surface. In such situations, the stresses should be brought back to the yield surface according to the method described below.

(iii) Procedure for Scaling Stress back to the Yield Surface

A special procedure developed in ref.[125] can be applied to bring the stresses back along the normal to the yield surface. Here, the correction scheme is very much similar to that used in the previous refinement for an improved estimation of r. When the stress is outside the yield surface, i.e. f>0; let this value be f_1. Assume now that the stress change or correction is in the direction of the normal to the yield surface, i.e.

$$\{\Delta\sigma\} = \zeta\{\partial f/\partial\sigma\} \qquad (6.31)$$

where ζ is a scaler quantity and $\{\Delta\sigma\}$ is the stress-correction vector. Substituting Eq.(6.31) into Eq.(6.26) and noting that $df=0-f_1$, the following results

$$-f_1 = \{\partial f/\partial\sigma\}^T\{\partial f/\partial\sigma\}\zeta \ . \qquad (6.32)$$

Solving for the scaler ζ from the above equation and substituting the value of ζ back to Eq.(6.31) yields

$$\{\Delta\sigma\} = -\frac{f_1\{\partial f/\partial\sigma\}}{\{\partial f/\partial\sigma\}^T\{\partial f/\partial\sigma\}} \ . \qquad (6.33)$$

Since the quantity $\{\partial f/\partial\sigma\}$ is calculated based on the stress outside the yield surface, it may not be exactly normal to the yield surface. Therefore, a number of successive approximations should be

preformed using Eq.(6.33) until the stress correction falls within a prescribed tolerance. In this study the tolerance used is $abs(df) < 10^{-6}$.

6.3 Finite Element Analysis of Reinforced Concrete Slabs

Finite element analysis of reinforced concrete slabs has been the subject of intensive investigation since the early seventies. This analysis was generally performed using an effective stiffness approach (refs.[128-130]) or layered element approach(refs.[24,131-133]). The effective stiffness approach can account for cracking and changing material properties in each element by using changing orthotropic flexural rigidities, but does not evaluate progressive cracking through the thickness of the slab. Also, this approach requires a good estimation of the effective stiffness matrix during all deformation stages which, sometimes, becomes very difficult. In the layered element approach the slab element is built up from a number of parallel layers of material and the reinforcing steel is introduced as a layer of material with orthotropic properties consistent with the amount and placement of steel. Unfortunately, this approach only accounts for vertical cracks and can not predict a shear failure in the slab. Besides the above mentioned drawback, both approaches do not allow the interface behaviour such as bond-slip and dowel action to be explicitly modelled in the analysis. Therefore, the present study adopts a discrete modelling approach similar to that used by Phillips and

Zienkiewicz[134] for beams and pressure vessels. In this approach, concrete and steel bars are modelled separately by two different finite elements. A similar model for slabs will be discussed in more detail later.

Despite the large amount of effort that has been put into numerical modelling of reinforced concrete slabs, there are still some drawbacks. This is because the behaviour of such structures is very complicated and extremely difficult to be modelled precisely. Of the many possible nonlinear effects, cracking and crushing of concrete, yielding of reinforcement and tension stiffening phenomenon are included in this study. Some of the effects such as bond-slip between concrete and steel bars, dowel action of reinforcement have been studied in the previous work(ref.[135]) and hence are not repeated here.

6.3.1 Concrete Element

The finite element employed for modelling of concrete is shown in Fig. 6.1(a). This element combines the eight degrees of freedom plane stress element for modelling in-plane action with the twelve degrees of freedom, non-conforming, plate bending element for modelling out-of-plane action. Thus, the combined element has five degrees of freedom per node (i.e. $u_i, v_i, w_i, w_{i,x}$ and $w_{i,y}$) and twenty degrees of freedom per element as indicated in Fig. 6.1(b). Here, $w_{i,x}=\partial w_i/\partial x$

and $w_{i,y}=\partial w_i/\partial y$ are the rotations about y and x axis, respectively.

As stated in Eq.(6.1), the displacement field within an element is described by interpolation polynomials and the nodal degrees of freedom as

$$\underset{3x1}{\{u\}} = \underset{3x20}{[N]}\ \underset{20x1}{\{a\}} \tag{6.34}$$

or

$$u = \sum_{i=1}^{4} N_i u_i$$

$$v = \sum_{i=1}^{4} N_i v_i$$

$$w = \sum_{i=1}^{12} \bar{N}_i w_i \ .$$

In Eq.(6.34), {a} is the vector of nodal displacements given by

$$\{a\}^T = \langle\ u_1, v_1, w_1, \frac{\partial w_1}{\partial x}, \frac{\partial w_1}{\partial y}, u_2, v_2, w_2, \frac{\partial w_2}{\partial x}, \frac{\partial w_2}{\partial y}, \ \ldots\ \rangle \tag{6.35}$$

and N_i, $\bar{N}_i$ are the shape functions for in-plane and out-of-plane actions, respectively. Mathematical forms concerning these shape functions are provided in Appendix F. It should be noted that for numerical integration purpose these functions are expressed in terms of the dimensionless coordinates s, t and r as indicated in Fig. 6.1(a) and have a range $(-1 \leq r,s,t \leq 1)$.

Under the assumptions of small displacement and the normals to the mid-surface of the plate remaining normal after deformation, it can be easily shown(ref.[122]) that the strain-displacement relationship take the following form

$$\{\varepsilon\} = [L]\{u\}$$

$$= \begin{bmatrix} \partial/\partial x & 0 & -z(\partial^2/\partial x^2) \\ \partial/\partial y & 0 & -z(\partial^2/\partial x^2) \\ \partial/\partial y & \partial/\partial x & -2z(\partial^2/\partial x \partial y) \end{bmatrix} \begin{bmatrix} u \\ v \\ w \end{bmatrix} \tag{6.36}$$

or in terms of the nodal displacements (by substituting Eq.(6.34) into Eq.(6.36))

$$\underset{3x1}{\{\varepsilon\}} = \underset{3x20}{[B]}\ \underset{20x1}{\{a\}}$$

where

$$[B] = \begin{bmatrix} \dfrac{\partial N_1}{\partial x} & 0 & -z\dfrac{\partial^2 \bar{N}_1}{\partial x^2} & -z\dfrac{\partial^2 \bar{N}_2}{\partial x^2} & \cdots \\ 0 & \dfrac{\partial N_1}{\partial y} & -z\dfrac{\partial^2 \bar{N}_1}{\partial y^2} & -z\dfrac{\partial^2 \bar{N}_2}{\partial y^2} & \cdots \\ \dfrac{\partial N_1}{\partial y} & \dfrac{\partial N_1}{\partial x} & -2z\dfrac{\partial^2 \bar{N}_1}{\partial x \partial y} & -2z\dfrac{\partial^2 \bar{N}_2}{\partial x \partial y} & \cdots \end{bmatrix} \tag{6.37}$$

The elasticity matrix $[D^e]$ is used in the formulation of the initial stiffness matrix and the calculation of elastic stress

components. For an isotropic plate the elasticity matrix is given by

$$[D^e] = \frac{E}{1-\upsilon^2}\begin{bmatrix} 1 & \upsilon & 0 \\ \upsilon & 1 & 0 \\ 0 & 0 & (1-\upsilon)/2 \end{bmatrix} \tag{6.38}$$

where E is the modulus of elasticity and υ is Poisson's ratio.

Now, that all the ingredients for calculation of the stiffness matrix have been introduced, the stiffness matrix is computed from

$$[k] = t_b \int_V [B]^T[D^e][B]dV \tag{6.39}$$

and the load vector using

$$\{r\} = t_b \int_S [N]^T\{t\}dS + \int_V [N]^T\{b\}dV \tag{6.40}$$

where t_b is the thickness of the plate.

Because of the complexities of integrands in Eqs.(6.39) and (6.40), numerical integration technique has to be used in calculation of the stiffness matrix and the load vector. In this study, Gaussian quadrature is used with three integration points in the s and t directions and five integration points in the r direction, Fig. 6.2. In doing so, these integrations must be transformed from (x,y,z) to (s,t,r) coordinate system by

$$x = x_0(s + 1)/2 \; ; \quad y = y_0(t + 1)/2 \; ; \quad z = t_b r/2 \tag{6.41}$$

where x_0 and y_0 represent the length of the element in x and y directions, respectively. Thus, Eq.(6.39) can now be written as

$$[k] = \int_0^{x_0} \int_0^{y_0} \int_{-t_b/2}^{t_b/2} [B]^T[D^e][B] \; dxdydz$$

$$= \frac{x_0 y_0 t_b}{8} \int_{-1}^{+1} \int_{-1}^{+1} \int_{-1}^{+1} [B]^T[D^e][B] \; dsdtdr$$

$$= \frac{x_0 y_0 t_b}{8} \sum_{i=1}^{3} \sum_{j=1}^{3} \sum_{k=1}^{5} H_i H_j H_k [B_i]^T [D]_{ijk} [B_i] \tag{6.42}$$

in which $[B_i]$ is the $[B]$ matrix calculated at the integration point (s_i, t_i, r_i); H_i, H_j and H_k are the weighting factors. The values of the weighting factors and the sampling points can be found in ref.[122].

Similarly, the load vector due to internal stresses is also integrated numerically in the following manner

$$\{P^n\} = \int_V [B]^T \{\sigma\} \; dV$$

$$= \frac{x_0 y_0 t_b}{8} \sum_{i=1}^{3} \sum_{j=1}^{3} \sum_{k=1}^{5} H_i H_j H_k [B(s_i, t_i, r_i)]^T (\sigma)_{ijk} \; . \tag{6.43}$$

Therefore, using Eqs.(6.42) and (6.43) the concrete element stiffness matrix and its load vector can be obtained. After the global stiffness matrix and the global load vector are assembled by addition of contributions from both concrete and steel elements, the unknown nodal displacements are solved using the skyline technique described in ref.[136].

6.3.2 Steel Element

A beam-column type of element had been successfully employed to represent the reinforcing steel bar in the previous works (refs.[135,137]) and therefore is also used in the present study. In the following, only the relevant parts (under the assumption of perfect bond between concrete and steel bars) are provided. The detailed information can be found in ref.[137]. If the behaviour of bond-slip and dowel action are also important, the formulation presented in ref.[135] should be implemented rather than one presented below.

Figure 6.3(a) shows a typical beam element used to model the steel reinforcement (with two nodes and three degrees of freedom per node), whereas Fig. 6.3(b) illustrates a steel element embedded within a concrete element along the x direction. Obviously, this steel (or beam) element has the length of the concrete element and is located at an eccentricity "e" from the mid-surface of the concrete element. In

the following, only the steel elements parallel to the x axis are considered. A similar derivation holds for steel elements in the y direction.

The displacement field along the centroidal axis of the steel element can be written as

$$u^s = \sum_{i=1}^{6} N_{si}\, a_{si} \tag{6.44}$$

$$w^s = \sum_{i=1}^{4} \bar{N}_{si}\, a'_{si} \tag{6.45}$$

where u^s is the axial displacement along the centroidal axis of the steel element, and w^s is the transverse displacement; N_{si} and $\bar{N}_{si}$ represent the shape functions which are listed in Appendix F. In Eqs.(6.44) and (6.45)

$$\{a_s\} = \langle u^s_1, w^s_1, \theta^s_1, u^s_2, w^s_2, \theta^s_2 \rangle \tag{6.46}$$

$$\{a'_s\} = \langle w^s_1, \theta^s_1, w^s_2, \theta^s_2 \rangle \tag{6.47}$$

which are the vectors of nodal displacements at the mid-surface of the concrete element as shown in Fig. 6.4. It should be pointed out here that the displacement field defined by u^s and w^s satisfy the kinematic constraints, e.g.

$$u^c = u^s - e(\partial w^s/\partial x) \tag{6.48}$$

in which u^c *is the in-plane displacement of the concrete element along the x direction at the mid-surface. See ref.[137] for details.*

Having defined the displacement field for the steel element, the strain-displacement relation can be determined from the following condition

$$\varepsilon_s = \partial u^s/\partial x - \bar{z}(\partial^2 w^s/\partial x^2) \tag{6.49}$$

which, after taking differentiations of Eqs.(6.44) and (6.45), results in

$$\varepsilon_s = [B_s]^T\{a_s\} \ . \tag{6.50}$$

In Eq.(6.50)

$$[B_s]^T = \langle\ -1/x_0,\ \ 6\zeta(e-\bar{z})/x_0^2,\ (3\zeta-1)(e-\bar{z})/x_0,$$
$$1/x_0,\ -6\zeta(e-\bar{z})/x_0^2,\ (3\zeta+1)(e-\bar{z})/x_0\ \rangle \ . \tag{6.51}$$

Here, ζ *and* $\bar{z}$ *are the dimensionless coordinates as shown in Fig. 6.3. Since the radius of steel bar usually is small in comparison with the eccentricity "e", the above equation can be replaced by*

$$[B_s]^T = \langle\ -1/x_0,\ 6e\zeta/x_0^2,\ e(3\zeta-1)/x_0,\ 1/x_0,\ -6e\zeta/x_0^2,\ e(3\zeta+1)/x_0\ \rangle \ . \tag{6.52}$$

The elasticity matrix $[D^e]$ for steel element contains only one constant E_s because the strain components other than the axial strain are assumed to be negligible. Thus, the steel element stiffness matrix is determined by

$$[k_s] = \int_{-x_0/2}^{x_0/2} E_s A_s [B_s]^T [B_s] \, d\zeta$$

$$= \sum_{i=1}^{3} E_s A_s H_i [B_s(\zeta_i)]^T [B_s(\zeta_i)] \qquad (6.53)$$

where H_i and ζ_i represent the weighting factors and the sampling points, respectively, and A_s is the area of cross-section of the steel bar. It should be noted that Eq.(6.53) is only valid for the stress level below the yield stress of steel bars. For stress level exceeding the yield stress in Eq.(6.53), the elastic constant E_s is replaced by $E_T=E_s/15$ which is the so-called tangent elastic modulus. It is assumed that E_s and E_T are the same for steel bars in tension and compression.

As mentioned before, the steel element load vector due to internal stresses has to be added to Eq.(6.43). The mathematical form is exactly the same as that in Eq.(6.43), i.e.

$$\{P_s^n\} = \int_{-x_0/2}^{x_0/2} [B_s]^T \{\sigma_s\} \, d\zeta$$

$$= \sum_{i=1}^{3} H_i [B_s(\zeta_i)]^T \{\sigma_s(\zeta_i)\} \qquad (6.54)$$

in which

$$\{\sigma_s\} = \begin{cases} E_s[B_s]^T\{a_s\} & \text{for } \sigma_s < \sigma_y \\ E_T[B_s]^T\{a_s\} & \text{for } \sigma_s \geq \sigma_y \end{cases} . \qquad (6.55)$$

For the perfect-bond assumed between concrete and steel, the degrees of freedom of steel nodes at concrete mid-surface can be transferred to those of the concrete element corner nodes by the following transformation matrix,

$$\underset{10x1}{\{a_s''\}} = \underset{10x20}{[T_s]} \; \underset{20x1}{\{a\}} \qquad (6.56)$$

where $\{a_s''\}$ is the vector of transformed degrees of freedom of steel nodes at concrete mid-surface, $\{a\}$ is the vector of degrees of freedom of concrete element at four corner nodes, and $[T_s]$ is the transformation matrix which is listed in Appendix G. The transformed stiffness matrix and the load vector can be written as

$$[\bar{k}_s] = [T_s]^T[k_s][T_s] \qquad (6.57)$$

$$\{\bar{P}_s^n\} = [T_s]^T\{P_s^n\} . \qquad (6.58)$$

In the case when the behaviour of bond-slip and dowel action are also to be included in the finite element modelling, the above

transformation is invalid and the so-called interface element should be incorporated in the formulation. An appropriate interface element together with relevant transformations has been developed in ref.[135].

Up to this point, formulations of element stiffness matrices and load vectors for both concrete and steel have been presented. In the following sections, these formulations will be employed, along with the proposed constitutive model for concrete discussed in Chapter 2, to investigate the nonlinear behaviour of reinforced concrete slabs such as cracking of concrete, tension stiffening phenomenon and total load-displacement characteristic, etc.

6.3.3 Modelling of Concrete Cracking and Tension Stiffening

It is well known that cracking of concrete is a major factor contributing to nonlinear behaviour of reinforced concrete members. Theoretically, the formation and propagation of microcracks in concrete cause physical discontinuities which are mainly localized and are different from those often discussed in continuum mechanics sense. This phenomenon had led to the development of the first finite element analytical model for cracking of concrete, i.e. discrete cracking model, refs.[17,18]. This approach constitutes the most rational method of representing cracks. In this approach, the cracks are modelled by the separation of nodal points and their locations are successively

redefined at each iteration during the analysis. Such continued redefinition of the nodal points not only alter the topology of the analytical model, but also destroys the narrow band width of the globe stiffness matrix and largely increases the computational effort required for the solution. These drawbacks have made discrete cracking model unrealistic. However, this model seems to be the best choice for a structural problem with a known crack location.

The second finite element model for cracking of concrete, i.e. the so-called smeared cracking model originally introduced by Rashid[19] and adopted in this study, overcomes the above mentioned drawbacks of a discrete cracking model. The original smeared cracking representation was based on the concept of a stress discontinuity in the maximum principal tensile stress direction while its strain component maintains continuity. In this concept, rather than representing a single crack, the approach assumes many finely spaced (or smeared) cracks perpendicular to the principal stress direction and usually adopts the maximum tensile strength of concrete as the criterion for cracking initiation. It has been found that this earlier version of smeared cracking model sometimes leads to numerical instability of solution, ref.[29].

To improve the smeared crack representation, many researchers[138-140] have suggested that the so-called tension stiffening phenomenon should be appropriately considered in an analytical model. This suggestion was primarily from the experimental

observations that at a major crack the concrete strength drops to zero and the steel bar carries the full load. However, concrete between the cracks still carries some tensile stress. In their studies, the tension stiffening effect was represented using two procedures. One procedure introduced by Scanlon[23] is to account for the tension stiffening effect by adding an arbitrary descending branch to the tensile stress-strain curve for concrete. The other procedure represents the effect by increasing the steel stiffness, ref.[25]. It seems that both procedures are not realistic and in fact are biased approaches in the sense that no real justification has been provided for the use of some artificial criteria such as the ultimate tensile strain of concrete and the shape of the descending branch or the increased tangent stiffness of reinforcing steel. One of the approaches, to get rid of these problems, is to use more rational constitutive model with strain softening description such as the model proposed in Chapter 2. The advantage of implementation of such a model is that the concrete cracking process and its induced tension stiffening effect can be modelled within the same framework, and no special numerical tricks are involved. All parameters used can be specified from the material tests rather than from numerical simulations and their comparison with the experimental results, ref.[14].

In the present approach, the initiation of cracks in concrete is governed by the portion of maximum strength envelope of concrete in the brittle regime, i.e. as described in Chapter 2 for $I<I_T$ (I_T is the transition pressure from ductile to brittle response). The tension

stiffening effect is considered as a post-cracking behaviour and has been numerically modelled by the proposed strain softening model. On the other hand, the crushing of concrete is controlled by the portion of maximum strength envelope in the ductile regime and the ultimate strain of concrete. This means that if $I > I_T$ *and maximum principal strain exceeds the ultimate strain, a crushing state is assumed to be reached. It should be noted that in the present model, cracking and crushing of concrete under tensile and compressive stresses, respectively, can be adequately modelled and the shear resistance after cracking is also accounted for by the model itself.*

In the next section, the approach discussed above is verified for a simply supported reinforced concrete slab subjected to an uniformly distributed load. It is expected that the model presented will improve the predicted results in terms of the global load-deflection response and also maintain the grid objectivity.

6.3.4. Numerical Examples

The numerical example presented here consists of detailed parametric study concerning the short-term deformation behaviour of a simply supported square reinforced concrete slab subjected to an uniformly distributed load. The experimental investigation of such structure was conducted by Taylor et al.[142]. The analytical results

using finite element method for the above mentioned slab were obtained by a number of investigators[26,31,94,140, 143,144]. Now it is re-analyzed here with the aim of verifying the proposed constitutive model for concrete in finite element modelling.

Figure 6.5 shows a plan view and a cross-section of the slab. It presents details of the reinforcing bars, the support system and the applied load. The material properties are summarized in Table 6.1. Because of the double symmetry, only one quarter of the slab needs to be considered in the finite element analysis. Three different meshes are used as shown in Fig. 6.6. The coarser mesh only consists of 4 elements whereas the finer mesh has 36 elements. In each analysis, two different load step sizes are employed, i.e. the small load step size involves 100 increments from zero loading up to failure, and the large step size uses 50 increments. In regard to the parametric study, there are two parameters of particular interest in the present investigation. One is the residual strength of concrete in the softening regime; the other is the rate of strain softening.

Figure 6.7 presents the comparison of the load-deflection responses of the slab (at the midpoint) obtained from the present analyses (using three different meshes) with the experimental curve from ref.[141]. Fig. 6.8 shows the results obtained by Chow[137]. Regarding finite element modelling details, the only difference between these two analyses is that Chow's model employed a linear-elastic constitutive model for concrete while the present model incorporates

the proposed elastoplastic constitutive relation. It can be seen from Fig. 6.7 that the overall predictions from the present analyses are in very good agreement with the test data. Moreover, improvements in the numerical predictions of deflection with the refinement of the finite element mesh can be observed. However, the results in Fig.6.8 indicate that the predicted response actually deteriorates with the improved grid in the cracking range. It is also found from the present analyses that the difference between the results using the two different incremental load step sizes is negligible due to implementation of the subincrement technique for evaluation of stresses, as mentioned in Section 6.2.3.

In Fig. 6.9, the influence of the residual strength of concrete (through parameter β_r) on the deflection of the slab is clearly indicated. The residual strength of concrete does have a significant influence on the predicted response. As the residual strength β_r varies from 5 % to 25 % of the maximum strength, the predicted response changes from very flexible to nearly the experimental response. It is found that the magnitude of the residual strength that results in a good prediction is in concordance with the value observed from experiments(refs.[94,145]), i.e. β_r=20% to 30%. On the other hand, for this particular example, the influence of the rate of strain softening on the predicted load-deflection characteristic is less important than that of the residual strength, as can be observed from Fig. 6.10. This can be explained by the fact that as soon as the stress starts to decrease due to cracking of concrete, the reinforcing steel

takes over. However, it is expected that the rate of strain softening has strong influence on the response of plain concrete structures which is the subject of the next section. The influence of the tensile strength of concrete, f_t', on the predicted response of the slab is shown in Fig. 6.11. As expected, the value of f_t' has signicant effect on the initial cracking process.

Therefore, it can be concluded that the proposed constitutive model in Chapter 2 is capable of modelling both cracking of concrete and tension stiffening effect in reinforced concrete slabs. Using such a rational model in a finite element modelling of reinforced concrete slabs results in the grid objectivity and a substantial reduction of the load step size sensitivity. Furthermore, the residual strength of concrete has considerable effect on the predicted response of slabs whereas the rate of strain softening has very small influence.

6.4 Finite Element Analysis of Strain Softening Response

In the last section the constitutive model described in Chapter 2 has been successfully applied to the finite element analysis of reinforced concrete slabs. Now the same model is incorporated into a finite element model for analysis of plain concrete structure with the objective to investigate the aspects related to unstable material response.

As mentioned previously, a conventional finite element analysis for a strain softening material may suffer from instabilities and high sensitivity to grid discretization. This problem has been discussed in refs.[82,86], but still remains unsolved. Now, this problem is re-addressed here by using the model described in Chapter 2. In what follows, a plain concrete beam subjected to a central concentrated load is analyzed by two different procedures. The first one is the standard procedure in which the rate of strain softening is assumed to be independent on the size of softening zone. In the second procedure, an appropriately defined 'size parameter', Eq.(2.21), is introduced. This parameter relates the rate of strain softening to the volume size associated with an integration point in the softening zone. Before discussing the numerical results, a brief discussion of the details of the finite element model employed is presented.

The finite element used here for modelling of concrete is the eight node isoparametric element with two degrees of freedom at each node, Fig. 6.12. The displacement field within this element is defined as follows

$$u = \sum_{i=1}^{8} N_i u_i \qquad (6.59a)$$

$$v = \sum_{i=1}^{8} N_i v_i \qquad (6.59b)$$

where N_i represents the appropriate shape functions which are listed in

Appendix H. For plane stress the strain-displacement relationship takes the following form

$$\{\varepsilon\} = \begin{bmatrix} \varepsilon_x \\ \varepsilon_y \\ \gamma_{xy} \end{bmatrix} = \underset{3x16}{[B]} \quad \underset{16x1}{\{a\}} \tag{6.60}$$

in which

$$[B] = \begin{bmatrix} \partial N_1/\partial x & 0 & \partial N_2/\partial x & 0 & \cdots \\ 0 & \partial N_1/\partial y & 0 & \partial N_2/\partial y & \cdots \\ \partial N_1/\partial y & \partial N_1/\partial x & \partial N_2/\partial y & \partial N_2/\partial x & \cdots \end{bmatrix} \tag{6.61}$$

and

$$\{a\}^T = \langle u_1, v_1, u_2, v_2, u_3, v_3, u_4, v_4, u_5, v_5, u_6, v_6, u_7, v_7, u_8, v_8 \rangle .$$

To construct the matrix [B] according to Eq.(6.61), the following transformation is required

$$\begin{bmatrix} \partial N_i/\partial x \\ \\ \partial N_i/\partial y \end{bmatrix} = [J]^{-1} \begin{bmatrix} \partial N_i/\partial \xi \\ \\ \partial N_i/\partial \eta \end{bmatrix} \tag{6.62}$$

In Eq.(6.62) $[J]^{-1}$ is the inverse of [J], i.e. the so-called Jacobin matrix given by

$$[J] = \begin{bmatrix} \partial x/\partial \xi & \partial x/\partial \eta \\ \partial y/\partial \xi & \partial y/\partial \eta \end{bmatrix} \tag{6.63}$$

where the x, y coordinates are interpolated by the same interpolation functions N_I as that in Eq.(6.59).

The formulation of the stiffness matrix can be obtained following the procedure outlined in section 6.2.1. When performing the integration of expressions given by Eqs.(6.9) and (6.10), the following transformations are required, i.e. for a volume integration (of unit thickness)

$$dV = dxdy = \det[J]d\xi d\eta \tag{6.64}$$

and for an integration on constant η surfaces

$$dS = \sqrt{(\partial x/\partial \xi)^2 + (\partial y/\partial \xi)^2}\, d\xi \ . \tag{6.65}$$

Once again the Gaussian quadrature technique has been applied. In the present analysis, the reduced 2x2 integration scheme is adopted in order to reduce the computational cost.

Figure 6.13 presents the geometry of the plain concrete beam selected for the present analysis. The beam is simply supported and subjected to a concentrated vertical load. In the analysis the beam has been discretized using 196 elements as shown in Fig. 6.13. The initial

stress approach has been used for nonlinear analysis. This problem has been solved in a load controlled fashion, i.e. the analysis is terminated as soon as the collapse load has been reached.

This problem is analyzed first using the conventional finite element approach in which the strain softening effect has been entirely attributed to the material behaviour (i.e. $\bar{\phi}_s=1$ in Eq.(2.17)). The corresponding numerical results are presented in Fig. 6.14. As mentioned before, such analysis may suffer from instability and considerable sensitivity to the details of discretization. Indeed, it is evident from Fig. 6.14 that the predicted collapse load is influenced by the type of mesh employed. In addition, the predicted collapse load also depends on the assumed rate of strain softening. This usually does not remain invariant with respect to sample geometry and hence, can not be uniquely defined.

The numerical results plotted in Fig. 6.15 are obtained using the second approach, in which the function $\bar{\phi}_s$ has been incorporated into the constitutive relations. For simplicity, $\alpha_1=1$ has been assumed in Eq.(2.22), resulting in

$$\bar{\phi}_s = 1 + [(V/V_s)^{\lambda} - 1] \ . \tag{6.66}$$

In a boundary value problem, V represents the volume associated with a quasi-uniform stress/strain field in the softening zone. In the finite

element context it can be interpreted as the volume associated with an integration point. The constant V_s corresponds to the volume for which the current strain softening characteristics, defined by H and u in Eq.(2.17), have been determined.

It can be seen from Fig. 6.15 that the analysis, employing Eq.(6.66), shows much less sensitivity to the details of descretization as compared to the standard approach. More importantly, it incorporates a "size parameter" reflecting a progressive increase in the rate of strain softening with increasing relative volume V/V_s of the sample. It should be noted that Eq.(6.66) has been selected quite arbitrarily in this study to demonstrate the effectiveness of the proposed approach. The form of this equation should be verified experimentally and it is likely that functions other than the power law, Eq.(6.66), will be more appropriate.

It has been demonstrated in this section that the conventional finite element analysis of strain softening material usually suffers from numerical instability and sensitivity to the details of discretization. In contrast, the proposed model, which incorporates the "size parameter", can reduce the numerical instability and the solution is virtually unaffected by the discretization. Hence, the proposed model performs much better than the more widely used standard approach in the context of finite element analysis of strain softening response.

TABLE 6.1 Material Properties of the Reinforced Concrete Slab

Concrete			Reinforcing Steel		
E	3242	KN/cm^2	E_s	20691	KN/cm^2
υ	0.18		E_t	1379	KN/cm^2
f_c'	3504	N/cm^2	σ_y	37.59	KN/cm^2
f_t'	360	N/cm^2			
ε_u	-0.003				

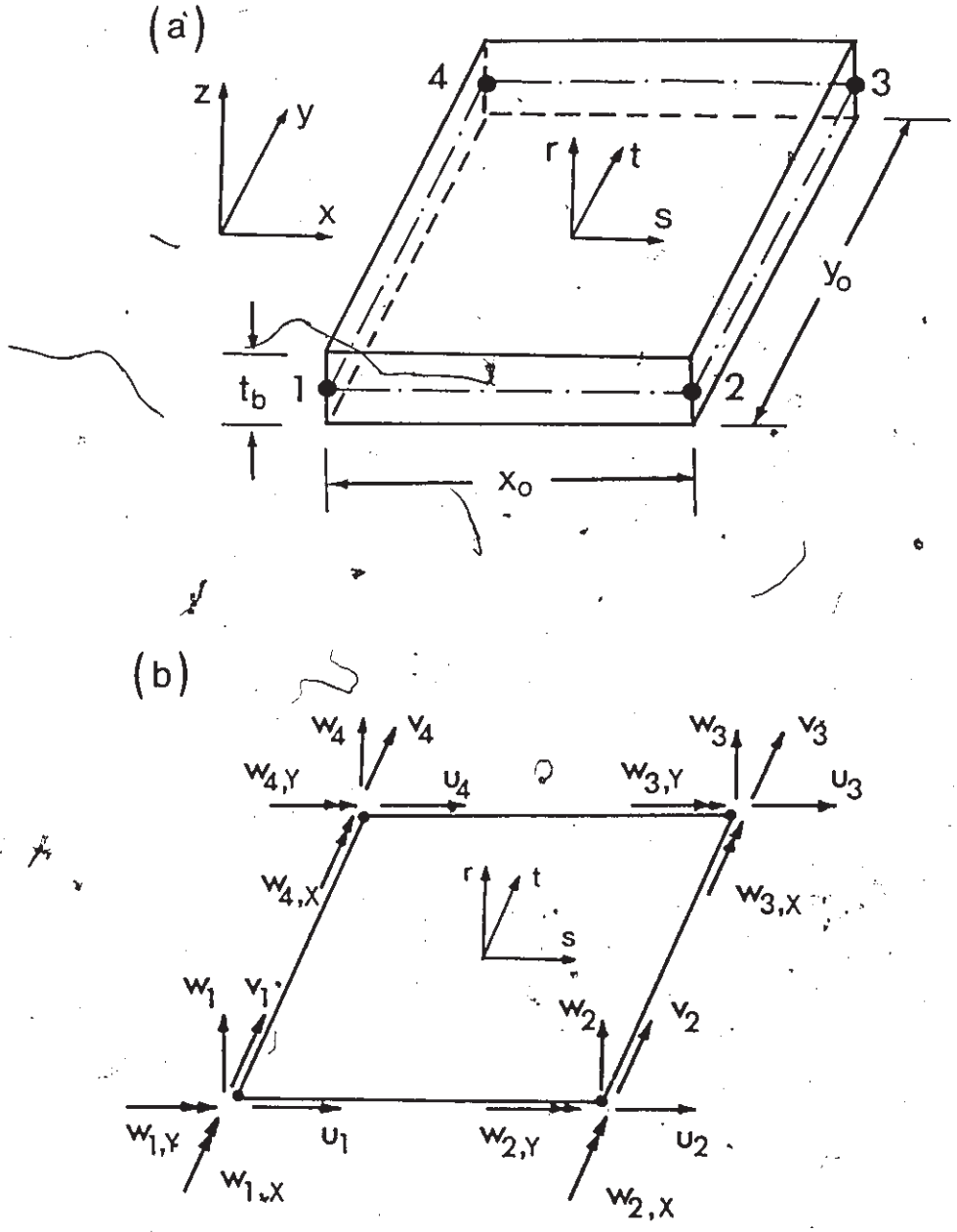

Fig. 6.1 *Rectangular Plate Bending Element: (a) Local Axes and Local Numbering System; (b) Nodal Displacement Components.*

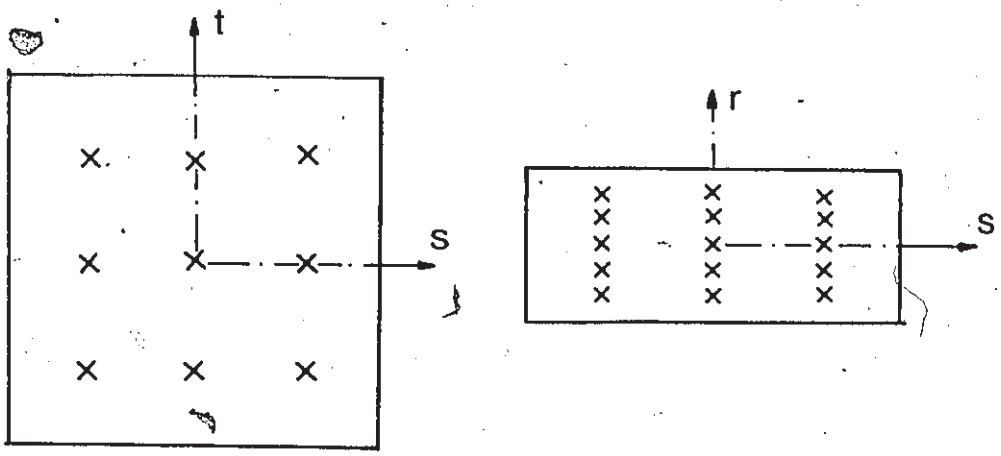

Fig. 6.2 Location of Gaussian Integration Points.

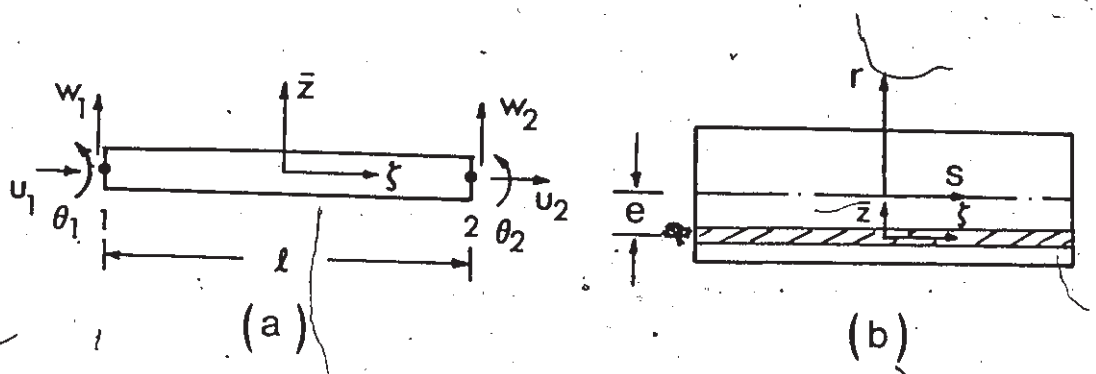

Fig. 6.3 Beam Element: (a) Local Axes and Nodal Degrees of Freedom; (b) Represention of a Steel Element Embeded within a Concrete Element along the x Direction.

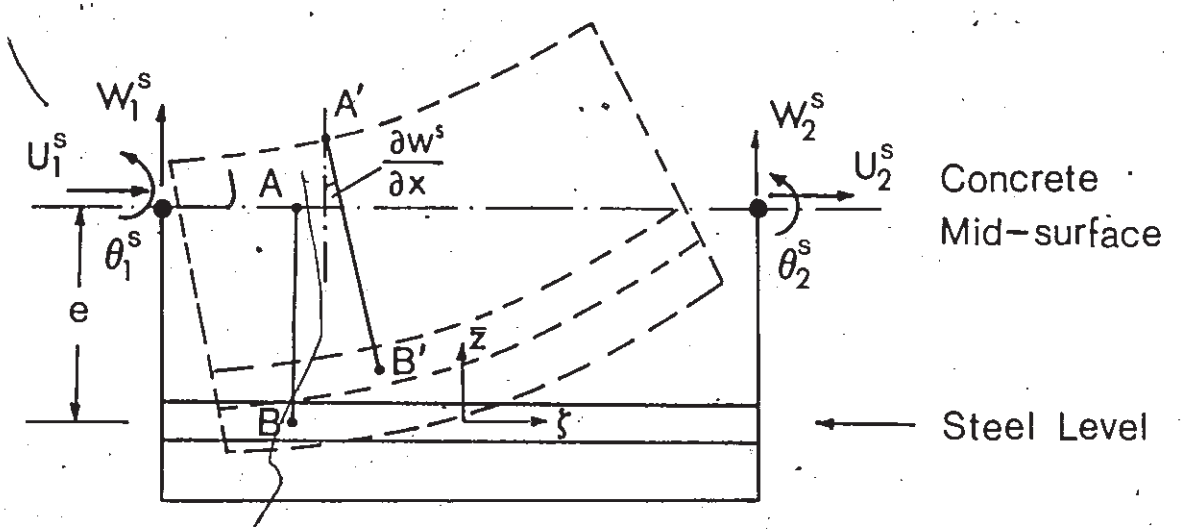

Fig. 6.4 Deformation of a Reinforced Concrete Plate Element.

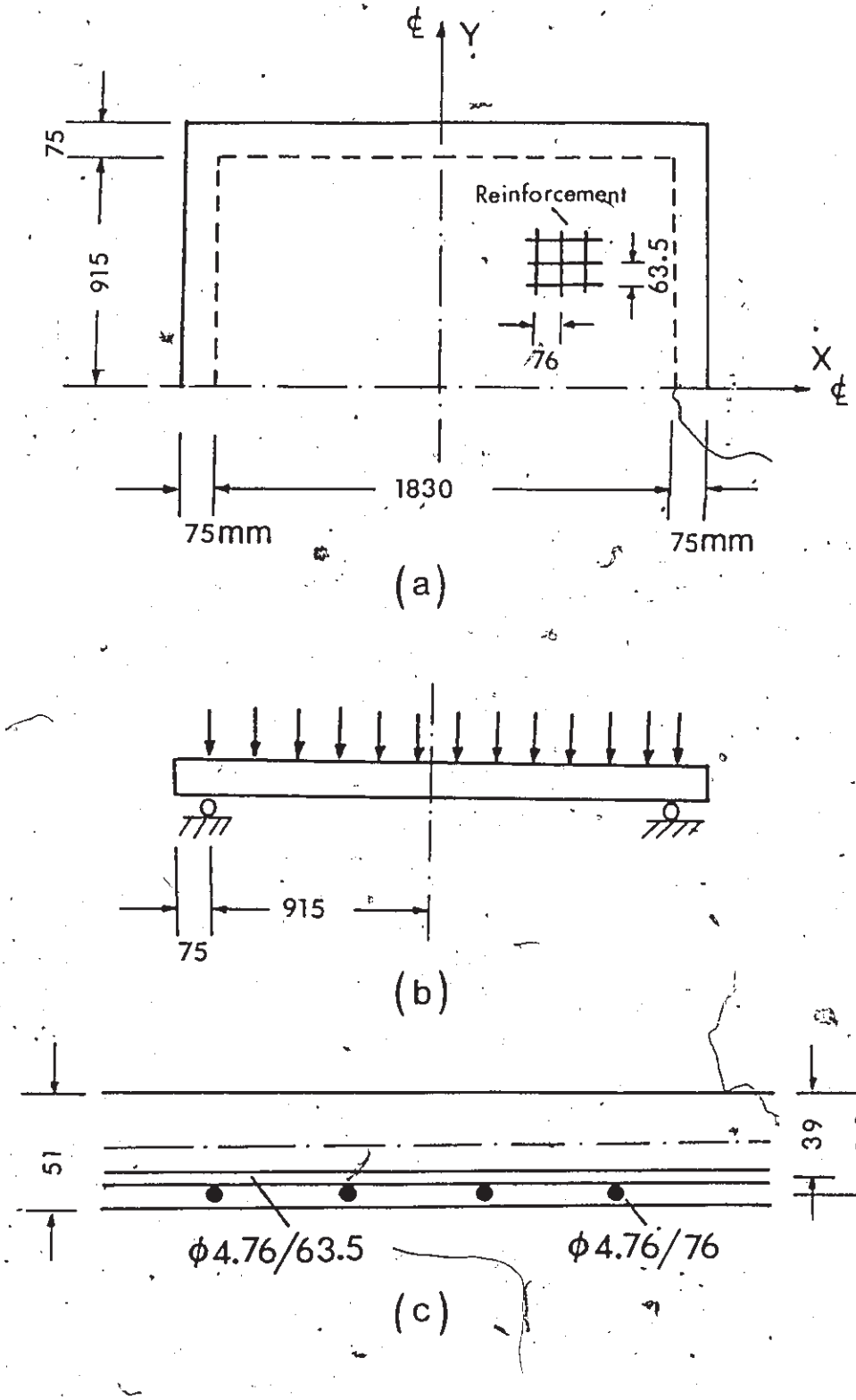

Fig. 6.5 Geometry and Cross Section of a Simply Supported Reinforced Concrete Slab Tested by Taylor et al.[142].

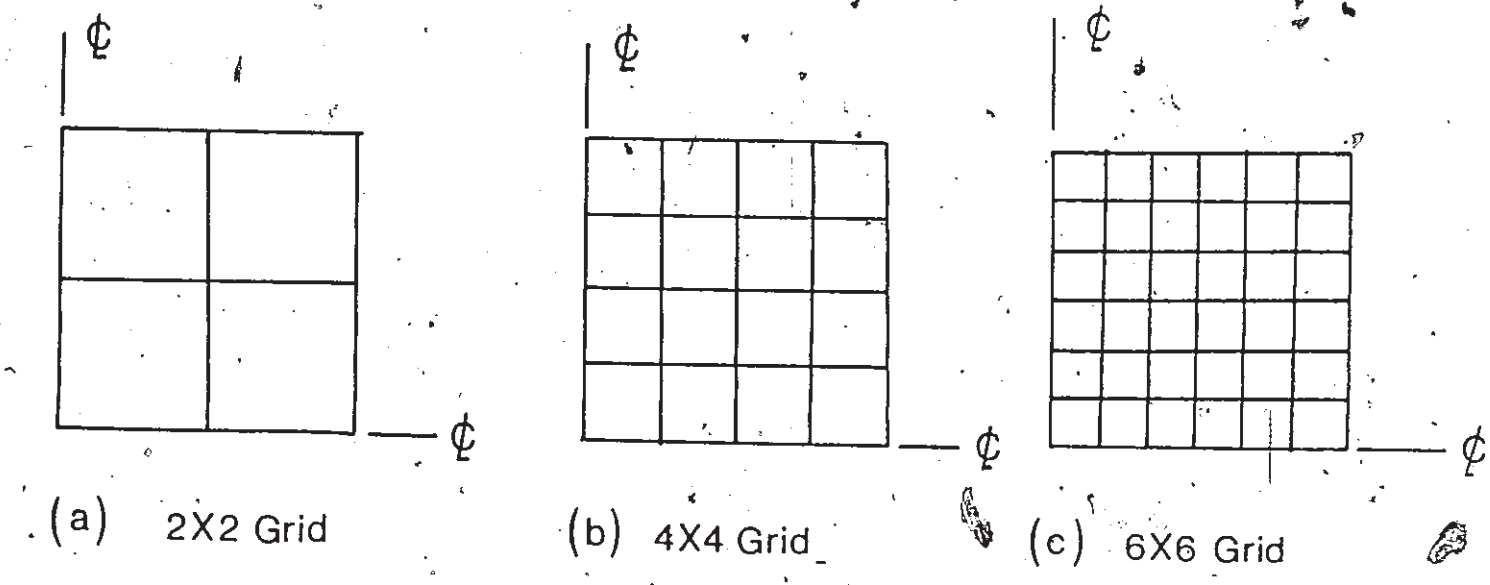

Fig. 6.6 Grid Layout for the Simply Supported Reinforced Concrete Slab.

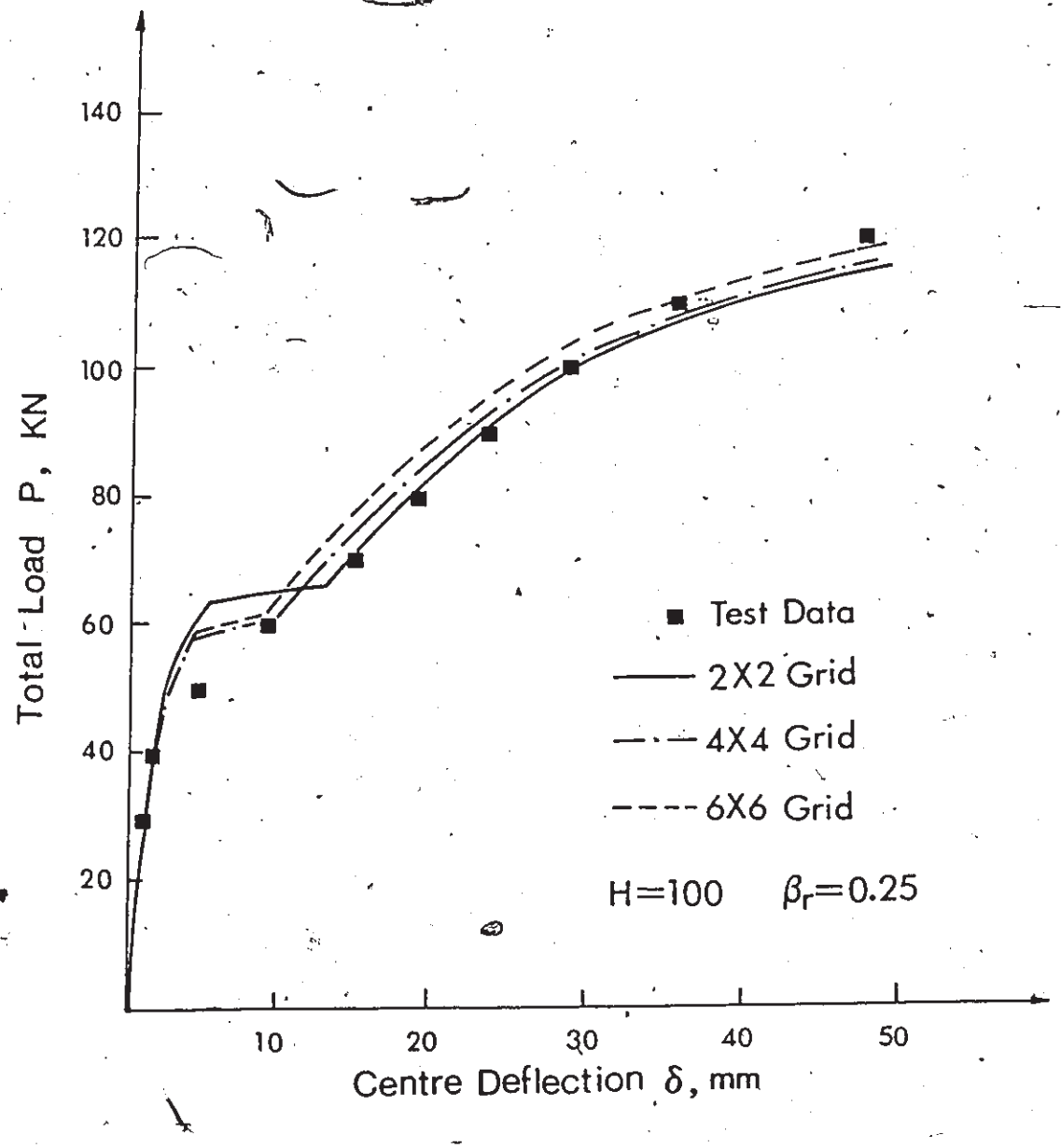

Fig. 6.7 Predicted Load-Displacement Response of the Slab at the Midpoint Using Different Grids.

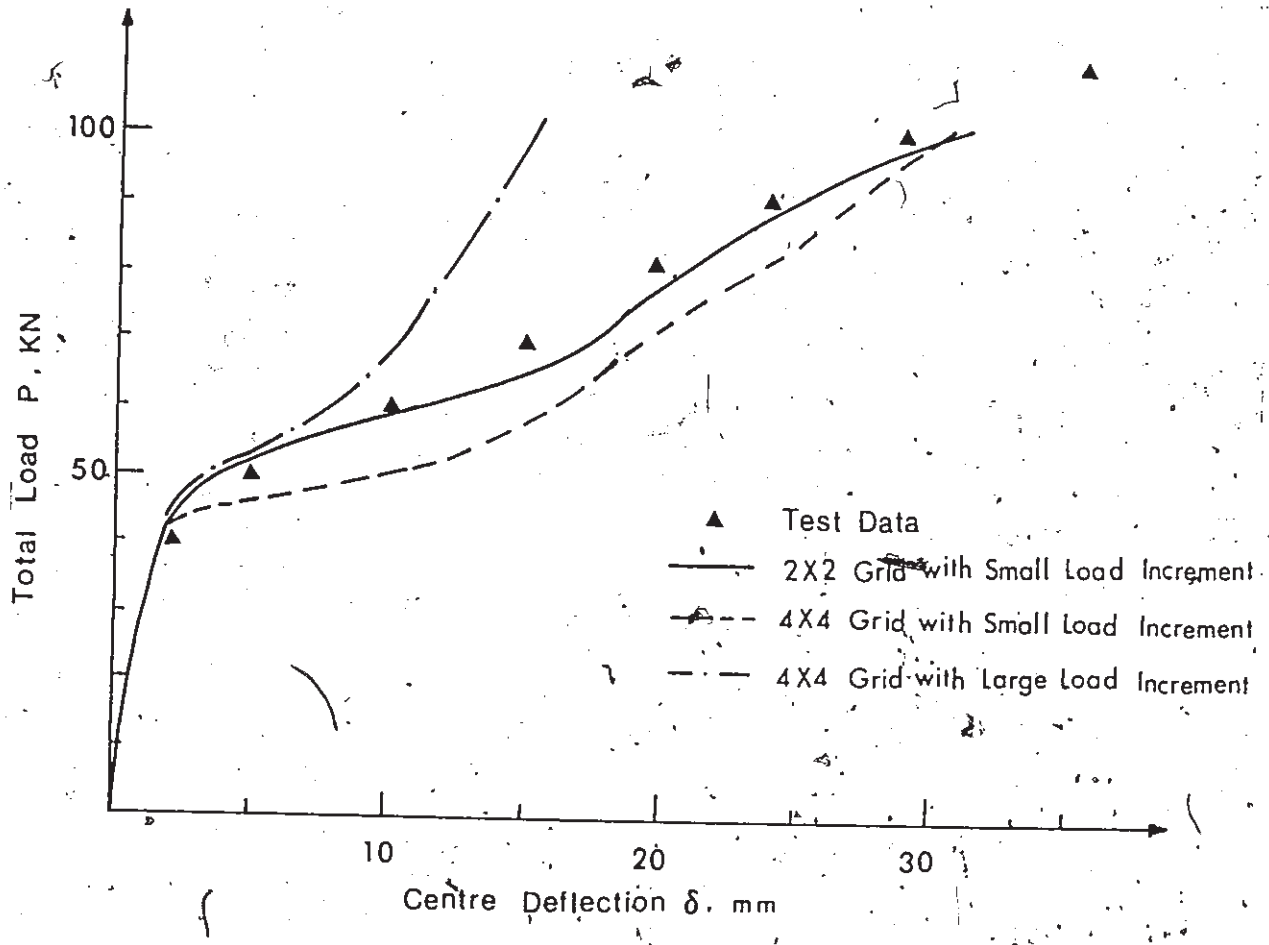

Fig. 6.8 Numerical Predictions by Chow[137].

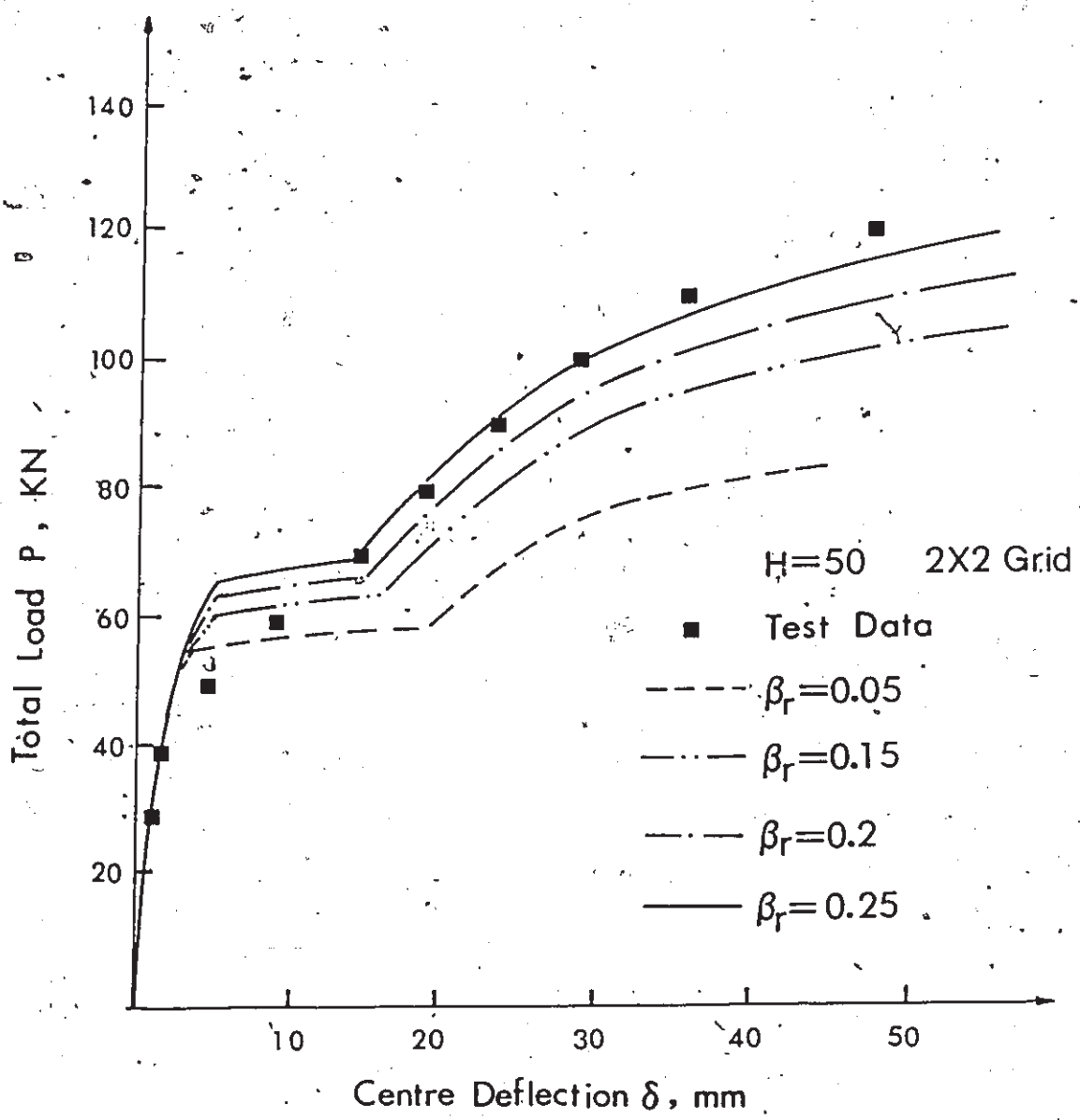

Fig. 6.9 Influence of Residual Strength of Concrete on the Predicted Deflection of the Slab.

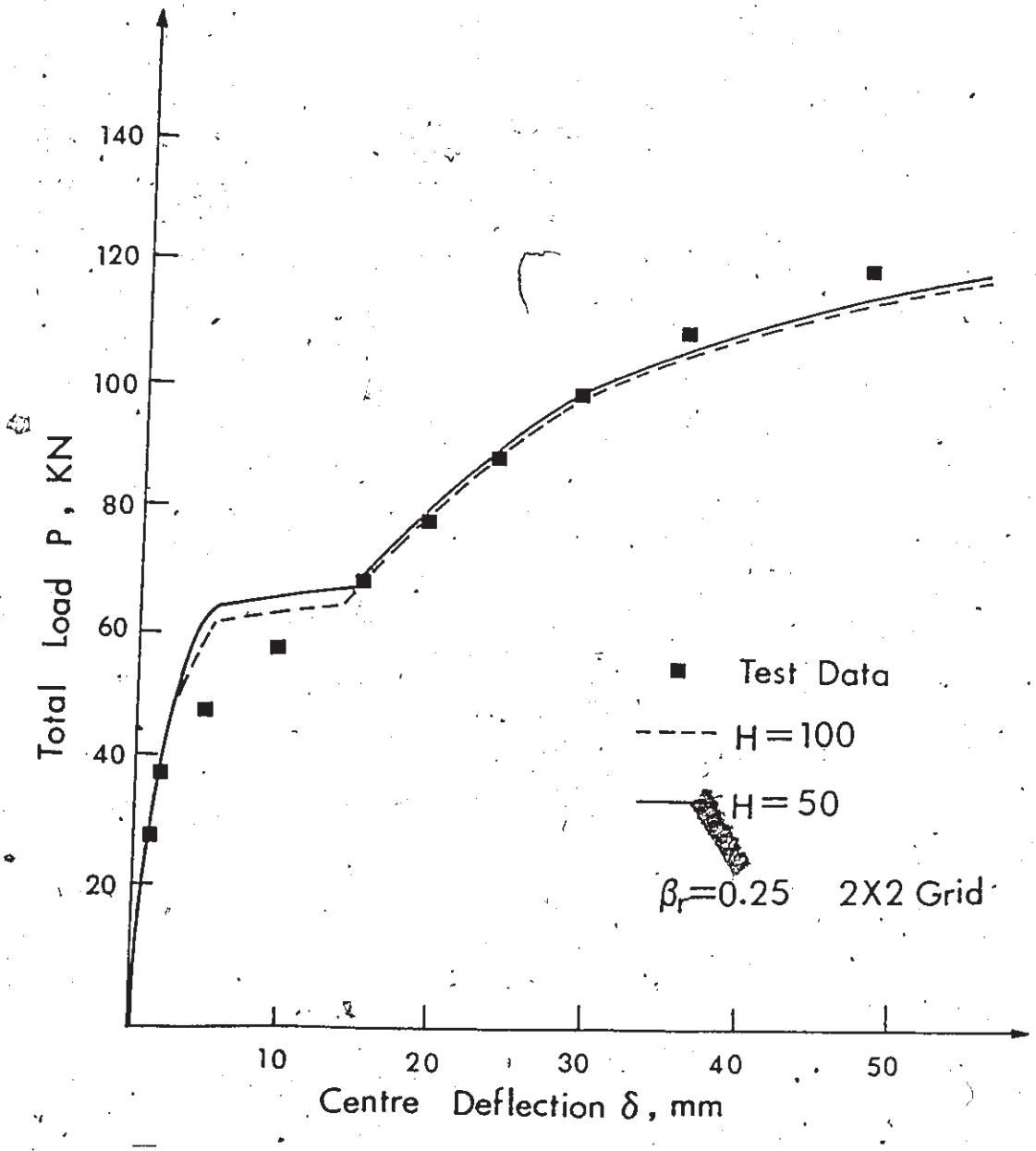

Fig. 6.10 Influence of Parameter H on the Predicted Deflection of the Reinforced Concrete Slab.

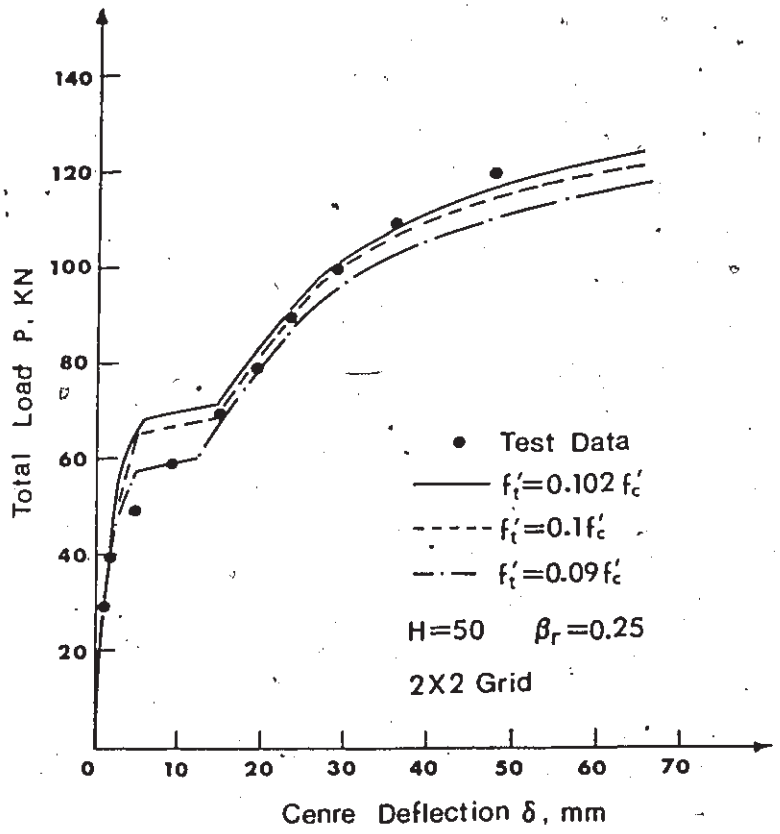

Fig. 6.11 Influence of the Value of f_t' on the predicted Deflection of the Slab.

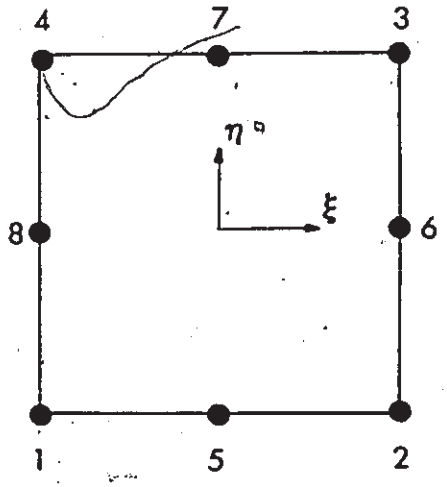

Fig. 6.12 Eight-Node Isoparametric Element

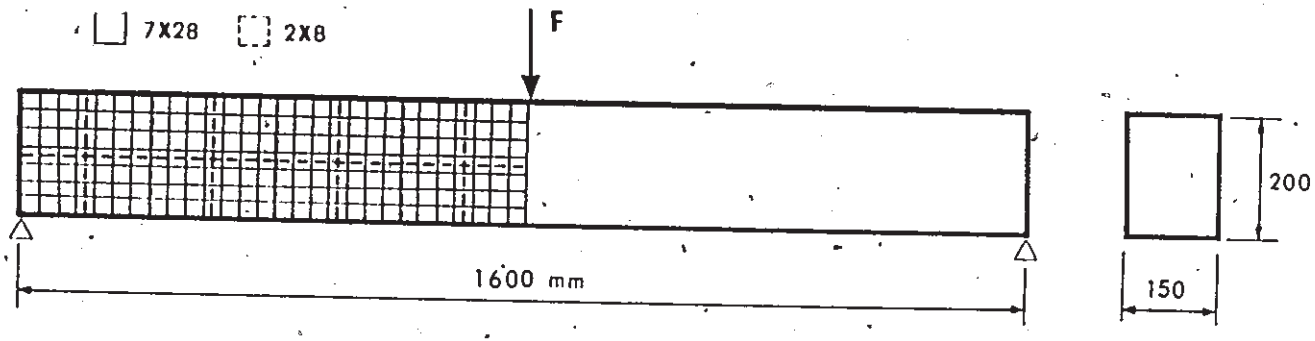

$E = 30000\ MPa$ $\quad f_c' = 30 MPa$

$\nu = 0.2$

$H = 10$ $\quad V_s = 750000\ mm^3$

$\mu = 2$ $\quad \lambda = 0.5$

$\bar{\phi}_r = 0.8$

$(\frac{f}{f_c'})_1 = 3$

Fig. 6.13 Geometry, Grid Layout and Material Properties of a Simply Supported Plain Concrete Beam.

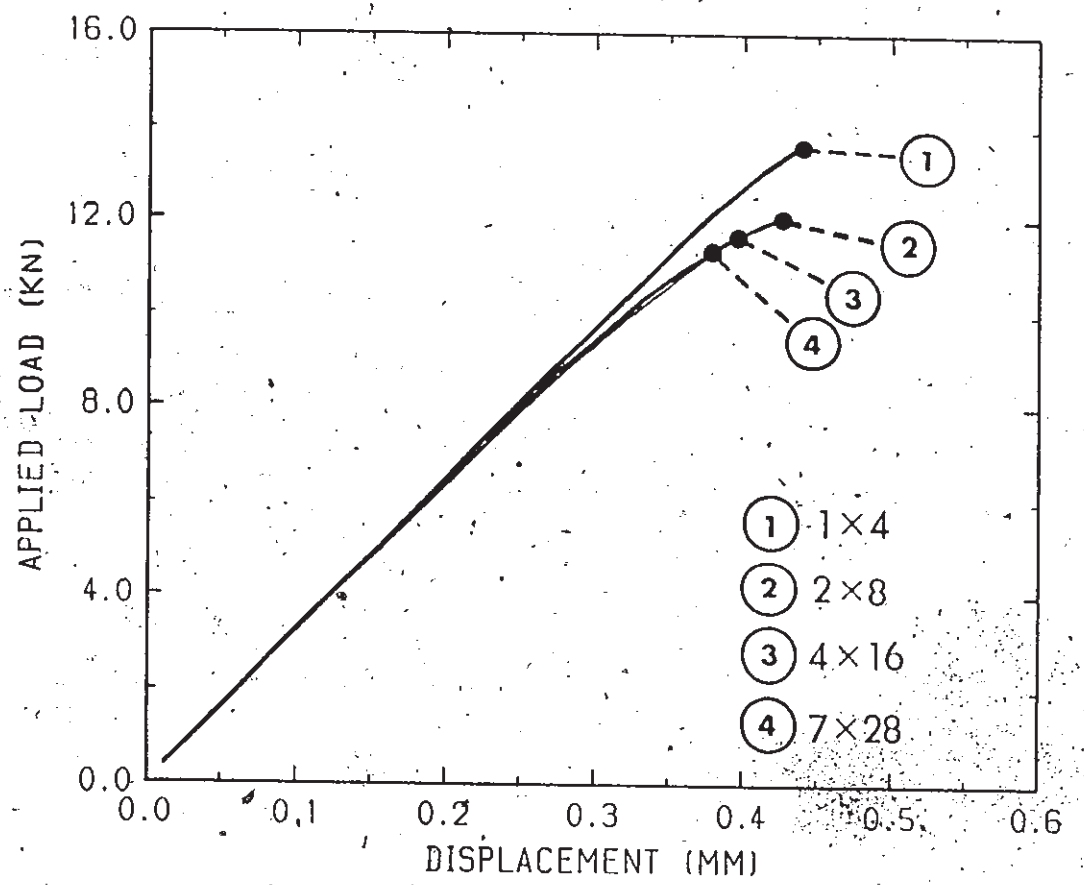

Fig. 6.14 Numerical Predictions by Conventional Finite Element Procedure.

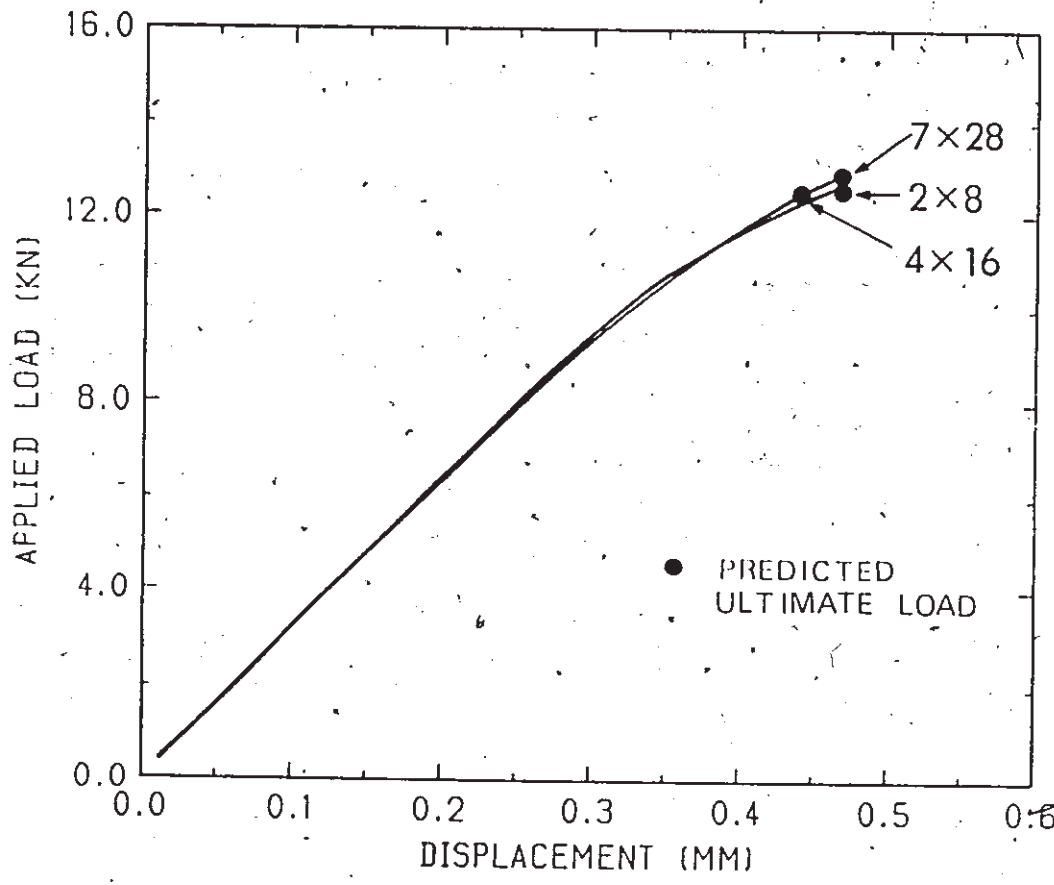

Fig. 6.15 Numerical Predictions by Unconventional Finite Element Procedure.

CHAPTER 7

CONCLUSIONS AND RECOMMENDATIONS

7.1 Summary and Conclusions

The present study has been concerned with the numerical modelling of mechanical behaviour of concrete structures. As a realistic numerical solution to a structural problem involving plain or reinforced concrete material depends, to a large extent, on the choice of an appropriate constitutive law, the emphasis of this study has been placed on investigating basic characteristics of concrete behaviour under general multiaxial loading conditions and establishing a rational constitutive theory for concrete. Furthermore, finite element models, which incorporate the proposed constitutive relations, have been developed for nonlinear analysis of reinforced concrete slabs as well as plain concrete beams.

Concrete is a composite material and contains numerous defects or microcracks. Under the action of externally applied loads the propagation and coalescence of these microcracks contribute to the generally observed nonlinear stress-strain behaviour and the irreversible deformation of concrete. At the same time, the material characteristics are strongly influenced by the magnitude of the confining pressure. A realistic representation of such a complex

behaviour of concrete has been achieved by adopting the framework of rate-independent theory of plasticity. The constitutive model proposed in this study is capable of describing the behaviour of concrete under both the monotonic and the cyclic loadings and adequately reflects certain typical trends in the response of concrete such as compaction-dilatancy transition, sensitivity of material characteristics to the confining pressure, the phenomenon of a smooth transition in failure mechanisms from a ductile to a brittle mode, cyclic degradation of material stiffness and strength.

From the mathematical point of view, the constitutive model invokes the concept of a failure locus which is introduced a priori as a path-independent criterion. During an initial active loading process the progressive deformation of concrete is described in terms of evolution of a family of yield surfaces, $f(\sigma_{ij},\xi)=0$. The instantaneous direction of plastic flow is determined by a non-associated flow rule which involves the existence of the family of plastic potential surfaces, $\Psi(\sigma_{ij})=$constant. The smobth transition from a ductile (stable) to a brittle (unstable) response is governed by an appropriate form of strain hardening/softening function. Upon stress reversal, the functional form of the current yield locus is incorporated into the material memory. It is postulated, by analogy to the bounding surface formulation, that this locus reflects the maximum load intensity attained during the past loading history. For the stress histories penetrating the interior of this surface, the deformation process is described by employing a set of neutral loading loci. This

locus defines the direction of stress rate for which the corresponding plastic strain rate instantaneously vanishes. Once again, the non-associated flow is used to determine the direction of plastic flow. However, the actual field of hardening moduli is defined relative to that along the maximum load intensity surface using an appropriate interpolation rule. If the stress reversal continues until the stress point reaches the maximum load intensity surface and tends to move outside it, the entire stress reversal history is erased from the material memory. The subsequent stress-strain behaviour is described by the same formula as that for the initial active loading process.

Before applying the model to simulate various loading histories, all the material parameters have to be appropriately identified. As a part of this study a detailed procedure for identification of the material parameters has been developed. In general, to predict monotonic response of concrete in the hardening regime, only one material constant f_c' is required in addition to the elastic properties. However, more parameters are involved when the unstable response and/or cyclic behaviour are to be accounted for. In either case the identification procedure is not difficult and requires conventional experimental tests. The model has been verified for a number of loading paths, including static and cyclic loading histories. The results of numerical simulations have been compared with the experimental data available in the literature. For the cases considered, the agreement between the numerical simulations and the experimental data has been observed to be very good.

In order to assure convexity of the yield surface and plastic potential in the octahedral plane, a general criterion for convexity has been derived using calculus and has been implemented to examine the various existing formulations. Two simple expressions defining the shape function $g(\theta)$ have been proposed in this study and they ensure a smooth and convex surface for K values near half.

In modelling of strain softening response, the approach based on an equivalent continuum concept, similar to that suggested in ref.[88], has been introduced. In this approach the strain softening is considered as a local phenomenon occurring, in a 'smeared' sense, at a material point. In order to account for the sensitivity of unstable characteristics to the size of the specimen, a so-called 'size parameter' has been introduced into the constitutive framework. This parameter has been defined in such a way as to relate the actual rate of strain softening to the volume of the sample. It has been assumed that the strain softening phenomenon is the result of localization of deformation into a shear band. Accordingly, the brittle-ductile transition in the behaviour of concrete can be treated as a bifurcation problem. From the constitutive instability criterion a necessary condition for strain localization has been derived. Moreover, in order to determine whether the bifurcation is physically feasible, an additional condition for strain localization has been postulated using the concept of maximum second rate of energy dissipation. Both conditions have been successfully employed to predict the brittle-ductile transition in concrete.

The second part of this study was to develop a finite element model which incorporates the proposed constitutive theory for nonlinear analysis of reinforced concrete slabs and plain concrete beams. The main purpose of this part was to verify whether the constitutive theory can adequately model both cracking and crushing of concrete in a real structural member during an increasing load process and whether it can improve the numerical predictions in terms of total load-deflection characteristics when compared with the previous studies by other researchers. In the finite element analysis of reinforced concrete slabs, the concrete plate has been represented by twenty degrees of freedom, non-conforming rectangular plate elements while the reinforcing steel bars have been accommodated as discrete beam elements. For analysis of plain concrete beams the eight-node isoparametric element has been used to discretize the concrete beam. In both analyses the 'initial stress' solution technique has been adopted together with the incremental load scheme. The numerical results of the slab analysis have been compared with the experimental data and the results obtained by other investigators. Significant improvement in the numerical predictions has been observed. The beam analysis involved both conventional and unconventional (i.e. incorporating the size parameter $\bar{\phi}_s$) finite element procedure. The comparison of numerical results obtained using two different procedures indicates that the unconventional analysis does reduce the sensitivity of the predicted collapse load to the details of discretization.

On the basis of this study, the following major conclusions can be restated:

(1) The elastoplastic constitutive framework can be considered as an effective tool for describing the complex behaviour of concrete.

(2) The proposed constitutive model captures the most important characteristics of concrete behaviour under static loading, e.g. compaction-dilatancy transition, sensitivity of material response to the applied confining pressure, brittle-ductile transition in failure mechanisms.

(3) The use of the concept of neutral loading surface to define conditions of neutral state of stress greatly simplifies the mathematical formulation for stress-reversal histories and the modified version of interpolation rule enables to simulate adequately the effect of cyclic degradation of the material stiffness and strength.

(4) The introduction of 'size effect' into constitutive framework allows to relate the actual rate of strain softening to the geometrical aspects of a sample. The finite element analysis of unstable response of plain concrete beam has demonstrated that the present approach incorporating the 'size effect' is certainly advantageous over conventional formulations which consider strain softening effects entirely as a material property.

(5) The brittle-ductile transition in the behaviour of concrete can be considered as a bifurcation problem and the transition pressure can be predicted from an appropriate analytical criterion.

(6) The finite element analysis of reinforced concrete slabs has clearly indicated that the proposed constitutive theory is capable of modelling both cracking of concrete and the effect of tension stiffening under a multiaxial state of stress. Moreover, the use of a rational model has resulted in a substantial reduction of sensitivity of finite element solution to the grid size and load step size.

(7) From the performed parametric study, it has been found that the residual strength of concrete has a considerable effect on the predicted response of slabs, whereas the rate of strain softening has a very small influence. However, the rate of strain softening has a strong influence on the response of plain concrete structures as observed from the results of conventional finite element analysis of the plain concrete beam presented in Chapter 6.

(8) The very important feature of the proposed constitutive model is that both brittle and ductile behaviour have been described within the same phenomenological framework. This is certainly advantageous in the context of finite element implementations as already observed.

7.2 Recommendations for Future Research

As the mechanical behaviour of concrete structures is extremely complicated, it is impossible to cover all aspects in a single research program. Instead, some of the most important characteristics of concrete behaviour have been investigated in the present study, thus leaving some problems for future investigations. In the following, some recommendations for future research are drawn from the present study.

(1) More experimental investigations on the strain softening response of concrete are required concerning the influence of the geometrical aspects of a sample and the applied confining pressure.

(2) More experimental data on the brittle-ductile transition of concrete behaviour is needed in order to further verify the proposed bifurcation theory.

(3) The cyclic response of concrete under general multiaxial loading conditions should be further studied both experimentally and analytically.

(4) Other aspects of the behaviour of concrete such as time-dependent response (creep and shrinkage), large deformations should also be investigated for a more complete understanding of the mechanical behaviour of concrete.

(5) The proposed constitutive theory should be further verified by analyzing different types of structural problems in order to further evaluate its reliability and

accuracy.

The above recommendations, as well as several points suggested throughout this study, appear to be a logical continuation of the present investigation.

APPENDIX A

DETERMINATION OF CURRENT PLASTIC POTENTIAL SURFACE

In order to define the current plastic potential surface, the following numerical procedure can be implemented:

(i) for $\Psi_0 \geq 0$ (or $\eta_c \leq \eta_0$)

Referring to Fig. 2.13, let define the parameter η_c as

$$\eta_c = \frac{\bar{\sigma}}{g(\theta)(a_3 f_c' + I^*)} \tag{A.1}$$

where, according to Eqs.(2.5) and (2.13)

$$\bar{\sigma} = \frac{\alpha g(\theta) f_c'}{2a_2}\left[-a_1 + \sqrt{a_1^2 + 4a_2\left(a_3 + \frac{I^*}{f_c'}\right)}\right] \tag{A.2}$$

Substituting the above relations into Eq.(2.12) and noting that $\bar{I}_0 = e(a_3 f_c' + I^*)$, an algebraic equation in terms of I^* is obtained. After solving this equation, an appropriate value of η_c can be determined which uniquely defines the current plastic potential surface.

(ii) for $\Psi_0 \leq 0$

In this case the value of parameter η_0, viz. Eq.(2.14), can be directly substituted in Eq.(2.12). Noting that $\bar{I}_0 = e a_0 f_c'$, Eq.(2.12) can be solved for a_0. Thus, the current plastic potential surface $\Psi = 0$ is completely defined.

APPENDIX B

STATIC ADMISSIBILITY OF THE $\bar{\sigma}$-$\bar{\varepsilon}$ CHARACTERISTICS

When the size parameter $\bar{\phi}_s$ is incorporated into the constitutive framework, Eq.(2.17), it is necessary to further investigate the condition concerning the static admissibility of the $\bar{\sigma}$-$\bar{\varepsilon}$ characteristics. During the strain softening phase progressive decrease in $\bar{\sigma}$ must be accompanied by the corresponding increase in the strain $\bar{\varepsilon}$, otherwise an abrupt loss of equilibrium will take place. In mathematical terms, the following conditions must be satisfied

$$d\bar{\varepsilon}^e + d\bar{\varepsilon}^p > 0 \tag{B.1}$$

where the superscripts refer to the elastic and plastic part of $\bar{\varepsilon}$, respectively.

According to Eq.(2.8), after differentiating, one have

$$\frac{d\beta}{d\xi} = \bar{\Phi} \frac{d\beta}{d\bar{\varepsilon}^p} \tag{B.2}$$

which gives

$$d\bar{\varepsilon}^p = \frac{\bar{\Phi}}{\beta'(\xi)} d\beta \tag{B.3}$$

where $B'(\xi)=dB/d\xi$. For the elastic part

$$d\bar{\varepsilon}^e = \frac{d\bar{\sigma}}{\sqrt{2}\,G} = \frac{\bar{\sigma}_f}{\sqrt{2}\,G}\,dB \tag{B.4}$$

where G represents the shear modulus. Now, combine the expressions for $d\bar{\varepsilon}^p$ and $d\bar{\varepsilon}^e$ to obtain

$$\left(\frac{\bar{\sigma}_f}{\sqrt{2}\,G} + \frac{\bar{\Phi}}{B'(\xi)}\right) dB > 0 \,. \tag{B.5}$$

In view of $dB<0$ at the strain softening phase, the above inequality reduces to

$$\frac{\bar{\sigma}_f}{\sqrt{2}\,G} + \frac{\bar{\Phi}}{B'(\xi)} < 0 \tag{B.6}$$

or after a simple rearrangement

$$\frac{dB}{d\xi} > -\sqrt{2}\,G\,\frac{\bar{\Phi}}{\bar{\sigma}_f} \tag{B.7}$$

For an arbitrary I, the function $dB/d\xi$ reaches its minimum when

$$\frac{d^2B}{d\xi^2} = 0, \tag{B.8}$$

In order to find this minimum let us simplify the function $B(\xi)$ in

Eq.(2.16) to the following form

$$\beta(\xi) \cong \beta_f[1 - \bar{\phi}_r[1 - \exp(-C(\xi-\xi_f))^2]] \tag{B.9}$$

After differentiation with respect to ξ, the following is obtained

$$\frac{d^2\beta}{d\xi^2} = -2\bar{\phi}_r C\beta_f \exp[-C(\xi - \xi_f)]^2[1 - 2C(\xi - \xi_f)^2]=0 \tag{B.10}$$

which leads to

$$\xi = \xi_f + \sqrt{\frac{1}{2C}} \tag{B.11}$$

so that

$$\min\left(\frac{d\beta}{d\xi}\right) = -\bar{\phi}_r\beta_f\sqrt{2C}\, e^{-1/2} \tag{B.12}$$

Substituting the above equation in the criterion for static admissibility in Eq.(B.7) yields

$$C < \frac{[G(\frac{\bar{\phi}}{\bar{\sigma}_f})]^2\, e^4}{(\bar{\sigma}_f\beta_f)^2} \tag{B.13}$$

Finally, in view of Eq.(2.17), the following inequality is arrived at

$$H < \frac{G^2 e^4}{\bar{\phi}_r^2 B_f \bar{\phi}_s \left[\dfrac{(1/f_c')_T - (1/f_c')_f}{a_3 + (1/f_c')_f}\right]} \left(\frac{\bar{\Phi}}{\bar{\sigma}_t}\right)^2 \qquad (B.14)$$

which represents a constraint imposed on the selection of the constant H in Eq.(2.17).

APPENDIX C

DETERMINATION OF CONSTITUTIVE TENSOR

According to Eq.(2.31), the mechanical behaviour of concrete is governed by an incremental constitutive relation

$$d\sigma_{ij} = D^{ep}_{ijkl}\, d\varepsilon_{kl} \qquad (C.1)$$

in which D^{ep}_{ijkl} is a fourth order tensor defined by

$$D^{ep}_{ijkl} = D^{e}_{ijkl} - \frac{D^{e}_{ijpq} \dfrac{\partial \dot{\Psi}}{\partial \sigma_{pq}} \dfrac{\partial \Psi}{\partial \sigma_{mn}} D^{e}_{mnkl}}{H_e + H_p} \qquad (C.2)$$

where

$$H_e = \frac{\partial f}{\partial \sigma_{pq}} D^{e}_{pqrs} \frac{\partial \Psi}{\partial \sigma_{rs}} \; ; \qquad H_p = - \frac{\partial f}{\partial \beta} \frac{\partial \beta}{\partial \xi} \left(dev \frac{\partial \Psi}{\partial \sigma_{ij}} dev \frac{\partial \Psi}{\partial \sigma_{ij}} \right)^{1/2} / \bar{\Phi} \; . \qquad (C.3)$$

To specify the form of D^{ep}_{ijkl}, the expressions, which define the appropriate gradient tensors, have to be provided. The gradient of yield function can be written in the following form

$$\frac{\partial f}{\partial \sigma_{ij}} = \frac{\partial f}{\partial I} \frac{\partial I}{\partial \sigma_{ij}} + \frac{\partial f}{\partial \bar{\sigma}} \frac{\partial \bar{\sigma}}{\partial \sigma_{ij}} + \frac{\partial f}{\partial \theta} \frac{\partial \theta}{\partial \sigma_{ij}} \; . \qquad (C.4)$$

From Eq.(2.1) that defines the stress invariants, the following derivatives are obtained

$$\frac{\partial I}{\partial \sigma_{ij}} = -\delta_{ij} \; ; \qquad \frac{\partial \bar{\sigma}}{\partial \sigma_{ij}} = \frac{s_{ij}}{2\bar{\sigma}} \; ; \qquad \frac{\partial J_3}{\partial \sigma_{ij}} = s_{ik}s_{kj} - \frac{2}{3}\bar{\sigma}^2\delta_{ij} \tag{C.5}$$

so that

$$\frac{\partial \theta}{\partial \sigma_{ij}} = \frac{\partial \theta}{\partial \bar{\sigma}} \frac{\partial \bar{\sigma}}{\partial \sigma_{ij}} + \frac{\partial \theta}{\partial J_3} \frac{\partial J_3}{\partial \sigma_{ij}} \tag{C.6}$$

where

$$\frac{\partial \theta}{\partial \bar{\sigma}} = \frac{3\sqrt{3}\, J_3}{2\bar{\sigma}^4 \cos 3\theta} \; ; \qquad \frac{\partial \theta}{\partial J_3} = -\frac{\sqrt{3}}{2\bar{\sigma}^3 \cos 3\theta} \; . \tag{C.7}$$

Then, Eqs.(2.3), (2.4) and (2.7), which define the yield locus, lead to

$$\frac{\partial f}{\partial f} = -\beta(\xi)g(\theta)\left[\frac{K_1(1-K)}{Kf_c'}\left(1 - \frac{g(\theta)(\sqrt{1+a} - \sqrt{1-a\sin 3\theta})}{\sqrt{1+a} - \sqrt{1-a}}\right) + \frac{f_c'}{2a_1\bar{\sigma}_c + a_1 f_c'}\right]$$

$$\frac{\partial f}{\partial \bar{\sigma}} = 1.0$$

$$\frac{\partial f}{\partial \theta} = -\frac{3a(1-K)\bar{\sigma}g(\theta)\cos 3\theta}{2K(\sqrt{1+a} - \sqrt{1-a})\sqrt{1-a\sin 3\theta}} \; . \tag{C.8}$$

Similarly, for the plastic potential surface, its gradient has the following form

$$\frac{\partial \Psi}{\partial \sigma_{ij}} = \frac{\partial \Psi}{\partial I}\frac{\partial I}{\partial \sigma_{ij}} + \frac{\partial \Psi}{\partial \bar{\sigma}}\frac{\partial \bar{\sigma}}{\partial \sigma_{ij}} + \frac{\partial \Psi}{\partial \theta}\frac{\partial \theta}{\partial \sigma_{ij}} \tag{C.9}$$

where

$$\frac{\partial \Psi}{\partial I} = -\frac{\bar{\sigma}}{I} + \eta_c g(\theta)$$

$$\frac{\partial \Psi}{\partial \bar{\sigma}} = 1.0$$

$$\frac{\partial \Psi}{\partial \theta} = -\frac{3a(1-K)\bar{q}g(\theta)\cos 3\theta}{2K(\sqrt{1+a} - \sqrt{1-a})\sqrt{1-a\sin 3\theta}} \tag{C.10}$$

Finally, in view of Eqs.(2.7), (2.16) and (2.20), the following derivatives are attained

$$\frac{\partial f}{\partial \beta} = -g(\theta)\bar{\sigma}_c \tag{C.11}$$

$$\frac{d\beta}{d\xi} = \frac{A}{(A + B\xi)^2} \tag{C.12a}$$

for strain hardening response; or

$$\frac{d\beta}{d\xi} = \frac{A(1-\bar{\phi}_r)}{(A+B\xi)^2} + \left[\frac{A}{(A+B\xi)^2} - \frac{C\gamma\xi(\xi-\xi_f)^{\gamma-1}}{A+B\xi}\right]\bar{\phi}_r \exp[-C(\xi-\xi_f)^{\gamma}] \tag{C.12b}$$

for strain softening response.

Eqs.(C.3) to (C.12) completely define the elastoplastic constitutive tensor D^{ep}_{ijkl} *and the plastic modulus* H_p.

APPENDIX D

AN EXPLICIT CONSTRAIN ON YIELD OR PLASTIC POTENTIAL SURFACE

According to the second law of thermodynamics, the condition of irreversibility can be written as the following

$$\sigma_{ij} d\varepsilon^{p}_{ij} \geq 0 \quad . \tag{D.1}$$

If material obeys an associated flow rule, the rate of energy dissipation, i.e. the left hand side of Eq.(D.1), during an active loading process is proportional to

$$\sigma_{ij} \frac{\partial f}{\partial \sigma_{ij}} = \sigma_{ij} \left(\frac{\partial f}{\partial I} \frac{\partial I}{\partial \sigma_{ij}} + \frac{\partial f}{\partial \bar{\sigma}} \frac{\partial \bar{\sigma}}{\partial \sigma_{ij}} + \frac{\partial f}{\partial \theta} \frac{\partial \theta}{\partial \sigma_{ij}} \right) . \tag{D.2}$$

Substitution of Eqs.(C.5), (C.6) and (C.7) into Eq.(D.2) yields

$$\sigma_{ij} \frac{\partial f}{\partial \sigma_{ij}} = \frac{\partial f}{\partial I} I + \frac{\partial f}{\partial \bar{\sigma}} \bar{\sigma} \quad . \tag{D.3}$$

Therefore, Inequality(D.1) can be replaced by

$$\frac{\partial f}{\partial I} I + \frac{\partial f}{\partial \bar{\sigma}} \bar{\sigma} \geq 0 \quad . \tag{D.4}$$

Inequality(D.4) is the explicit constrain on the yield surface, It is obvious now that Inequality(D.4) does not involve θ, and thus it is

not affected by the shape of the yield surface in octahedral plane. Furthermore, inequality(D.4) does not require convexity of the yield surface in meridional plane either.

It should be noted that the above conclusion also holds for the plastic potential surface in the case when the non-associated flow rule is used to define the direction of plastic strain increment.

APPENDIX E

MATHEMATICAL DETAILS OF NECESSARY CONDITION FOR STRAIN LOCALIZATION

(i) The coefficients in Eq.(5.18) are evaluated by

$$
\begin{aligned}
B_1 &= A_1\alpha^e_{11} - A_4\alpha^e_{12} + A_7\alpha^e_{14} \\
B_2 &= A_1\bar{\alpha}_{11} + A_2\alpha^e_{11} - A_4\bar{\alpha}_{12} - A_5\alpha^e_{12} + A_7\bar{\alpha}_{14} + A_8\alpha^e_{14} \\
B_3 &= A_2\bar{\alpha}_{11} + A_3\alpha^e_{11} - A_5\bar{\alpha}_{12} - A_6\alpha^e_{12} + A_8\bar{\alpha}_{14} + A_9\alpha^e_{14} \\
B_4 &= A_3\bar{\alpha}_{11} + A_6\bar{\alpha}_{12} + A_9\bar{\alpha}_{14}
\end{aligned}
\qquad (E.1)
$$

where

$$
\begin{aligned}
A_1 &= \alpha^e_{22}\alpha^e_{44} - \alpha^e_{24}\alpha^e_{42} \\
A_2 &= \alpha^e_{22}\bar{\alpha}_{44} + \bar{\alpha}_{22}\alpha^e_{44} - \alpha^e_{24}\bar{\alpha}_{42} - \bar{\alpha}_{24}\alpha^e_{42} \\
A_3 &= \bar{\alpha}_{22}\bar{\alpha}_{44} - \bar{\alpha}_{24}\bar{\alpha}_{42} \\
A_4 &= \alpha^e_{21}\alpha^e_{44} - \alpha^e_{24}\alpha^e_{41} \\
A_5 &= \alpha^e_{21}\bar{\alpha}_{44} + \bar{\alpha}_{21}\alpha^e_{44} - \alpha^e_{24}\bar{\alpha}_{41} - \bar{\alpha}_{24}\alpha^e_{41} \\
A_6 &= \bar{\alpha}_{21}\bar{\alpha}_{44} - \bar{\alpha}_{24}\bar{\alpha}_{41} \\
A_7 &= \alpha^e_{21}\alpha^e_{42} - \alpha^e_{22}\alpha^e_{41} \\
A_8 &= \alpha^e_{21}\bar{\alpha}_{42} + \bar{\alpha}_{21}\alpha^e_{42} - \alpha^e_{22}\bar{\alpha}_{41} - \bar{\alpha}_{22}\alpha^e_{41} \\
A_9 &= \bar{\alpha}_{21}\bar{\alpha}_{42} - \bar{\alpha}_{22}\bar{\alpha}_{41}
\end{aligned}
\qquad (E.2)
$$

(ii) For material under plane strain uniaxial compression, the necessary condition for bifurcation is given by the following

$$H_p \le (H_p)_{cr} - \frac{E}{2(1+\upsilon)(1-2\upsilon)} \left[-a' + \sqrt{a'^2 - (1-2\upsilon)b'}\right] \qquad (E.3)$$

where

$$a' = \upsilon(L_{31} + L_{13}) + (1-\upsilon)(L_{11} + L_{33})$$

$$b' = 4L_{11}L_{33} - (L_{31} + L_{13})^2 \,. \qquad (E.4)$$

In Eq.(E.4), parameters L_{ij} are defined by

$$L_{11} = \frac{\partial\Psi}{\partial\sigma_1}\frac{\partial f}{\partial\sigma_1} + \frac{\partial\Psi}{\partial\sigma_2}\frac{\partial f}{\partial\sigma_2} + \upsilon\left(\frac{\partial\Psi}{\partial\sigma_1}\frac{\partial f}{\partial\sigma_2} + \frac{\partial\Psi}{\partial\sigma_2}\frac{\partial f}{\partial\sigma_1}\right)$$

$$L_{13} = \frac{\partial\Psi}{\partial\sigma_1}\frac{\partial f}{\partial\sigma_3} + \upsilon\left(\frac{\partial\Psi}{\partial\sigma_1}\frac{\partial f}{\partial\sigma_2} + \frac{\partial\Psi}{\partial\sigma_2}\frac{\partial f}{\partial\sigma_3} - \frac{\partial\Psi}{\partial\sigma_2}\frac{\partial f}{\partial\sigma_2}\right)$$

$$L_{31} = \frac{\partial\Psi}{\partial\sigma_3}\frac{\partial f}{\partial\sigma_1} + \upsilon\left(\frac{\partial\Psi}{\partial\sigma_3}\frac{\partial f}{\partial\sigma_2} + \frac{\partial\Psi}{\partial\sigma_2}\frac{\partial f}{\partial\sigma_1} - \frac{\partial\Psi}{\partial\sigma_2}\frac{\partial f}{\partial\sigma_2}\right)$$

$$L_{33} = \frac{\partial\Psi}{\partial\sigma_3}\frac{\partial f}{\partial\sigma_3} + \frac{\partial\Psi}{\partial\sigma_2}\frac{\partial f}{\partial\sigma_2} + \upsilon\left(\frac{\partial\Psi}{\partial\sigma_3}\frac{\partial f}{\partial\sigma_2} + \frac{\partial\Psi}{\partial\sigma_2}\frac{\partial f}{\partial\sigma_3}\right) . \qquad (E.5)$$

When Inequality(E.3) is satisfied, two shear bands may form. The inclination of the two bands is determined by

$$\theta_0 = \pm\tan^{-1}\sqrt{\frac{2\upsilon(1+\upsilon)(H_p)_{cr} - E(L_{13}+L_{31})}{2(1-\upsilon^2)(H_p)_{cr} + 2EL_{11}}} \,. \qquad (E.6)$$

It should be noted that angle θ_0 is the angle between the normal to the plane of localization and the σ_3-axis.

APPENDIX F

SHAPE FUNCTIONS OF CONCRETE AND STEEL ELEMENTS

(i) Shape Functions of Concrete Element

$$N_1 = (1 - s)(1 - t)/4$$

$$N_2 = (1 + s)(1 - t)/4$$

$$N_3 = (1 + s)(1 + t)/4$$

$$N_4 = (1 - s)(1 - t)/4 \qquad (F.1)$$

$$\bar{N}_1 = 1 - (\frac{1+s}{2})(\frac{1+t}{2}) - (2-s)(\frac{1+s}{2})^2(\frac{1-t}{2}) - (\frac{1-s}{2})(2-t)(\frac{1+t}{2})^2$$

$$\bar{N}_2 = x_0(\frac{1-s}{2})^2(\frac{1+s}{2})(\frac{1-t}{2})$$

$$\bar{N}_3 = y_0(\frac{1-s}{2})(\frac{1+t}{2})(\frac{1-t}{2})^2$$

$$\bar{N}_4 = (\frac{1+s}{2})^2(\frac{1-t}{2})(2-s) - (\frac{1+s}{2})(\frac{1+t}{2})(\frac{1-t}{2})t$$

$$\bar{N}_5 = -x_0(\frac{1-s}{2})(\frac{1+s}{2})^2(\frac{1-t}{2})$$

$$\bar{N}_6 = y_0(\frac{1+s}{2})(\frac{1+t}{2})(\frac{1-t}{2})^2$$

$$\bar{N}_7 = (2-s)(\frac{1+s}{2})^2(\frac{1+t}{2}) + (\frac{1+s}{2})(\frac{1+t}{2})(\frac{1-t}{2})t$$

$$\bar{N}_8 = -x_0\left(\frac{1-s}{2}\right)\left(\frac{1+s}{2}\right)^2\left(\frac{1+t}{2}\right)$$

$$\bar{N}_9 = -y_0\left(\frac{1+s}{2}\right)\left(\frac{1-t}{2}\right)\left(\frac{1+t}{2}\right)^2$$

$$\bar{N}_{10} = \left(\frac{1-s}{2}\right)\left(\frac{1+t}{2}\right)^2(2-t) - \left(\frac{1+s}{2}\right)\left(\frac{1-s}{2}\right)\left(\frac{1+t}{2}\right)s$$

$$\bar{N}_{11} = x_0\left(\frac{1+s}{2}\right)\left(\frac{1-s}{2}\right)^2\left(\frac{1+t}{2}\right)$$

$$\bar{N}_{12} = -y_0\left(\frac{1-s}{2}\right)\left(\frac{1-t}{2}\right)\left(\frac{1+t}{2}\right)^2$$

(F.2)

(ii) Shape Functions of Steel Element

$$N_{s1} = 1 - (2-\zeta)\left(\frac{1+\zeta}{2}\right)^2$$

$$N_{s2} = \ell\left(\frac{1-\zeta}{2}\right)^2\left(\frac{1+\zeta}{2}\right)$$

$$N_{s3} = \left(\frac{1+\zeta}{2}\right)^2(2-\zeta)$$

$$N_{s4} = -\ell\left(\frac{1-\zeta}{2}\right)\left(\frac{1+\zeta}{2}\right)^2$$

(F.3)

$$\bar{N}_{s1} = \frac{1-\zeta}{2}$$

$$\bar{N}_{s2} = \frac{6e}{\ell}\left(\frac{1+\zeta}{2}\right)\left(\frac{\zeta-1}{2}\right)$$

$$\bar{N}_{s3} = e\left[1 - 4\left(\frac{1+\zeta}{2}\right) + 3\left(\frac{1+\zeta}{2}\right)^2\right]$$

$$\bar{N}_{s4} = \frac{1+\zeta}{2}$$

$$\bar{N}_{s5} = \frac{6e}{\ell}\left(\frac{1+\zeta}{2}\right)\left(\frac{1-\zeta}{2}\right)$$

$$\bar{N}_{s6} = e\left[-2\left(\frac{1+\zeta}{2}\right) + 3\left(\frac{1+\zeta}{2}\right)^2\right]$$

(F.4)

APPENDIX G

STEEL TRANSFORMATION MATRIX

$$
\begin{bmatrix} u_1 \\ v_1 \\ w_1 \\ \frac{\partial w_1}{\partial x} \\ \frac{\partial w_1}{\partial y} \\ u_2 \\ v_2 \\ w_2 \\ \frac{\partial w_2}{\partial x} \\ \frac{\partial w_2}{\partial y} \end{bmatrix} =
\begin{bmatrix}
N_1 & & & N_2 & & & N_3 & & & N_4 & & \\
 & N_1 & & & N_2 & & & N_3 & & & N_4 & \\
 & \bar{N}_1 & \bar{N}_2 & \bar{N}_3 & \bar{N}_4 & \bar{N}_5 & \bar{N}_6 & \bar{N}_7 & \bar{N}_8 & \bar{N}_9 & \bar{N}_{10} & \bar{N}_{11} & \bar{N}_{12} \\
 & \frac{\partial \bar{N}_1}{\partial x} & \frac{\partial \bar{N}_2}{\partial x} & \frac{\partial \bar{N}_3}{\partial x} & \frac{\partial \bar{N}_4}{\partial x} & \frac{\partial \bar{N}_5}{\partial x} & \frac{\partial \bar{N}_6}{\partial x} & \frac{\partial \bar{N}_7}{\partial x} & \frac{\partial \bar{N}_8}{\partial x} & \frac{\partial \bar{N}_9}{\partial x} & \frac{\partial \bar{N}_{10}}{\partial x} & \frac{\partial \bar{N}_{11}}{\partial x} & \frac{\partial \bar{N}_{12}}{\partial x} \\
 & \frac{\partial \bar{N}_1}{\partial y} & \frac{\partial \bar{N}_2}{\partial y} & \frac{\partial \bar{N}_3}{\partial y} & \frac{\partial \bar{N}_4}{\partial y} & \frac{\partial \bar{N}_5}{\partial y} & \frac{\partial \bar{N}_6}{\partial y} & \frac{\partial \bar{N}_7}{\partial y} & \frac{\partial \bar{N}_8}{\partial y} & \frac{\partial \bar{N}_9}{\partial y} & \frac{\partial \bar{N}_{10}}{\partial y} & \frac{\partial \bar{N}_{11}}{\partial y} & \frac{\partial \bar{N}_{12}}{\partial y} \\
N_1 & & & N_2 & & & N_3 & & & N_4 & & \\
 & N_1 & & & N_2 & & & N_3 & & & N_4 & \\
 & \bar{N}_1 & \bar{N}_2 & \bar{N}_3 & \bar{N}_4 & \bar{N}_5 & \bar{N}_6 & \bar{N}_7 & \bar{N}_8 & \bar{N}_9 & \bar{N}_{10} & \bar{N}_{11} & \bar{N}_{12} \\
 & \frac{\partial \bar{N}_1}{\partial x} & \frac{\partial \bar{N}_2}{\partial x} & \frac{\partial \bar{N}_3}{\partial x} & \frac{\partial \bar{N}_4}{\partial x} & \frac{\partial \bar{N}_5}{\partial x} & \frac{\partial \bar{N}_6}{\partial x} & \frac{\partial \bar{N}_7}{\partial x} & \frac{\partial \bar{N}_8}{\partial x} & \frac{\partial \bar{N}_9}{\partial x} & \frac{\partial \bar{N}_{10}}{\partial x} & \frac{\partial \bar{N}_{11}}{\partial x} & \frac{\partial \bar{N}_{12}}{\partial x} \\
 & \frac{\partial \bar{N}_1}{\partial y} & \frac{\partial \bar{N}_2}{\partial y} & \frac{\partial \bar{N}_3}{\partial y} & \frac{\partial \bar{N}_4}{\partial y} & \frac{\partial \bar{N}_5}{\partial y} & \frac{\partial \bar{N}_6}{\partial y} & \frac{\partial \bar{N}_7}{\partial y} & \frac{\partial \bar{N}_8}{\partial y} & \frac{\partial \bar{N}_9}{\partial y} & \frac{\partial \bar{N}_{10}}{\partial y} & \frac{\partial \bar{N}_{11}}{\partial y} & \frac{\partial \bar{N}_{12}}{\partial y}
\end{bmatrix}
\begin{bmatrix} u_1 \\ v_1 \\ w_1 \\ w_{1,x} \\ w_{1,y} \\ u_2 \\ v_2 \\ w_2 \\ \vdots \\ w_{4,x} \\ w_{4,y} \end{bmatrix}
$$

APPENDIX H

SHAPE FUNCTIONS OF EIGHT-NODE ISOPARAMETRIC ELEMENT

$$
\begin{aligned}
N_1 &= -(1-\xi)(1-\eta)(\xi+\eta+1)/4 \\
N_2 &= (1+\xi)(1-\eta)(\xi-\eta-1)/4 \\
N_3 &= (1+\xi)(1+\eta)(\xi+\eta-1)/4 \\
N_4 &= (1-\xi)(1+\eta)(-\xi+\eta-1)/4 \\
N_5 &= (1-\xi^2)(1-\eta)/2 \\
N_6 &= (1+\xi)(1-\eta^2)/2 \\
N_7 &= (1-\xi^2)(1+\eta)/2 \\
N_8 &= (1-\xi)(1-\eta^2)/2
\end{aligned}
\qquad (H.1)
$$

BIBLIOGRAPHY

1. ASCE Committee on Concrete and Masonrey Structures, A State-of-the-Art Report on Finite Element Analysis of Reinforced Concrete. Published by ASCE, 1982.

2. Evans, R.J. and Pister, K.S. "Constitutive Equations for a Class of Nonlinear Elastic Solids", Int. Journ. Solids Struct., Vol.2, No.3, (1966), 427-445.

3. Liu, T.C.Y., Nilson, A.H. and Slate, F.O. "Biaxial Stress-Strain Relations for Concrete", Journal of Struct. Div., ASCE, Vol.98, No.ST5, (1972), 1025-1034.

4. Palaniswamy, R. and Shah, S.P. "Fracture and Stress-Strain Relationship of Concrete under Triaxial Compression", Journal of Struct. Div., ASCE, Vol.100, No.ST5, (May 1974), 901-915.

5. Cedolin, L., Crutzen, Y.R.J. and Poli, S.D. "Triaxial Stress-Strain Relationships for Concrete", Journ. Engng. Mech. Div., ASCE, Vol.103, No.EM3, (1977), 423-439.

6. Chen, A.C.T. and Chen, W.F. "Constitutive Relations for Concrete", Journ. Engng. Mech. Div., ASCE, Vol.101, No.EM4, (1975), 465-481.

7. William, K.J. and Warnke, E.P. "Constitutive Models for the Triaxial Behaviour of Concrete", IABSE Seminar Concr. Struct. Subjected to Triaxial Stresses, Bergamo, Italy, 1974, IABSE Proc., Vol.19, (1975), 1-30.

8. Chen, E.S. and Buyukozturk, O. "Constitutive Model for Concrete in Cyclic Compression", Journal of Engng. Mech., ASCE, Vol.111, No.6, (June 1985).

9. Han, D.J. and Chen, W.F. "A Nonuniform Hardening Plasticity Model for Concrete Materials", Mech. of Materials, Vol.4, (1985), 33-58.

10. Yang, B.L., Dafalias, Y.F. and Herrmann, L.R. "A Bounding Surface Plasticity Model for Concrete", Journal of Engng. Mech., ASCE, Vol.111, No.3, (March 1985).

11. Fardis, M.N., Alibe, B. and Tassoulas, A.M. " Monotonic and Cyclic Constitutive Law for Concrete", Journal of Engng. Mech., ASCE, Vol.109, No.2, (April 1983), 516-536.

12. Bazant, Z.P. and Bhat P.D. "Endochronic Theory of Inelasticity and Failure of Concrete", Journ. Engng. Mech. Div., ASCE, Vol.102, No.EM4, (1976), 701-722.

13. Valanis, K.C. and Read, H.E. "An Endochronic Plasticity Theory for Concrete", Mech. of Materials, Vol.5, (1986), 277-295.

14. Bazant, Z.P. and Kim, S.S. "Plastic-Fracturing Theory for Concrete", Journ. Engng. Mech. Div., ASCE, Vol.105, No.EM3, (1979), 407-428.

15. Dragon, A. and Mroz, Z. "A Continuum Model for Plastic-Brittle Behaviour of Rock and Concrete", Int. Journ. Engng. Sci., Vol.17, (1979), 121-137.

16. Valanis, K.C. "A Theory of Viscoplasticity without a Yield Surface, I: General Theory; II: Application to Mechanical Behaviour of Metals", Arch. Mech., Vol.23, No.4, (1971), 517-551.

17. Ngo, D. and Scordelis, A.C. "Finite Element Analysis of Reinforced Concrete Beams", Journal of ACI, Vol.64, No.3, (1967), 152-163.

18. Nilson, A.H. "Nonlinear Analysis of Reinforced Concrete by Finite Element Method", Journal of ACI, Vol.65, No.9, (1968), 757-766.

19. Rashid, Y.R. "Analysis of Prestressed Concrete Pressure Vessels", Nuclear Engng. and Design, Vol.7, No.4, (1968), 334-344.

20. Franklin, H.A. Nonlinear Analysis of Reinforced Concrete Frames and Panels. Ph.D. Thesis, Univ. of California, Berkeley, March 1970.

21. Suidan, M. and Schnobrich, W.C. "Finite Element Analysis of Reinforced Concrete", Journ. Struct. Div., ASCE, Vol.99, No.ST10, (1973), 2109-2122.

22. Darwin, D. and Pecknold, D.A. "Analysis of R.C. Shear Panels under Cyclic Loading", Journ. Struct. Div., ASCE, Vol.102, No.ST2, (1976), 355-369.

23. Scanlon, A. Time Dependent Deflections of Reinforced Concrete Slabs. Ph.D. Thesis, University of Alberta, Edmonton, Canada, 1971.

24. Lin, C.S. and Scordelis, A.C. "Nonlinear Analysis of RC Shells of General Form", Journal of Struct. Div., ASCE, Vol.101, No.ST3, (1975).

25. Gilbert, R.I. and Warner, R.F. "Nonlinear Analysis of Reinforced Concrete Slabs with Tension Stiffening", UNICIV Report No. R-167, University of New South Wales, Kensington, Australia, 1977.

26. Floegl, H. and Mang, H. "On Tension Stiffening in Cracked Reinforced Concrete Slabs and Shells Considering Geometric and Physical Nonlinearity", Ingenieur-Archiv, Vol.51, (1981), 215-242.

27. Argyris, J.H., Faust, G., Szimmat, J., Warnke, E.P. and William, K.J. "Recent Developments in the Finite Element Analysis of Prestressed Concrete Reactor Vessels", Nucl. Engng. Design, Vol.28, (1974).

28. Zienkiewicz, O.C., Owen, D.R.J., Phillips, D.V. and Nayak, G.C. "Finite Element Method in the Analysis of Reactor Vessels", Nucl. Engng. Design, Vol.20, 1972.

29. Bazant, Z. and Cedolin, L. "Blunt Cracks Band Propagation in Finite Element Analysis", Journal of Engng. Mech. Div., ASCE, Vol.105, No.EM2, (1979), 297-315.

30. Hillerborg, A., Modeer, M. and Petersson, P. "Analysis of Crack Formation and Crack Growth in Concrete by Means of Fracture Mechanics and Finite Elements", Cement and Concrete Research, Vol.6, No.6, (1976), 773-782.

31. Pietruszczak, S. "A Flow Theory for Soil: Concept of Multiple Neutral Loading Surfaces", Computers and Geotechnics, Vol.2, (1986), 185-203.

32. Nevill, A.M. Properties of Concrete. Pitman, London, 1977.

33. Mindess, S. and Young, J.F. Concrete. Prentice-Hall, New Jersey, 1981.

34. Avram, C., Facaoaru, I., Filimon, I., Mirsu, O. and Tertea, I. Concrete Strength and Strain. Elsevier, New york, 1981.

35. Mehta, P.K. Concrete: Structure, Properties, and Materials. Prentice-Hall, New Jersey, 1986.

36. Aoyama, H. and Noguchi, H. "Mechanical Properties of Steel and Concrete under Load Cycles Idealizing Seismic Action", Proc. 25th IABSE-CEB Symp., Rome, (1979).

37. Newman, K. "Concrete Systems", Composite Materials, Edited by Holliday, L., Elsevier, Amsterdam, (1966), 336-452.

38. Brooks, A.E. and Newman, K. Proc. Int. Conf. Struct. Concr. London, 1968, Cement and Concrete Association, London.

39. Shah, S.P. High Strength Concrete. Univ. Ill. Proc. Workshop Chicago 1977, Univ. of Ill., Chicago.

40. Hegemier, G.A. and Read, H.E. "On Deformation and Failure of Brittle Solids: Some Outstanding Issues", Mechanics of Materials, Vol.4, (1985), 215-259.

41. Hsu, T.T.C., Slate, F.O., Sturman, G.M. and Winter, G. "Microcracking of Plain Concrete and the Shape of the Stress-Strain Curve", Journal of ACI, Vol.60, No.2, (Feb. 1963), 209-224.

42. Spooner, D.C., Pomeroy, C.D. and Dougill, J.W. "Damage and Energy Dissipation in Cement Pastes in Compression", Magazine of Concr. Research, London, Vol.27, No.2, (March 1976), 21-29.

43. Newman, K. "Criteria for the Behaviour of Plain Concrete under Complex States of Stress", Proc. Int. Conf. Struct. Concr., London, (1968), 255-274.

44. Winter, G. and Nilson, A.H. Design of Concrete Structures. 4th Edition, McGraw-Hill, New York, 1979.

45. Kotsovos, M.D. and Newman, J.B. "Behaviour of Concrete under Multiaxial Stress", Journal of ACI, Vol.74, No.9, (1977), 443-446.

46. Chen, W.F. Plasticity in Reinforced Concrete. McGraw-Hill, New york, 1982.

47. Hughes, B.P. and Chapman, G.P. "The Deformation of Concrete and Microconcrete in Compression and Tension with Particular Reference to Aggregate Size", Magazine of Concr. Research, London, Vol.18, No.54, (March 1966), 19-24.

48. Guo, Z.H. and Zhang, X.Q. "Investigation of Complete Stress-Deformation Curves for Concrete in Tension", ACI Materials Journal, (July/August 1987), 278-285.

49. McHenry, D. and Shideler, J.J. "Review of Data on Effect of Speed in Mechanical Testing of Concrete", Proc. Symp. on Speed in Testing, STP-185, ASTM, Philadelphia, (1956), 72-82.

50. Kupfer, H., Hilsdorf, H.K. and Rusch, H. "Behaviour of Concrete under Biaxial Stresses", Journal of ACI, Vol.66, No.8, (August 1969), 656-666.

51. Tasuji, M.E., Slate, F.O. and Nilson, A.H. "Stress-Strain Response and Fracture of Concrete in Biaxial Loading", Journal of ACI, Vol.75, No.7, (July 1978), 306-312.

52. Tasuji, M.E., Nilson, A.H. and Slate, F.O. "Biaxial Stress-

Strain Relationship for Concrete", Magazine of Concr. Research, London, Vol.31, No.109, (Dec. 1979), 217-224.

53. Liu, T.C.Y., Nilson, A.H. and Slate, F.O. "Stress-Strain Response and Fracture of Concrete in Uniaxial and Biaxial Compression", Journal of ACI, Vol.69, No.5, (May 1972), 291-295.

54. Nelissen, L.J.M. "Biaxial Testing of Normal Concrete", Heron, the Netherland, Vol.18, No.1, (1972).

55. Taylor, M.A. Jain, A.K. and Ramey, M.R. "Path Dependent Biaxial Compressive Testing of an All-Lightweight Aggregate Concrete", Journal of ACI, Vol.69, No.12, (Dec. 1972), 758-764.

56. Richart, F.E., Brandtzaeg, A. and Brown, R.L. "The Failure of Plain and Spirally Reinforced Concrete in Compression", Univ. Ill. Eng. Exp. St. Bull. 190, (April 1929).

57. Balmer, G.G. "Shearing Strength of Concrete under High Triaxial Stress-Computation of Mohr's Envelope as a Curve", Struc. Res. Lab. Rep. SP-23, Denver, Colo. (Oct. 1949).

58. Cowan, H.I. "The Strength of Plain, Reinforced and Prestressed Concrete under the Action of Combined Stresses with Particular Reference to the Combined Bending and Torsion of Rectangular Section", Magazine of Concr. Research, No.14, (Dec. 1953), 75-86.

59. Berg, O.Y. "Research on the Concrete Strength Theory, Building Research and Documentation", Contributions and Discussions, First Committee International du Batimant Congress, Rotterdam, the Netherlands, (1959), 60-69.

60. Green, S.J. and Swanson, S.R. "Static Constitutive Relations for Concrete", Air Force Weapons Lab. Tech. Rep. No.AFWL-TR-72-2, Kirtland Air Force Base, (1973).

61. Palaniswamy, R.G. Fracture and Stress-Strain Law of Concrete under Triaxial Compressive stresses. Ph.D. thesis, Univ. of Ill. at Chicago Circle.

62. Kotsovos, M.O. and Newman, J.B. "Generalized Stress-Strain Relations for Concrete", Journal of Engng. Mech. Div., ASCE, Vol.104, No.EM4, (August 1978), 845-856.

63. Gerstle, K.H., Linse, D.H., et al. "Strength of Concrete under Multi-axial Stress States", Proc. McHenry Symp. Concr. Concr. Struct., Mexico city, (1976), ACI Publ. SP55, 103-131.

64. Kotsovos, M.D. "Effect of Stress Path on the Behaviour of Concrete under Triaxial Stress States", Journal of ACI, Vol.76,

No.2, (Feb. 1979), 213-223.

65. Pietruszczak, S., Jiang, J. and Mirza, F.A. "An Elastoplastic Constitutive Model for Concrete", Int. Journal Solids Struct., in press.

66. Bresler, B. and Pister, K.S. "Strength of Concrete under Combined Stress", Journal of ACI, Vol.55, (Sept. 1958), 321-345.

67. Lade, P.V. "Three-Parameter Failure Criterion for Concrete", Journal of Engng. Mech. Div., ASCE, Vol.108, No.EM5, (1982), 850-863.

68. Ottossen, N.S. "A Failure Criterion for Concrete", Journal of Engng. Mech. Div., ASCE, Vol.103, No.EM4, (August 1977), 527-535.

69. Reimann, H. "Kritische Spannungszustande der Betons bei mehrachsiger, ruhender Kurzzeitbelastung", Dtsch. Auschuss Stahlbeton, Vol.175, (1965).

70. Hsieh, S.S., Ting, E.C. and Chen, W.F. " An Elastic- Fracture Model for Concrete", Proc. 3rd Engng. Mech. Div. Spec. Conf., ASCE, Austin, Tex., (1979), 437-440.

71. Chen, W.F. and Han, D.J. "A Five-Parameter Mixed Hardening Model for Concrete Materials", Proc. Int. Symp. Plasticity Today, Udine, Italy, (1983).

72. Podgorski, J. "General Failure Criterion for Isotropic Media", Journal of Engng. Mech., ASCE, Vol.111, No.2,(Feb. 1985), 188-201.

73. Schreyer, H.L. and Babcock, S.M. "A Third-Invariant Plasticity Theory for Low-Strength Concrete", Journal of Engng. Mech., ASCE, Vol.111, No.4, (April 1985).

74. Chen, W.F. "Constitutive Relations for Concrete and Rock", Mechanics of Geomaterials: Rocks, Concrete, Soils, Edited by Bazant, Z.P., William Prager Symp. on Mech. of Geomaterials: Rocks, concrete, Soils, Northwestern Univ., Evanston, Ill., (1983).

75. Jiang, J. and Pietruszczak, S. "Convexity of Yield Loci for Pressure Sensitive Materials", Computers and Geotechnics, in press.

76. Chen, E.S. and Buyukozturk, O. "Constitutive Model for Concrete in Cyclic Compression", Journal of Engng. Mech., ASCE, Vol.111, No.6, (June 1985).

77. Hill, R. The Mathematical Theory of Plasticity. Oxford Univ.

Press, London, 1950.

78. Mendelson, A. Plasticity: Theory and Applications. Macmillan Publishing Co., Inc., New York, 1968.

79. Kachanov, L.M. Foundations of Theory of Plasticity. North-Holland Publishing Company, Amsterdam, 1971.

80. Poorooshasb, H.B. and Pietruszczak, S. "On Yield and Flow of Sand: a Generalized Two Surface Model", Computers and Geotechincs, Vol.1, No.1, (1985), 33-58.

81. van Mier, J.G.M. Strain-Softening of Concrete under Multiaxial Loading Conditions, Ph.D. Thesis, Eindhoven Univ. of Tech., Eindhoven, the Netherlands, (1984).

82. Sandler, I.S. "Strain Softening for Static and Dynamic Problems", ASME Winter Annual Meeting, Proc. Symp. on Constitutive Equations: Micro, Macro and Computational Aspects, CEQ, New Orleans, (Dec. 1984).

83. Read, H.E. and Hegemier, G.A. "Strain Softening of Rock, Soil and Concrete-A review Article", Mech. of Materials, Vol.3, (1984), 271-294.

84. Shah, S.P. and Slate, F.O. "Internal Microcracking, Mortar-Aggregate Bond and the Stress-Strain Curve of Concrete", Proc. Int. Conf. on the Struct. of Concr. and its Behaviour under Load, London, 1965, Cement and Concrete Association, London, (1968).

85. Maher, A. and Darwin, D. "Mortar Constituent of Concrete in Compression", Journal of ACI, Vol.100, (March/April 1982).

86. Pietruszczak, S. and Mroz, Z. "Finite Element Analysis of Deformation of Strain-Softening Materials", Int. Journal Numer. Meth. Engng., Vol.17, (1981), 327-334.

87. Kotsovos, M.D. "Mathematical Description of the Strength Properties of Concrete under Generalized Stress", Magazine of Concr. Research, Vol.31, No.108, (1979), 151-158.

88. Gardner, N.J. "Triaxial Behaviour of Concrete", Journal of ACI, Vol.66, No.2, (1969), 136-146.

89. Mills, L.L. and Zimmerman, R.M. "Compressive Strength of Plain Concrete under Multiaxial Loading Conditions", Journal of ACI, Vol.69, No.10, (1970), 802-807.

90. Launary, P. and Gachon, H. "Strain and Ultimate Strength of Concrete under Triaxial Stress", Spec. Publ. ACI SP-34, (1970), 269-282.

91. Kotsovos, M.D. and Newman, J.B. "A Mathematical Description of the Deformation Behaviour of Concrete under Complex Loading", Magazine of Concr. Research, Vol.31, No.107, (1979), 77-90.

92. Chinn, J. and Zimmerman, R.M. "Behaviour of Plain Concrete under Various High Triaxial Compression Loading Conditions", Tech. Report No.WL TR 64-163, Air Force Weapons Lab., Albuquerque, NM.

93. Gopalaratnam, V.S. and Shah, S.P. "Softening Response of Concrete in Direct Tension", Journal of ACI, Vol.82, No.3, (1985), 310-323.

94. Dilger, W.H., Koch, R. and Kowalczyk,R. "Ductility of Plain and Confined Concrete under Different Strain", Journal of ACI, Vol.81, No.1, (1984), 73-81.

95. Wang, P.T., Shah, S.P. and Naaman, A.E. "Stress-Strain Curves of Normal and Lightweight Concrete in Compression", Journal of ACI, Vol.75, No.11, (1978), 603-611.

96. Prager, W. "Recent Developments in the Mathematical Theory of Plasticity", Journal of Applied Physics, Vol.20, No.3, (1949), 235-241.

97. Mroz, Z. "Non-associated Flow Laws in Plasticity", Journal de Mecanique, Vol.2, No.1, (1963), 21-42.

98. Drucker, D.C. "A More Fundamental Approach to Stress- Strain Relations", Proceedings 1st National Congress for Applied Mechanics, ASME, (1951), 487-491.

99. Drucker, D.C. "On Uniqueness in the Theory of Plasticity", Quarterly of Applied Mathematics, Vol.14, No.1, (1956), 35-42.

100. Drucker, D.C. "A Definition of Stable Inelastic Material", Journal of Applied Mechanics, ASME, Vol.26, (1959), 101-106.

101. Gudehus, G. "Elastoplastische Stoffgleichungen fur Trockenen Sand", Ingenieur-Archiv, Vol.42, (1973), 151-169.

102. Argyris, J.H. et al. "Recent Developments in the Finite Element Analysis of PCRV", Nuclear Engng. and Design, Vol.28, (1974), 42-75.

103. Boswell, L.F. and Chen, Z. "A General Failure Criterion for Plain Concrete", Int. Journal Solids Struct., Vol.23, (1987), 621-630.

104. Lade, P.V. and Duncan, J.M. "Elastoplastic Stress-Strain Theory for Cohesionless Soil", Journal of Geotech. Engng. Div., ASCE, Vol.101, (1975), 1037-1053.

105. Matsuoka, H. and Nakai, T. "Stress-Deformation and Strength Characteristics of Soil under Three Different Principal Stresses", Proc. Japan Soc. Civil Engrs., Vol.232, (1974), 59-70.

106. Ellis, R. and Gulick, D. Calculas with Analytic Geometry. Harcourt Brace Jovanovich, Inc., New York, 1978.

107. Zienkiewicz, O.C. and Pande, G.N. "Some Useful Forms of Isotropic Yield Surfaces for Soil and Rock mechanics", Finite Elements in Geomechanics, Edited by Gudehus, G., John Wiley and Sons, Inc., New York, (1977), 179-180.

108. Lin, F.B. and Bazant, Z.P. "Convexity of Smooth Yield Surface of Frictional Material", Journal of Engng. Mech., ASCE, Vol.112, (1986), 1259-1262.

109. Dafalias, Y.F. and Herrmann, L.R. "Bounding Surface Plasticity. II: Application to Isotropic Cohesive Soils", Journal of Engng. Mech., ASCE, Vol.112, No.12, (1986), 1263-1291.

110. Shinha, B.P., Gerstle, H.K. and Tulin, L.G. "Stress-Strain Relations for Concrete under Cyclic Loading", Journal of ACI, Vol.61, No.2, (1964), 195-211.

111. Shah, S.P. and Winter, G. "Response of Concrete to Repeated Loadings", RILEM, Proc. Int. Symp. on the Effects of Repeated Loading on Materials and Structural Elements, Mexico City, (1966).

112. Karsan, I.D. and Jirsa, J.O. "Behaviour of Concrete under Compression Loadings", Journal of Struct. Div., ASCE, Vol.95, No.ST12, (1969), 2543-2563.

113. Beams, G.W., Gerstle, K.H. and Ko, H.Y. "Response of Concrete to Cyclic Biaxial Compressive Loads", presented at the April 1982, ASCE National Convention, Las Vegas, Nev. (Preprint 81-015).

114. Scavuzzo, R., Stankowski, J., Gerstle, K.H. and Ko, H.Y. "Stress-Strain Curves for Concrete under Multiaxial Load Histories", Report of the Department of Civil, Environmental, and Architectural Engineering, Univ. of Colorado, Boulder, Colo. (Aug. 1983).

115. Pietruszczak, S. and Stolle, D.F.E. "Modelling of Sand Behaviour under Earthquake Excitation", Int. Journal Num. Analy. Meth. Geomech., Vol.11, (1987), 221-240.

116. Poorooshasb, H.B. and Pietruszczak, S. "A Generalized Flow Theory for Sand", Soil and Foundations, Vol.26, No.2, (1986), 1-15.

117. Thomas, T.Y. Plastic Flow and Fracture in Solids. Academic Press, New York, 1961.

118. Hill, R. "Acceleration Waves in Solids", Journal of Mech. Phys. Solids, Vol.10, (1962), 1-16.

119. Vermeer, P.A. "A Simple Shear-Band Analysis Using Compliance", IUTAM Conf. on Deformation and Failure on Granular Materials, Delft, Holland, (1982), 439-499.

120. Rudinicki, J.W. and Rice, J.R. "Condition for the Localization of Deformation in Pressure-Sensitive Dilatant Materials", Journal of Mech. Phys. Solids, Vol.23, (1975), 371-394.

121. Reklaitis, G.V., Ravindran, A. and Ragsdell, K.M. Engineering Optimization Methods and Applications. John Wiley and Sons, Inc. 1983

122. Zienkiewicz, O.C. The Finite Element Method. McGraw-Hill, London, 1977.

123. Meyer, C. and Okamura, H. Finite Element Analysis of Reinforced Concrete Structures. Proceedings of the U.S.-Japan Seminar on Finite Element Analysis of Reinforced Concrete, Published by ASCE, 1986.

124. Zienkiewicz, O.C., Valliappan, S. and King I.P. "Elasto-Plastic Solutions of Engineering Problems 'initial stress', finite element approach", Int. Journ. Numer. Meth. Engng., Vol.1, (1969), 75-100.

125. Nayak, G.C. and Zienkiewicz, O.C. "Elasto-Plastic Stress Analysis. A Generalization for Various Constitutive Relations Including Strain Softening", Int. Journ. Numer. Meth. Engng., Vol.5, (1972), 113-135.

126. Nayak, G.C. and Zienkiewicz, O.C. "Note on the 'Alpha'-Constant Stiffness Method for Analysis of Nonlinear Problems", Int. Journ. Numer. Meth. Engng., Vol.4, (1972), 579-582.

127. Siriwardane, H.J. and Desai, C.S. "Computational Procedures for Nonlinear Three-Dimensional Analysis with Some Advanced Constitutive Laws", Int. Journ. Numer. Analy. Meth. Geomech., Vol.7, (1983), 143-171.

128. Jofriet, J.C. and McNiece, G.M. "Finite Element Analysis of Reinforced Concrete Slabs", Journal of Struc. Div., ASCE, Vol.97, No.ST3, (1971).

129. Bell, J.C. A Complete Analysis of Reinforced Concrete Slabs and Shells. Ph.D. Thesis, Dept. of Civil Engng., University of Canterbury, Christchurch, New Zealand, 1970.

130. Bell, J.C. and Elms, D. "Partially Cracked Finite Element", Journal of Struc. Div., ASCE, Vol.97, No.ST7, (1971).

131. Scanlon, A. and Murray, D.W. " An Analysis to Determine the Effect of Cracking in Reinforced Concrete Slabs", Proc. of the Specialty Conference on Finite Element Methods in Civil Engineering, Montreal, Canada, (1972).

132. Hand, F.R., Pecknold, D.A. and Schnobrich, W.C. "Nonlinear Layered Analysis of RC Plates and Shells", Journal of Struc. Div., ASCE, Vol. 99, No.ST7, (1973).

133. Bashur, F.K. and Darwin, D. "Nonlinear Model for Reinforced Concrete Slabs", Journal of Struc. Div., ASCE, Vol.104, No.ST1, (1978).

134. Phillips, D.V. and Zienkiewicz, O.C. "Finite Element Non-Linear Analysis of Concrete Structures", Proc. Instn. Civ. Engrs., Part 2, Vol.61, (1976), 59-88.

135. Jiang, J. Analysis of Reinforced and Prestressed Concrete Slabs by Finite Element Method. M.Eng. Thesis, Dept. of Civil Engng. and Engng. Mech., McMaster University, Hamilton, Canada, 1985.

136. Bathe, K.J. and Wilson E.L. Numerical Methods in Finite Element Analysis. Prentice-Hall, New Jersey, 1976.

137. Chow, W.K.M. Finite Element Modelling of Prestressed Concrete Slabs. M.Eng. Thesis, Dept. of Civil Engng. and Engng. Mech., McMaster University, Hamilton, Canada, 1984.

138. Kabir, A.F. "Nonlinear Analysis of Reinforced Concrete Panels, Slabs and Shells for Time Dependent Effects", UC-SESM Report No. 76-6, University of California at Berkeley, 1976.

139. Saouma, V. Automated Nonlinear Finite Element Analysis of Reinforced Concrete: A Fracture Mechanics Approach. Ph.D. Thesis, Cornell University, Ithaca, New york, 1981.

140. van Greunen, J. "Nonlinear Geometric, Material and Time Dependent Analysis of Reinforced and Prestressed Concrete Slabs and Panels", UC-SESM Report No. 79-3, University of California at Berkeley, 1979.

141. Leibengood, L.D. and Darwin, D. "Parameters Affecting FE Analysis of Concrete Structures", Journal of Struc. Engng., ASCE, Vol.112, No.2, (1986), 326-341.

142. Taylor, R., Maher, D.R.H. and Hayes, B. "Effect of the Arrangement of Reinforcement on the Behaviour of Reinforced Concrete Slabs", Magazine of Concrete Research, Vol.98, No.55, (1966).

143. Berg, S. Nonlinear Finite Element Analysis of Reinforced Concrete Plates, Ph.D. Thesis, Division of Structural Mechanics, The Norwegian Institute of Technology, Trondheim, 1973.

144. Arnesen, A. "An Analysis of Reinforced Concrete Shells Considering Material and Geometric Nonlinearities", Report No. 79-1, Division of Structural Mechanics, The Norwegian Institute of Technology, Trondheim, 1979.

145. Gopalaratnam, V.S. and Shah, S.P. "Softening Response of Plain Concrete in Direct Tension", Journal of ACI, Vol.82, No.3, (1985), 310-323.